DAILY TO YEARLY VARIATIONS IN RIP CURRENT ACTIVITY OVER KILOMETER SCALES

Gregory P. Dusek

A dissertation submitted to the faculty of the University of North Carolina at Chapel Hill in partial fulfillment of the requirements for the degree of Doctor of Philosophy in the Department of Marine Sciences (Physical Oceanography)

Chapel Hill
2011

Approved by:

Dr. Harvey Seim

Dr. Rick Luettich

Dr. Antonio Rodriguez

Dr. Jeffrey Hanson

Dr. George Voulgaris

ABSTRACT

GREGORY P. DUSEK: Daily to Yearly Variations in Rip Current Activity Over Kilometer Scales
(Under the direction of Dr. Harvey Seim)

Rip currents are seaward directed jets of water that originate nearshore and frequently occur along many U.S. beaches. Rip currents are well known to be the number-one public safety risk at the beach, yet there are research voids, particularly in regard to rip current forecasting. This dissertation seeks to describe the factors that influence the daily to yearly variations in rip current activity and provide the statistical basis for a probabilistic rip current forecast model. First, an open-source toolbox to process and analyze directional wave spectra from Acoustic Doppler Current Profilers (ADCPs) is presented. The toolbox, Doppler Profiler Waves Processing toolbox (DPWP), proves to be a flexible alternative to the instruments' proprietary software and provides comparable performance. DPWP processes all ADCP data used in this dissertation. Second, an analysis of historical rip current rescue data collected by Kill Devil Hills (KDH) Ocean Rescue on the Outer Banks of North Carolina from 2001 to 2009 is described. This analysis suggests that rip currents are most likely when there are large significant wave heights, a shore-normal wave direction and at low tidal elevations. The presence of two swells increased the likelihood of rescues when there were large differences between the mean directions of each swell. Alongshore location is important, as the southern half of KDH tends to be more favorable to hazardous rip occurrence than

northern KDH. Third, daily variations in observed rip intensity are related to wave field and surf zone bathymetry features. Rip intensity was found to increase substantially when the daily averaged significant wave height exceeded about 0.7 m, and then increase gradually as the significant wave height approached 2 m. Rip intensity was also found to be greatest at locations where there were substantial surf zone bars that varied in depth (~ 0.5 m) over 50 m alongshore. Lastly, a probabilistic rip current forecast model is created using rip current observations and a logistic regression formulation. Given a set of input predictor variables, the probabilistic model predicts the likelihood of hazardous rip current occurrence (0 to 1). Using rip current rescues to indicate hazardous rip current occurrence the probabilistic model has a Brier Score of 0.15 (0 is perfect prediction) compared to a minimum Brier Score of 0.45 for the present National Weather Service (NWS) Weather Forecast Office model. The change in score represents a 67% improvement in prediction for the probabilistic model compared to the NWS model.

To my wife Katrina. Without her sacrifice, support and friendship this work would not have been possible.

ACKNOWLEDGEMENTS

First and foremost I would like to thank my advisor, Dr. Harvey Seim. The completion of this dissertation would not have been possible without his continued support and guidance. I would also like to thank my committee members: Dr. Jeffrey Hanson, Dr. Rick Luettich, Dr. Antonio Rodriguez and Dr. George Voulgaris. I truly appreciate the time they spent providing feedback on the various chapters in this dissertation as well as sitting through the sometimes marathon committee meetings. They are all experts in their fields and have served as invaluable resources.

The fieldwork necessary to provide the observations used in this dissertation would not have been possible without the help of numerous organizations and individuals. Chief among these is Kill Devil Hills Ocean Rescue, who provided all of the rip current observations used in this research. I would especially like to thank head lifeguard David Elder. His enthusiasm and tireless commitment to this research was a primary reason for a successful outcome. Instrument deployment and bathymetry surveys were supported by the University of North Carolina Coastal Studies Institute. In particular I would like to thank Mike Muglia, who captained our deployments and served as the head diver. Much of the equipment and supplies used for instrument deployment and bathymetry surveys were from the U.S. Army Corps of Engineers Field Research Facility. I would like to thank Mike Forte for his surveying expertise and guidance using

RTK GPS systems. Finally, I would like to thank Nick Spore and Justin Robey who volunteered to spend part of their summers helping me venture into the surf zone and perform beach profiles.

Some of the data used in this dissertation has been provided by the U.S. Army Corps of Engineers Field Research Facility, primarily wave, tide and weather observations and bathymetry surveys offshore of Kill Devil Hills. In addition, the National Weather Service provided rip current forecast data. I would in particular like to thank Scott Kennedy with his help and for all of the effort he has put into rip current forecasting. I would also like to thank Su Zhang and Dr. J.S. Marron of UNC Chapel Hill for their assistance with the logistic regression formulation.

Funding sources includes NOAA IOOS Grant NA07NOS4730212 and U.S. Army Corps of Engineers Grant W912BU-9-P-0236, as well as the Graduate School Dissertation Completion Fellowship. This material is based in part upon work supported by the US Department of Homeland Security under Award Number: 2008-ST-061-ND 0001. The views and conclusions contained in this document are those of the author and should not be interpreted as necessarily representing the official policies, either expressed or implied, of the US Department of Homeland Security.

Lastly, I would like to thank my wife, Katrina for reading my drafts or listening to my practice talks and always providing thoughtful feedback. For putting up with my many trips to the beach, and for letting me waste some of her vacation time surveying all of Kill Devil Hills. But most importantly for her continued support and devotion.

TABLE OF CONTENTS

LIST OF TABLES

LIST OF FIGURES

CHAPTER 1

INTRODUCTION

Rip currents are relatively narrow, seaward directed jets of water that originate in the surf zone. Often incorrectly referred to as "rip tides", rip currents are the number one cause for rescues and drownings at the beach in the United States. Over the past decade there have been on average over 20 reported rip related drownings and over 30,000 reported rip rescues each year in the U.S. (www.usla.org). Despite these statistics rip currents are relatively poorly understood by the beach going public and attempts to forecast rip currents, to inform the public of the possible risk, remain fairly simplistic. Perhaps the primary reason for this is a lack of scientific research focusing on large scale variations in rip current activity. Although rip currents have been studied extensively over the past 20 years, there is very little research regarding rip current activity over large spatial (> 1 km) and temporal (days to years) scales. An understanding of rip current variations over these large scales is essential if we wish to accurately predict the likelihood of rip currents occurring at different locations along the coastline on at least a daily basis. This dissertation will focus on determining the relationship between physical processes and large scale variations in rip current activity, and quantifying this relationship to create a probabilistic rip current forecast model.

1.1 Scientific Background

Rip currents are surf zone currents that are typically 10s of meters wide and extend 100 m or more offshore with velocities generally 1 m/s or less, although occasionally in excess of 2 m/s (MacMahan et al., 2006). Rip currents can be visually identified by surf zone regions without breaking waves, and are often characterized by foam or sediment laden water that forms a cloud or "rip head" just outside the surf zone (Figure 1.1). Rip currents were first observed scientifically in 1941 (Shepard et al., 1941), with the first complete theoretical description provided in 1969 (Bowen, 1969; Bowen and Inman, 1969).

Rip currents are dynamically forced by alongshore variations in radiation stress resulting from varying wave heights alongshore. Radiation stress is defined as the transport of wave-induced momentum (Longuet-Higgins and Stewart, 1964). Following Holthuijsen (2007), for a stationary first order approximation, the cross-shore gradient in radiation stress, S_{xx}, is balanced by the hydrostatic pressure gradient:

$$\frac{dS_{xx}}{dx} = -\rho g(d + \bar{\eta})\frac{d\bar{\eta}}{dx} \quad (1.1)$$

where ρ is the density of seawater, g is gravitational acceleration, d is the still water depth and $\bar{\eta}$ is the change in mean water level. Essentially, a negative cross-shore radiation stress gradient results in a positive hydrostatic pressure gradient or an increase in water level (i.e. a set-up). A negative cross-shore radiation stress gradient occurs shoreward of where waves first start to break (i.e. the outer surf zone) and larger breaking waves result in a correspondingly more negative cross-shore radiation stress gradient. Thus, larger breaking waves result in a greater set-up or higher water level in the surf

Figure 1.1 A rip current can be seen in the center of the photograph, identified by the region without breaking waves and foam transported outside of the surf zone.

zone compared to smaller breaking waves. Alongshore variations in breaking wave heights then result in a gradient of the alongshore set-up (e.g. HI-LOW-HI) that forces a flow of water from the regions of large breaking waves to the regions of smaller waves and drives rip current circulation.

Since alongshore differences in the breaking wave height are the primary driver of rip currents, the characteristics of the nearshore wave field and tidal elevation will significantly impact rip current occurrence and intensity. Numerous observational studies have determined that there is an increase in rip current activity and intensity with increasing wave height (Brander, 1999; Brander and Short, 2000; MacMahan et al., 2005) and as wave incidence approaches shore-normal (Engle et al., 2005; Svendsen et al., 2000). Additionally, rip current activity increases as tidal elevation decreases (Brander and Short, 2000; Engle et al., 2002; MacMahan et al., 2005; Scott et al., 2009). Rip

currents tend to be more intense at low tide when there is increased breaking over the surf zone bar and the water level may be low enough over the surf zone bar that return flow within the surf zone is directed towards rip channels, strengthening rip intensity. The relation of wave period with rip currents is less certain. Although studies have suggested that the occurrence of strong rip currents increases as wave period increases (Engle et al., 2002; Scott et al., 2009), the relationship is not conclusive. When two swells are present, the resulting bi-modal wave field can cause crossing wave trains nearshore, which may be a mechanism for forming a hazardous rip current. Crossing wave trains were shown to cause rip currents in lab studies (Fowler and Dalrymple, 1991).

The surf zone bathymetry also plays a significant role in rip current activity. Although there are ways to generate rip currents from purely hydrodynamic forcing (e.g. crossing wave trains) (Dalrymple, 1978; Fowler and Dalrymple, 1991; Johnson and Pattiaratchi, 2004), rip currents are often associated with alongshore variability in the bathymetry and more specifically in the surf zone bar (Brander, 1999; Brander and Short, 2000; Haller et al., 2002; MacMahan et al., 2005). Generally, rip current activity will be more significant in areas of a prominent surf zone bar, as alongshore variations in the height of the bar will drive variations in the breaking wave height, which is the primary mechanism for rip current formation (Bowen, 1969; Dalrymple, 1978; Haller et al., 2002). The idealized bar morphology conducive for rip current generation is an alongshore uniform bar with breaks or rip channels, leading to relatively large breaking waves over the bar, and smaller breaking waves in the channel. It is important to note that this idealized morphology probably rarely occurs, rather the surf zone bar structure is often much more complex in both the alongshore and cross-shore direction. Although it

has been shown that small alongshore variations in the bathymetry (1 in 300 alongshore variation) can lead to rip current circulation (MacMahan et al., 2008), the expectation is that strong or hazardous rip currents are more commonly driven by large alongshore variations in bar morphology (e.g. breaks bisecting the bar; Brander, 1999).

There is a strong morphodynamic relationship between the surf zone bar system, rip current activity and the local wave conditions (Brander, 1999; Brander and Short, 2000). It has been shown that immediately following a large wave event a relatively alongshore-uniform bar is developed on the outer boundary of the surf zone (van Enckevort and Ruessink, 2003; van Enckevort et al., 2004). As wave energy decreases, the bar migrates towards shore, developing alongshore non-uniformities (van Enckevort et al., 2004). These non-uniformities often consist of rip channel type features and thus rip current activity will often be greater in the days following large wave events. The extent of the wave event will in part determine whether there is full or partial reset of the bar. For relatively large events, an alongshore-uniform bar will develop, and non-uniformities may take a week or more to fully develop (van Enckevort et al., 2004). However, a partial reset of the bar (i.e. not to a fully alongshore uniform state) may occur under moderate wave events, in which non-uniformities will be significant immediately following the wave event (Garnier et al., 2008). The non-uniformities (i.e. an alongshore varying bar with rip channels) thus provide the mechanism for rip circulation described previously.

1.2 Rip Current Forecasting

Due to the many variables involved with generating a rip current, accurate rip current prediction is difficult (Calvete et al., 2007). An accurate forecast system is a valuable resource for public outreach and thus there has been an effort over the past two decades to create a viable rip current forecast model. Lushine (1991) was the first to attempt rip prediction when he analyzed the relationship of drownings due to rip currents in southeast Florida to a variety of meteorological and oceanographic data. Lushine determined that rip current drownings were well correlated with increasing wind speed, shore-normal wind direction, increasing wave height and low tide. He used his results to aid in the creation of an empirical rip current forecasting or prediction index called LURCS (LUshine Rip Current Scale), in which various inputs (wind speed and direction, wave height, tide) were assigned a numerical value and added together resulting in a rip current risk assessment. For example, 15 kt onshore winds, a 3 ft wave height and low tide would result in a category 5 risk, or a high likelihood for strong rip currents. Lascody (1998) performed a similar analysis as Lushine, but in east central Florida and with rip current lifeguard rescues instead of drownings, thus providing a much larger data set. In addition to re-affirming that rip currents were correlated to the wave height, low tide, wind speed and wind direction, Lascody found that wave period was also a factor and that rip currents were more likely during instances of long period swell (> 12 s). Thus, Lascody formulated the ECFL (east central Florida) LURCS index, which followed a similar method as Lushine's LURCS, but with the addition of swell period as a factor. Four years later, Engle et al. (2002) performed additional analyses of lifeguard rescue data in east central Florida and made further changes to the ECFL LURCS index. Engle

et al. found that wind speed and direction were not an important factor in determining rip current likelihood, but rather that the wave field (peak period, peak direction and height) and the tide were the most accurate indicators of hazardous rip activity. Thus, a modified ECFL LURCS index utilizing these factors was created and successfully back tested.

The modified ECFL LURCS index (or a slight variation) is the rip current forecasting method predominantly used today by National Weather Service (NWS) Weather Forecast Offices (WFOs). The Newport/Morehead City WFO has implemented a form of the ECFL LURCS forecasting index with some success; however, the accuracy of the NWS WFO model has been hindered by a lack of observations assessing the impact of physical factors on hazardous rip current occurrence over large spatial (< 1km) and temporal (days to years) scales. The index method and categorical output of the NWS WFO model also has inherent functional limitations, for example, the output of a three-category forecast compared to a fully continuous probabilistic model. These limitations suggest significant opportunity for improving the forecast system currently in place and that any substantial improvements would require a deviation from the present forecast index approach.

1.3 Dissertation Layout

Although the dynamics of rip currents are fairly well understood, much of the scientific research detailed above has focused on a singular rip system over relatively short timescales (< 1 month). This leaves uncertainty regarding which physical factors most influence the occurrence of rip currents over large spatial (> 1 km) and temporal scales (days to years). This lack of understanding has prevented significant improvement

in the accuracy of the present rip current forecast models, which are one of the mechanisms for public awareness of hazardous rip current conditions. Thus, there is an impetus to better understand the physical processes driving large scale rip activity or more importantly those driving large-scale hazardous rip activity (i.e. rip currents intense enough to pose a safety risk to bathers). This dissertation seeks to determine the relationships between physical processes and large scale variations in rip current activity, and to utilize these relationships to create a probabilistic rip current forecast model. The layout of the dissertation is as follows:

Chapter 2: Evaluation of an open-source directional wave spectral toolbox applied to Doppler profiler data

As rip currents are highly dependent on the wave field, observational wave data is an essential part of rip current research. Some of the wave data utilized in this dissertation were collected using Acoustic Doppler Current Profilers (ADCPs), instruments deployed on the sea floor that use sound waves to measure the wave field. As the ADCPs output their data in binary code, computer software is needed to translate the binary code into water level data, to directional wave spectra and eventually to wave spectral statistics (e.g. significant wave height, peak period and mean direction). Although there exists proprietary software to process the binary output, the closed nature of this software is potentially limiting. Thus an open-source spectral toolbox has been created to process the binary output from ADCPs and is detailed in this chapter.

Chapter 3: Analysis of rip current rescues at Kill Devil Hills, North Carolina

Lifeguards at Kill Devil Hills, a 7.5 km stretch of beach on the Outer Banks of North Carolina, have recorded the time and location of every rip current rescue made from 2001 to 2009. During this time, hourly wave and tidal data is available at the nearby U.S. Army Corps of Engineers Field Research Facility. The resultant data set includes 741 observations of rip rescues and over 20,000 hourly observations of the wave field and tidal elevation. Assuming that a rip rescue indicates hazardous rip current occurrence, this data set has been used to determine what wave field and tidal conditions favor hazardous rip current activity. In part, the results of this research have determined that significant wave height, mean direction and directional spread contribute to rip current activity.

Chapter 4: The influence of the wave field and surf zone bathymetry on daily variations in rip current intensity

In addition to the rip rescue record, lifeguards at Kill Devil Hills performed daily surf zone observations in the summer of 2008 and 2009 to determine the occurrence and relative intensity of rip currents near their lifeguard chair. In concert with these observations, bi-hourly wave field observations were collected by two ADCPs in the region and cross-shore beach and surf zone profiles were collected at seven locations throughout the summers of 2008 and 2009. These data were used to develop probability distributions of rip intensity for various wave field statistics and to relate rip intensity to surf zone bathymetry profile metrics. In addition, since the interpretation of rescue data is complicated by the number of people in the water, the lifeguard observations provide an unambiguous and continuous data record of rip current occurrence and intensity.

Chapter 5: A probabilistic rip current forecast model

A probabilistic rip current forecast model is developed from lifeguard rip current observations using a logistic regression formulation. Given a set of input predictor variables, the probabilistic model predicts the likelihood of hazardous rip current occurrence (0 to 1). The inclusion of each predictor is determined through both a physical and statistical basis. The predictors utilized in the model include significant wave height, vector mean wave direction, tidal elevation, and if the forecast occurs in a 72-hour post- wave event window. A hindcast of the probabilistic model demonstrates improved performance compared to the present NWS WFO forecast model. Using rip current rescues to indicate hazardous rip current occurrence the probabilistic model has a Brier Score of 0.15 (0 is perfect prediction) compared to a minimum Brier Score of 0.45 for the NWS model. The change in score represents a 67% improvement in prediction for the probabilistic model compared to the NWS model.

Chapter 6: Conclusions and future research

Dissertation conclusions are presented along with a number of research questions that remain to be addressed.

CHAPTER 2

EVALUATION OF AN OPEN-SOURCE DIRECTIONAL WAVE SPECTRAL TOOLBOX APPLIED TO DOPPLER PROFILER DATA

2.1 Introduction

Collecting accurate measurements of nearshore directional waves is invaluable for many applications, from sediment transport (e.g. Boon et al., 1996) to evaluating wave models (e.g. Gorman et al., 2003). Recently the use of acoustic Doppler devices has become a popular choice for measuring directional wave data in shallow water since they are portable, simple to use and relatively inexpensive. Two of the more common types of these devices are the Nortek AWAC (Acoustic Wave And Current sensor) and the TRDI (Teledyne RD Instruments) ADCP (Acoustic Doppler Current Profiler).

There have been numerous studies validating the performance of both the AWAC (e.g. Siegel et al., 2004; Pedersen and Lohrmann, 2004) and the ADCP (e.g. Hoitinik and Schroevers, 2004; Jeans et al., 2003; Rorbaek and Andersen, 2000, Strong et al., 2000; Work and Bystrom, 2005) through comparison to more traditional pressure or buoy-based accelerometer directional wave measurements. In addition, the performance of the ADCP and AWAC in providing wave measurements have been compared against each other, generally with favorable results (Birch et al., 2004). However, in much of the

previous work the comparisons were made using the proprietary software of each company.

Two recent publications have demonstrated the effectiveness of ADCP directional wave measurements without the use of the proprietary software. Hoitink et al. (2007) developed a linear filtration technique to remove turbulence and noise from the along-beam radial velocity measurements and determined that with or without this filtration the frequency spectra generated from ADCP measurements compared favorably to Datawell Waverider buoy spectra. Herbers and Lentz (2010) determined that generally the directional spectra resultant from ADCP along-beam radial velocity measurements agreed favorably with Waverider spectra. They found that during low energy conditions noise levels in the radial velocity data lead to directional spread measurements biased high, however that frequency spectra and measurements of mean direction were accurate when compared to the Waverider estimates.

In both of these publications the authors utilized their own independent processing methods to analyze the ADCP data. This enabled them to determine why there may be inaccuracies in the spectra generated from ADCP measurements and allowed them to make modifications to the processing methods to improve the quality of their results. This flexibility would be impossible for those utilizing just the proprietary software. Although the authors of the aforementioned publications have developed a method for processing ADCP data, there is no open-source code publically available to process ADCP directional wave measurements. Thus, a majority of users are forced to rely on the proprietary software to process their data. Not only can the closed nature of the proprietary software be potentially limiting, but also the proprietary software for each

device is limited to a particular hardware platform and can limit the manner in which real-time data systems can be configured.

To address the need for an independent processing scheme an open-source Doppler Profiler Waves Processing toolbox (DPWP) has been created. This toolbox utilizes a similar processing scheme for both the AWAC and ADCP raw data and generates wave spectra within MATLAB® utilizing a modified version of the toolbox DIWASP (Directional Wave Spectra Toolbox; Johnson, 2002). DIWASP has been used effectively to process Datawell Waverider buoy data into directional wave spectra (Cruz et al., 2007), however the ability of DIWASP to generate directional wave spectra from ADCP or AWAC data has not been demonstrated.

The purpose of this paper is to validate the DPWP toolbox as an affective alternative to the proprietary software when processing ADCP or AWAC directional wave measurements and is organized as follows. First a description of the processing scheme is presented. Then, a month long data sample from the 8m pressure array in Duck, NC is used to validate DPWP compared to an independent processing scheme created by the Army Corps of Engineers Field Research Facility. An ADCP located within the array permits a comparison of the directional wave spectra generated from ADCP *p*-*u*-*v*-*w*, range and along beam radial velocity measurements to the spectra generated from the 8m array. Finally, the DPWP toolbox is applied to the Nortek AWAC and a side-by-side comparison between the ADCP and the AWAC located at Bogue Banks, NC is made using DPWP.

2.2 Data Processing Methods

2.2.1 Description of processing scheme

The toolbox we have developed to process raw data from either the ADCP or AWAC currently employs a two-step process (Figure 2.1). The initial step is to format the raw binary data output from either the ADCP or the AWAC using a program written in Python. For either the ADCP or the AWAC this code accomplishes a similar goal, to convert the raw binary data to a format compatible with the second step in the processing. For both instrument platforms the input data can be either a single hourly sample or a long stream of samples, and can be either waves data alone or interleaved waves and currents data. The second step of processing is completed in MATLAB® and includes the generation of directional wave spectra utilizing a modified version of the DIWASP wave spectral toolbox (Johnson, 2002). In addition to the output of a directional wave spectrum, the DIWASP toolbox provides a graphical representation and information about the spectrum (significant wave height with confidence intervals, peak period, direction of peak period and dominant direction). See Appendix A for a more detailed description of the processing scheme and a link to the code repository.

2.2.2 Data inputs

For the analysis of the ADCP directional wave spectra, three separate data inputs are utilized: pressure and *u*-*v*-*w* velocities, along-beam range to surface, and the along-beam radial velocity measurements. Although the record lengths vary, both ADCPs used in the study were deployed with similar options (Table 2.1). In each case for every wave sample, the ADCP output pressure measurements, along-beam range measurements and

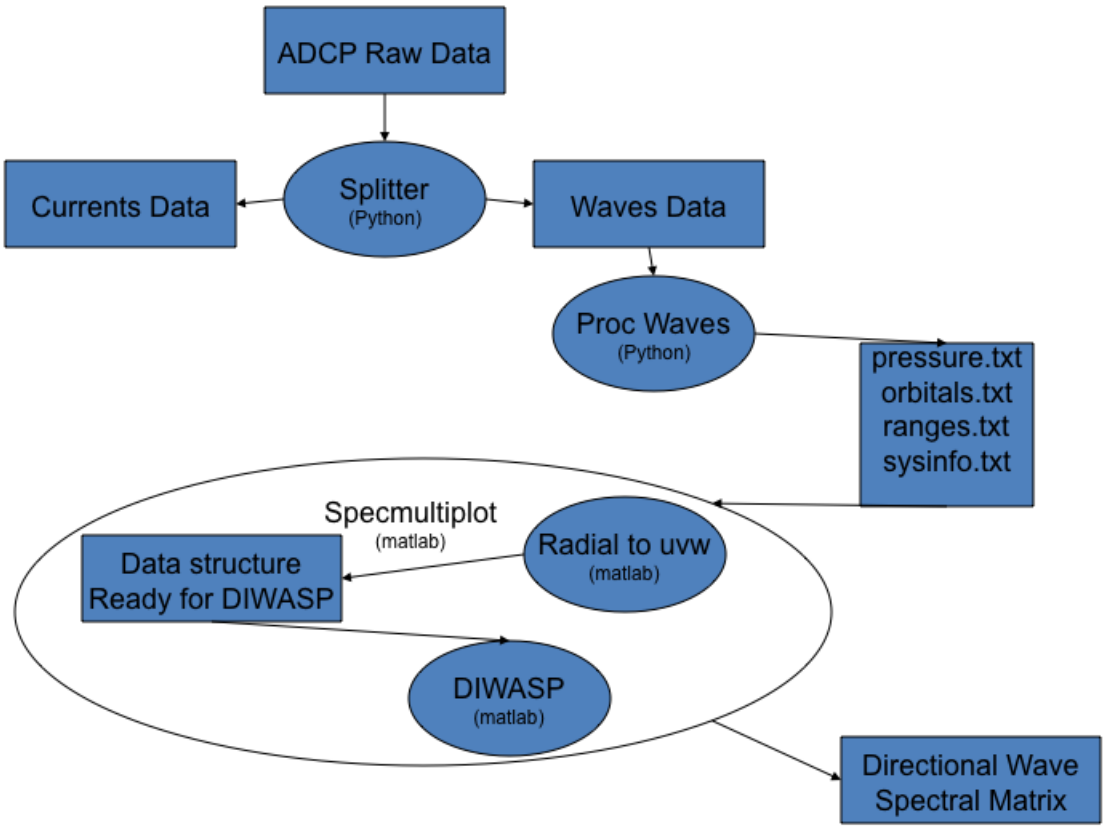

Figure 2.1 A flowchart of the processing scheme used by the Doppler Profiler Waves Processing Toolbox. Processing steps (ovals) in Python and MATLAB and data inputs/outputs (rectangles) are indicated.

along-beam radial velocity measurements sampled at 2 Hz. The *u*-*v*-*w* velocities were calculated by combining all four along-beam velocity measurements at each of five bin heights. The range data was transformed to surface elevation measurements by accounting for the beam angle and distance from the ADCP to the horizontal location where the beam intersects the oceans surface. The radial velocities are the direct along-beam velocity measurements at each beam (four total) and each bin (five total) location for a total of 20 radial velocity measurements. Each beam from the upper three bins (unless the top bin has excessive bad data points), a total of 12 radial velocity inputs, are utilized in DIWASP when generating the directional spectra. In each case the outliers or

bad data points outside of four standard deviations of the mean were removed from the raw data time-series.

Table 2.1 A list of the hardware and user options selected for the ADCPs and AWAC used for the study

	FRF ADCP	**Bogue Pier ADCP**	**Bogue Pier AWAC**
Model	RDI Workhorse Sentinel	RDI Workhorse Sentinel	Nortek AWAC w/ AST
Frequency	1200 kHz	1200 kHz	1000 kHz
Firmware	16.21	16.28	1.17 AST
Bin Size	0.5 m	0.5 m	0.5 m
No. of Bins	30	50	20
Blanking Dist.	1.05 m	1.05 m	0.40 m
Ping Frequency	2 Hz	2 Hz	2 Hz / AST - 4Hz
Records per Burst	4096	2400	2048
Time of Burst	34.13 min (per hour)	20 min (per hour)	17.07 min (per hour)

For each data-type a transfer function is used to relate the measurement to a sea-surface elevation following linear wave theory (Hashimoto 1997, sec 9.2). The pressure transfer function *H* is given by:

$$H_p(k,\omega,\theta) = \rho g \frac{\cosh(kz)}{\cosh(kd)} \text{ , (2.1)}$$

and the *u*-*v*-*w* transfer functions are respectively:

$$H_u(k,\omega,\theta) = \omega \frac{\cosh(kz)}{\sinh(kd)} \cos\theta \quad H_v(k,\omega,\theta) = \omega \frac{\cosh(kz)}{\sinh(kd)} \sin\theta$$

$$H_w(k,\omega,\theta) = -i\omega \frac{\sinh(kz)}{\sinh(kd)} \quad (2.2)$$

where θ is the wave propagation direction, $\omega = 2\pi f$ or the angular frequency (f = frequency in Hz), ρ is the fluid density, g is gravitational acceleration, k is the scalar wave number, z is the elevation from the bottom and d is the water depth. The along-beam radial velocity transfer function was added to DIWASP when it was included in DPWP. The radial velocity transfer function is given in by:

$$H_{rad}(k,\omega,\theta) = \omega \frac{\exp\{ikr\sin\alpha\cos(\theta-\beta)\}}{\sinh kd} \cdot[\cosh\{k(r\cos\alpha+z)\}\sin\alpha\cos(\theta-\beta) - i\sinh\{k(r\cos\alpha+z)\}\cos\alpha] \quad (2.3)$$

where the polar coordinates of (α,β,r) representing the beam angle from the vertical, the horizontal axis angle of the beam sample cell, and the along-beam distance to the sample cell respectively. For the range data no transfer function is needed since it is a direct measure of the surface elevation.

In addition, a low and high frequency cut-off are applied to the radial velocity transfer function to prevent very low (< 0.05 Hz) and high frequency (> 0.4 Hz) noise from being disproportionately represented in the transferred surface elevation spectrum:

$$H_{rad}(f \le 0.05,\theta) = H_{rad}(0.05,\theta) \quad \text{and} \quad H_{rad}(f < 0.40,\theta) = H_{rad}(0.40,\theta). \quad (2.4)$$

Cut-off values were chosen since on the east coast of the U.S. a majority of surface gravity wave energy will be found within 0.05 Hz to .40 Hz. Additionally, the presence of infragravity motions at low frequencies (Hoitink et al., 2007) and excessive noise at high frequencies (Herbers and Lentz, 2010) can reduce the quality of both the frequency and directional spectra.

2.2.3 Spectral Estimation Technique

The frequency spectrum of the water's surface, *G(f)*, is generated from the auto-spectra of the chosen data input by applying the transfer function, *H*. A directional spreading function, *E*, is estimated and applied to the frequency spectra to generate full 2-d (2 dimensional) directional spectra, $G(f,\theta)$. Two of the directional spectra estimation methods available within the DPWP toolbox are utilized: the Iterative Maximum Likelihood Method (IMLM) and the Extended Maximum Entropy Principle Method (EMEP).

The IMLM was initially developed by Pawka (1983) to improve upon the Maximum Likelihood Method or MLM (Capon, 1969). Otlman-Shay and Guza (1984) present an alternative method of computing the iterative term in the IMLM. The initial MLM estimation of the directional spreading function, for a given angular frequency (ω) and wave number (k) is of the form:

$$E(\theta \mid k,\omega) = D\left[\sum_{n=1}^{N}\sum_{m=1}^{N} X_{nm}^{-1}(\omega)H_n(k,\omega,\theta)H_m^*(k,\omega,\theta)\exp\{ik[(x_n - x_m)\cos\theta + (y_n - y_m)\sin\theta\}\right]^{-1} \quad (2.5)$$

where N is the number of "sensors" or in the case of the ADCP, the number of measurement locations. $X_{nm}^{-1}(\omega)$ is the inverse of the cross spectral matrix and $H(k,\omega,\theta)$ is the transfer function. The values of x and y represent the horizontal location of the "sensor" and D is a proportionality constant to ensure the correct integrated energy density. For a given k and ω the IMLM algorithm is defined as:

$$E_{IMLM}^{i}(\theta) = E_{IMLM}^{i-1}(\theta) + \varepsilon_i(\theta), \quad (2.6)$$

where $\varepsilon_i(\theta)$ is the modification to the i-1 iteration. In DPWP a default value of 50 iterations was chosen to assure that the solution would sufficiently converge. In the DPWP IMLM code, the modification term is a slight variation to the formulations provided by either Pawka (1983) or Oltman-Shay and Guza (1984) and is defined as:

$$\varepsilon_i = \gamma\left[\{E^0_{IMLM}(\theta) - T^i_{MLM}(\theta)\} + \alpha\{T^i_{MLM}(\theta) - T^{i-1}_{MLM}(\theta)\right], \quad (2.7)$$

where $T^i_{MLM}(\theta)$ is the MLM spectral estimate calculated from the cross-spectral matrix reconstructed from $E^{i-1}_{IMLM}(\theta)$ and where $T^{i-1}_{MLM}(\theta)$ is the previous MLM spectral estimate. The values of γ and α represent variable parameters that affect the convergence rate of the IMLM estimate. For the DPWP code the original values provided in DIWASP version 1.1 were chosen (γ, α = 0.1).

Some changes were made to the original IMLM function within DIWASP to improve the results, most notably when utilizing the ADCP radial velocity measurements. Due to high noise levels in the radial velocity measurements, $T^i_{MLM}(\theta)$ often estimated negative values that became increasingly negative with each iteration, yielding an unusable directional spectrum. This response of the IMLM when dealing with measurements with high noise levels or contaminated with errors has been previously documented (Hashimoto, 1997). The negative estimates result from an inaccurate calculation of the inverse of the reconstructed cross-spectral matrix when performing the iterative MLM estimation. To improve the results of the inversion some pre-conditioning is performed on the cross-spectral matrix and an improved inversion technique is applied. Additionally, any negative values in $T^i_{MLM}(\theta)$ are adjusted to 0 to avoid poor estimation of the $\varepsilon_i(\theta)$ modification term (following WAFO toolbox; Brodtkorb et al., 2000).

The EMEP was developed by Hashimoto et al. (1994) to improve upon and increase the flexibility of the Maximum Entropy Principle Method (MEP; Kobune and Hashimoto, 1985). The EMEP extends the MEP to allow for input of a large number of mixed instrument measurements (e.g. ADCP radial velocity measurements). The formulation of the EMEP is as follows:

$$E(\theta \mid \omega) = \frac{\exp\left[\sum_{n=1}^{N}\{a_n(\omega)\cos n\theta + b_n(\omega)\sin n\theta\}\right]}{\int_0^{2\pi}\exp\left[\sum_{n=1}^{N}\{a_n(\omega)\cos n\theta + b_n(\omega)\sin n\theta\}\right]d\theta}, \quad (2.8)$$

where $a_n(\omega)$ and $b_n(\omega)$ (n =1,…,N) are unknown parameters and *N* is order of the model. For the DPWP a value of N=50 is used to assure that the optimal model order is achieved. The EMEP code will iteratively estimate the spreading function until order 50 or until the optimal order is reached. If the computation becomes unstable a control parameter is included to under-relax the computation (For a complete description see Hashimoto et al, 1994).

2.2.4 Spectral Statistics and Error Metrics

The spectral statistics calculated to assess the performance of DPWP include significant wave height, peak period, mean direction and directional spread. Significant wave height, approximated by H_{mo} is defined as:

$$H_s \approx H_{mo} = 4\sqrt{e}, \quad (2.9)$$

where *e* is the total spectral energy and equates to:

$$e = \iint G(f,\theta)\,d\theta\,df, \quad (2.10)$$

Peak period is defined as:

$$T_p = 1/f_p \text{ , (2.11)}$$

where f_p is the interpolated peak frequency using a three-point parabolic fit to the 1-d spectral peak. Mean wave direction is the vector mean wave direction (as in Hanson et al., 2009) defined as:

$$\bar{\theta} = \tan^{-1}\left(\frac{\overline{\sin\theta}}{\overline{\cos\theta}}\right), \text{ (2.12)}$$

where:

$$\overline{\sin\theta} = \frac{1}{e}\iint G(f,\theta)\sin\theta\partial\theta\partial f \text{ , (2.13)}$$

$$\overline{\cos\theta} = \frac{1}{e}\iint G(f,\theta)\cos\theta\partial\theta\partial f \text{ . (2.14)}$$

The directional spread, σ, is calculated for the 2-d directional spectrum (Kuik et al., 1988; O'Reilly et al., 1996). It can be approximated by:

$$\sigma = [2(1-m)]^{1/2} \text{ , (2.15)}$$

where:

$$m = (a^2 + b^2)^{1/2} \quad \text{(2.16)}$$

and a and b are the two lowest Fourier coefficients for a given frequency f of the directional distribution of wave energy $G(\theta|f)$ such that:

$$a(f) = \int_0^{2\pi} d\theta\cos\theta G(\theta \mid f) \text{ and } b(f) = \int_0^{2\pi} d\theta\sin\theta G(\theta \mid f) \text{ . (2.17)}$$

Following Hanson et al. (2009) the metrics used to quantify error are bias, root-mean-squared (RMS) error and scatter index (SI) for significant wave height, peak period

and directional spread and angular bias and circular correlation for mean direction. In addition, normalized error metrics were computed.

2.2.5 Confidence Limits

A calculation to estimate the 95% confidence intervals for frequency spectra and significant wave height is included in DPWP. The degrees of freedom are calculated using an effective number of data points, or N^* for each time series (Emery and Thomson, 2004).

$$N^* = \frac{N}{\left[\sum_{\tau+-\infty}^{\infty} \rho_{xx}(\tau)\rho_{yy}(\tau) + \rho_{xy}(\tau)\rho_{yx}(\tau)\right]} \quad (2.18)$$

where ρ represents the normalized cross- or auto-covariance function for some lag τ.

Once N^* is calculated for all time series pairs, an N^* matrix of size SxS is generated where S is the number of time series. The average of the off-diagonal N^* matrix quantities is calculated and used in eq. (2.19) to calculate the equivalent degrees of freedom (Emery and Thomson, 2004).

$$D_{eq} = w(N^* / M)S \quad (2.19)$$

where w is the window constant and M is the half-width of the window. The confidence bounds are calculated assuming that the true frequency spectrum $G(f)$ must fall within the following interval:

$$\frac{D_{eq}\tilde{G}(f)}{\chi^2_{1-\alpha/2,D_{eq}}} < G(f) < \frac{D_{eq}\tilde{G}(f)}{\chi^2_{\alpha/2,D_{eq}}} \quad (2.20)$$

Where $\tilde{G}(f)$ is the estimated frequency spectrum and χ^2 is the chi-square value for a particular α and D_{eq} and α is representative of the (1-α)100% confidence level.

2.3 Validation of DPWP Processing

To determine the effectiveness of the DPWP toolbox it is desirable to validate DIWASP and the DPWP toolbox through a statistical comparison of a time series of spectra utilizing an independent data source. To perform this analysis we have chosen to utilize data collected from an ADCP and the 8m pressure array located at the Army Corps of Engineers Field Research Facility (FRF) in Duck, NC. The array has been used for generating directional wave spectra for over 20 years and is considered among the most robust and accurate directional wave data available (Long and Oltman-Shay, 1991). The ADCP is a 1200kHz Workhorse Sentinel (Table 2.1) located within the 8m array. The first step in the validation of DPWP processing is to use DPWP to process 8m array data using both the IMLM and EMEP methods and compare the results to the output from the FRF's own independent processing scheme (Long and Atmadja, 1994). Following this analysis the ADCP data processed by DPWP and Teledyne RDI's proprietary Wavesmon software will be compared to the processed 8m array data to determine the validity of the ADCP DPWP processing method. When utilizing Wavesmon, the default options are used in each instance.

2.3.1 DPWP processing of 8m array data

The 8m pressure array consists of 15 pressure gauges located in 8m of water and about 900m offshore. Four consecutive 2048-second profiles are recorded at 2 Hz,

providing a record of 16384 points every 3 hours. The FRF processes and generates their directional wave spectra using their own software based around an IMLM estimation method. A complete description of this method can be found in Long and Atmadja (1994). The FRF processing uses a directional resolution of 2 degrees and a frequency resolution of 0.00977 Hz with minimum and maximum values of 0.0444 Hz and 0.3179 Hz respectively. The DPWP processing options include a directional resolution of 2 degrees, a frequency resolution of .01 Hz going from 0.01 Hz to 0.4 Hz and a Fast Fourier Transform (FFT) window size of 256. Data collected from Feb 1, 2007 to Feb 27, 2007 has been processed to validate and compare the DPWP EMEP and IMLM methods.

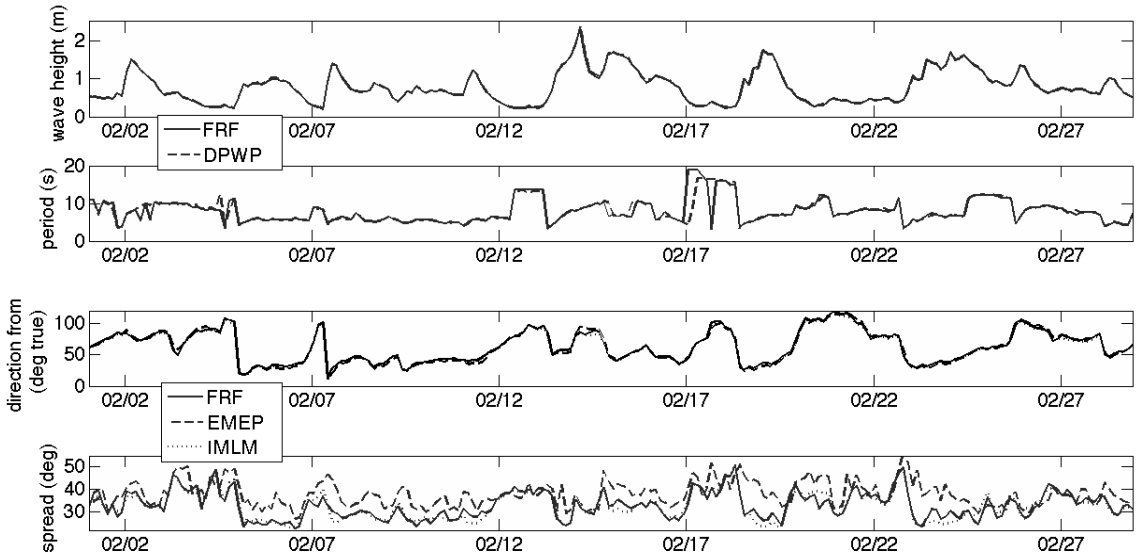

Figure 2.2 Time series plots showing a data comparison between the 8m array data processed by the FRF and the same data processed by DPWP. From top to bottom the plots are: significant wave height, peak period, mean direction and directional spread. The significant wave height for the FRF spectra is always within the 95% confidence limits of the DPWP measurement (not drawn due to clarity).

A visual analysis of the time series plots of the significant wave height, peak period, mean wave direction and directional spread generally show very good agreement

between the FRF and DPWP processed spectra (Figure 2.2). Since the application of either the EMEP or IMLM method only effects the directional spectra, they are only shown in the mean direction and directional spread plots.

The significant wave height is nearly identical throughout the time series with a maximum difference of only .06 m. The wave height of the FRF method is never outside of the 95% confidence levels of the DPWP wave height measurements. The plot of the peak period shows good agreement for a majority of time steps. The minor differences can be predominantly attributed to differences in the frequency resolution between the two processing methods. The more significant deviations seen are instances of a bimodal wave field where the two spectral peaks are very close in height, however the absolute peak is different in each processing method. The plot of the mean direction shows very good agreement between both the EMEP and IMLM method with the FRF method, as there is a maximum difference of only 7 degrees between the IMLM and the FRF methods, and 11 degrees between the EMEP and FRF methods. There are slightly greater differences evident in the time series of the directional spread, especially when considering the EMEP method. While the FRF and IMLM methods both demonstrate similar relatively tight directional spread (and a maximum difference of 8 degrees), the spread for the EMEP method is consistently greater and occasionally by as much as 15 degrees.

An example of the 1-d frequency and directional spectra (Figure 2.3) demonstrates the close similarities between the DPWP and FRF processing methods for the frequency spectra and the deviations in the directional spreading that occur between the various methods. The frequency spectra are very similar and the FRF spectrum is

nearly always within the 95% confidence limits of the DPWP spectrum. Conversely, while the IMLM directional spectrum is very similar to the FRF spectrum, the EMEP spectrum has energy distributed across all directional bins. This energy distribution results in a depressed peak and an increased directional spread measurement. The increased spread measurements tend to occur more often during short period wave conditions. Additionally, although this spreading negatively impacts the quality of the directional spectra for the EMEP method, the effect on bulk directional statistics is slight.

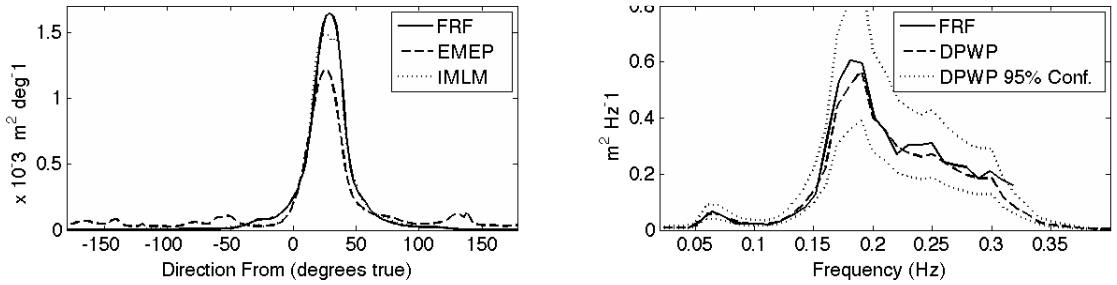

Figure 2.3 Spectral plots for a 2 hour and 16 minute record from the FRF 8m array in February 2007. The plot on the left is the 1-d directional spectra of the 8m array data processed by the FRF, DPWP EMEP and DPWP IMLM. The plot on the right is the 1-d frequency spectra of the 8m array data processed by the FRF and DPWP, as well as the 95% confidence limits for the DPWP spectra.

Table 2.2 Frequency spectra error metrics resulting from the comparative statistical analysis of each wave spectra data set collected at the USACE FRF.

	8m DPWP vs 8m FRF	**ADCP radial vs 8m DPWP**	**ADCP puvw vs 8m DPWP**	**ADCP range vs 8m DPWP**	**ADCP WMON vs 8m DPWP**
Sig Wave Height					
bias	< 0.01	< 0.01	-0.01	0.05	< 0.01
RMS error	0.02	0.07	0.05	0.12	0.06
SI	0.02	0.09	0.06	0.13	0.07
Norm bias	> 0.99	> 0.99	> 0.99	0.94	> 0.99
Norm RMS error	0.98	0.93	0.95	0.87	0.93
Norm SI	0.98	0.92	0.94	0.87	0.93
Peak Period					
bias	0.01	-0.23	-0.11	0.03	-0.22
RMS error	1.63	1.45	1.51	1.46	1.84
SI	0.21	0.19	0.19	0.19	0.24
Norm bias	> 0.99	0.97	> 0.99	> 0.99	0.97
Norm RMS error	0.81	0.83	0.82	0.83	0.78
Norm SI	0.79	0.81	0.81	0.81	0.76
Peak Period (with bi-modal points removed)					
bias	-0.03	-0.07	0.02	-0.01	-0.18
RMS error	0.34	0.5	0.56	0.46	0.70
SI	0.04	0.06	0.07	0.06	0.09
Norm bias	> 0.99	> 0.99	> 0.99	> 0.99	0.98
Norm RMS error	0.96	0.94	0.93	0.94	0.91
Norm SI	0.96	0.94	0.93	0.94	0.91

Table 2.3 Directional spectra error metrics resulting from the comparative statistical analysis of each wave spectra data set collected at the USACE FRF.

	8m DPWP EMEP vs 8m FRF	**8m DPWP IMLM vs 8m FRF**	**ADCP WMON vs 8m DPWP**	**ADCP radial EMEP vs 8m DPWP**	**ADCP radial IMLM vs 8m DPWP**
Direction					
angular bias	-0.84	-1.27	4.13	3.46	2.81
Norm angular b	> 0.99	> 0.99	0.98	0.98	0.98
Circular Correlation	> 0.99	> 0.99	0.98	> 0.99	0.98
Directional Spread					
bias	4.92	-0.22	7.75	8.23	-1.64
RMS error	7.04	1.99	8.84	12.07	4.11
SI	0.13	0.06	0.10	0.22	0.12
Norm bias	0.85	0.99	0.76	0.75	0.95
Norm RMS error	0.79	0.94	0.73	0.63	0.88
Norm SI	0.87	0.94	0.90	0.78	0.88

	ADCP range EMEP vs 8m DPWP	**ADCP range IMLM vs 8m DPWP**	**ADCP puvw EMEP vs 8m DPWP**	**ADCP puvw IMLM vs 8m DPWP**
Direction				
angular bias	4.52	3.71	10.78	7.52
Norm angular b	0.97	0.98	0.94	0.96
Circular Correlation	0.91	0.92	0.79	0.99
Directional Spread				
bias	25.71	26.88	30.09	-0.37
RMS error	27.55	28.69	34.53	5.32
SI	0.17	0.17	0.27	0.17
Norm bias	0.22	0.18	0.09	0.99
Norm RMS error	0.16	0.13	< 0.01	0.84
Norm SI	0.83	0.83	0.73	0.83

The results from the above error analysis (Tables 2.2 and 2.3) show that the DPWP processing method provides an accurate depiction of the wave field in nearly every regard. For the 2 output values calculated from the frequency spectra (significant wave height, peak period) the computed bias is minimal and can be considered insignificant given the resolution of the output values. The bias for the mean direction is also minimal for both the EMEP and IMLM methods, however when considering the spread the EMEP method shows a tendency to be biased high as was evident in the time series plot. The SI and RMS error computed for the significant wave height indicate very good agreement, as their normalized values of 0.98 are very close to 1 (perfect correlation). In addition the circular correlation for the mean direction is 0.99 for both the EMEP and IMLM, which depicts nearly perfect directional correlation between the different processing methods. The peak period shows some variability between the DPWP and FRF methods, as the values for the normalized SI and RMS error are 0.79 and 0.81 respectively. This difference is indicative of the instances of bimodal wave fields as mentioned above.

There are numerous instances in the data record where there is a bimodal wave field with both a low and high frequency peak. For nine of the instances (out of 224 data points) the peaks are very close in magnitude and each processing method indicates a different peak as the max value. When these instances are removed from the data record (Table 2.2, bottom), both the SI and RMS error decrease by about a factor of 4 and both normalized values improve to 0.96.

The above analysis demonstrates that within a small margin of error, the DPWP toolbox, using both the EMEP and IMLM estimation methods, is an accurate indicator of

the directional wave field. However, the IMLM may be optimal due to its more constrained directional spread.

2.3.2 Comparison of the ADCP and 8m array spectra

We next validate the ADCP observations processed using DPWP against the processed 8m array spectra over the same 1 month time period in February 2007. The TRDI Wavesmon processed ADCP data is also included in this comparison. Since the ADCP at the FRF samples for 34 minutes while the 8m array samples for 2 hours and 16 minutes, we have shortened the 8m array record to the first 34 minutes sampled of every 3 hour period. The 8m array data is processed in DPWP with the IMLM method utilizing the same options in DPWP as used in the previous analysis, which includes a directional resolution of 2 degrees, a frequency resolution of .01 Hz going from 0.01 Hz to 0.4 Hz and a Fast Fourier Transform (FFT) window size of 256. DPWP is used to process the three available types of ADCP data: radial velocities, pressure and *u*-*v*-*w* velocities, and the range to surface measurements. With all three data types both the EMEP and the IMLM methods are used to estimate the directional spreading. The ADCP data is processed with the same DPWP options selected for the 8m array.

The error metrics calculated when comparing the 2-d directional wave spectra of each processing option to the 8m array spectra suggest which DPWP directional estimation method and ADCP data types are superior. The error metrics suggest that all ADCP data types provide frequency spectra of similar quality (Table 2.2). The radial velocity data and *p*-*u*-*v*-*w* data have essentially no bias in significant wave height (less than 0.01 m in each case) or in peak period once the bi-modal points are removed (less

than 0.1 seconds in each case). Additionally the RMS error and SI values are fairly low for the significant wave height and peak period of both data types. The radial velocities achieve an RMS error of 0.07 m and SI of 0.09 for the significant wave height and 0.5 seconds and 0.06 respectively for the peak period. The pressure and *u*-*v*-*w* velocities achieve similar values of an RMS error of 0.05 m and an SI of 0.06 for the significant wave height and 0.56 seconds and 0.07 for the peak period. Both data types also perform at least as well in these regards when compared to the Wavesmon output. Furthermore, when a visual analysis of the 1-d frequency spectra is performed the 8m array spectra nearly always fall within the 95% confidence limits of both the radial velocity and *p*-*u*-*v*-*w* spectra (Figure 2.4). These results indicate that either of these data types provide an adequate measure of the frequency spectra and may be viable options when processing ADCP data. The range data performance is similar to the other data types when calculating the peak period, however the significant wave height estimates tend to be slightly biased high (0.05 m) and with a higher RMS error (0.12 m). The bias for the range data is most significant in low energy conditions and suggests that there may be complications with the range beam accurately reflecting off the surface during these conditions.

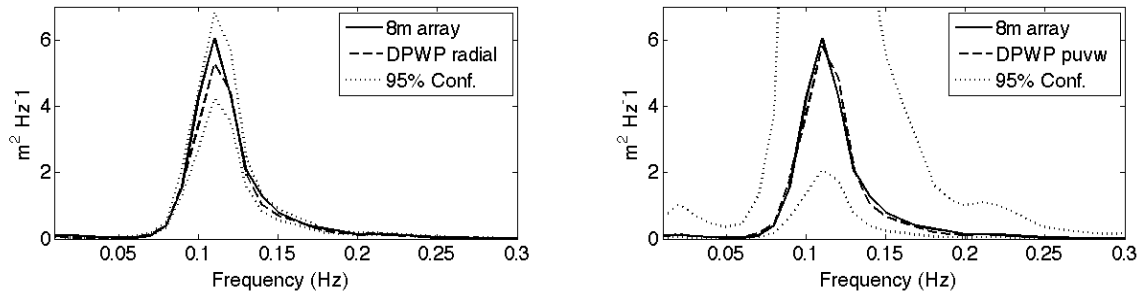

Figure 2.4 Spectral plots from a 34 minute record from the 8m array and co-located ADCP at the FRF in February 2007. The plot on the left is the 1-d frequency spectrum of the 8m array data and the DPWP radial velocity data. The plot on the right is the 1-d frequency spectrum of the 8m array data and the DPWP p-u-v-w data.

The metrics quantifying the error in the direction statistics for the 2-d spectra more clearly identify which ADCP data type and directional estimation method is optimal. Out of all three data types (radial, range, *p*-*u*-*v*-*w*) the radial velocity inputs provide the most accurate measurements of the mean direction (Table 2.3). The radial data processed via EMEP achieves normalized values of 0.98 and 0.99 for the angular bias and circular correlation respectively with the IMLM radial reaching 0.98 for both measures. These results are inline with the Teledyne RDI Wavesmon software, which also has values of 0.98 for both measures. The other data types and processing methods generally perform only slightly worse in regard to mean direction, with the exception of the *p*-*u*-*v*-*w* inputs with the EMEP method which has poor circular correlation (0.79) suggesting that the EMEP method may not be well suited for the *p*-*u*-*v*-*w* inputs.

The radial velocity data inputs also perform well when comparing measurements of the directional spread. The EMEP radial spectra are slightly less constrained directionally than the 8m array with a bias of 8 degrees and an RMS error of 12 degrees. The IMLM radial spectra are more constrained directionally than the 8m array, achieving a bias of -1.6 degrees and an RMS error of 4 degrees. The IMLM *p*-*u*-*v*-*w* spectra performed similarly to the IMLM radial velocity spectra in regard to directional spread. However, the EMEP *p*-*u*-*v*-*w* provided the least constrained directional spectra of all data type and estimation method pairings, again suggesting that the EMEP method is not well suited for the *p*-*u*-*v*-*w* data input.

The range data provide spectra with significantly greater directional spread than the 8m array measurements in most instances, as the bias is greater than 25 degrees for both the IMLM and EMEP method. The directional spread is especially large for the

range data during instances of relatively long period and thus large wavelength waves (Figure 2.5). In these instances the directionality of the estimate often breaks down due to the limited aperture of the surface elevation measurements relative to the wavelength. The aperture diagonally along the surface of the ADCP array can be calculated using the depth (8 m) and the angle of the beams (20 degrees from vertical). This relationship indicates that the aperture will be 72.8% of the depth, which in 8 m water depth gives an aperture width of 5.8 m. The range data often fails to provide adequate directional resolution when the period of the waves exceeds 12 seconds. The wavelength λ of a 12 second wave, given by $\lambda = T\sqrt{\frac{g\lambda}{2\pi}\tanh(\frac{2\pi h}{\lambda})}$, with h =8 m, T=12 s is 102 m. Thus, adequate directional resolution is unlikely with range observations when the aperture becomes 6% or less of the wavelength, or similarly if the depth is less than about 8% of the wavelength. The range data generally provided a reasonable directional spread once the wave period was at or below 9 seconds with mixed results when the period was between 10-12 seconds. Therefore, a good estimate is that the range data is valid when the depth is equal to or greater than 11% of the wavelength.

An analysis of the directional error metrics indicates that the radial velocity measurements are the optimal ADCP data type to input into DPWP to achieve accurate and directionally constrained spectra. In addition, the IMLM method appears to outperform the EMEP method when utilizing either the radial velocity or the *p*-*u*-*v*-*w* data types, most notably in regard to directional spread. This assessment is verified by time series plots of the bulk statistics of the IMLM radial velocity spectra compared to the 8m array DPWP spectra (Figure 2.6). All four spectral statistics (significant wave height, peak period, mean direction and spread) of the IMLM radial velocity spectra compare

very closely to the 8m array spectra. The significant wave height is nearly identical, and always within the 95% confidence limits. The peak period is very similar except for the instances of bimodal seas as referenced earlier. The mean direction and spread are also very close, with the mean direction of the ADCP spectra tending to be slightly biased from the south and the spread being slightly less than the 8m array spectra. Although the EMEP processed radial velocity data and the IMLM *p*-*u*-*v*-*w* data also compare favorably to the 8m array spectra, the metrics and time series plots suggest that the IMLM radial velocity pairing is optimal and thus is the default processing option selected for the DPWP toolbox.

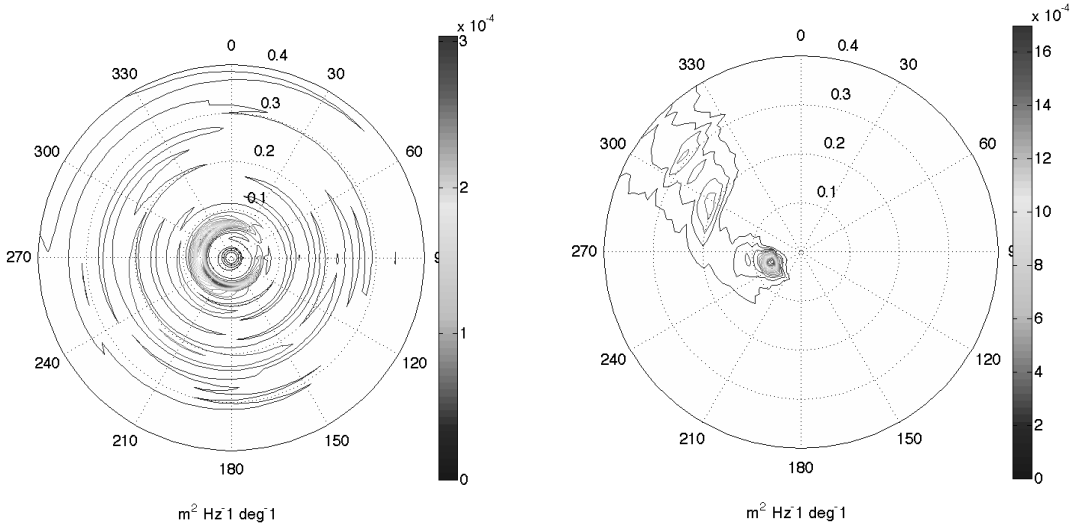

Figure 2.5 Plots of the 2-d directional spectra from a 34 minute record from the FRF ADCP in February 2007. Shown are polar plots of the ADCP range data (left) and the ADCP radial velocity data (right) via the DPWP IMLM. Radial coordinates are frequency in Hz.

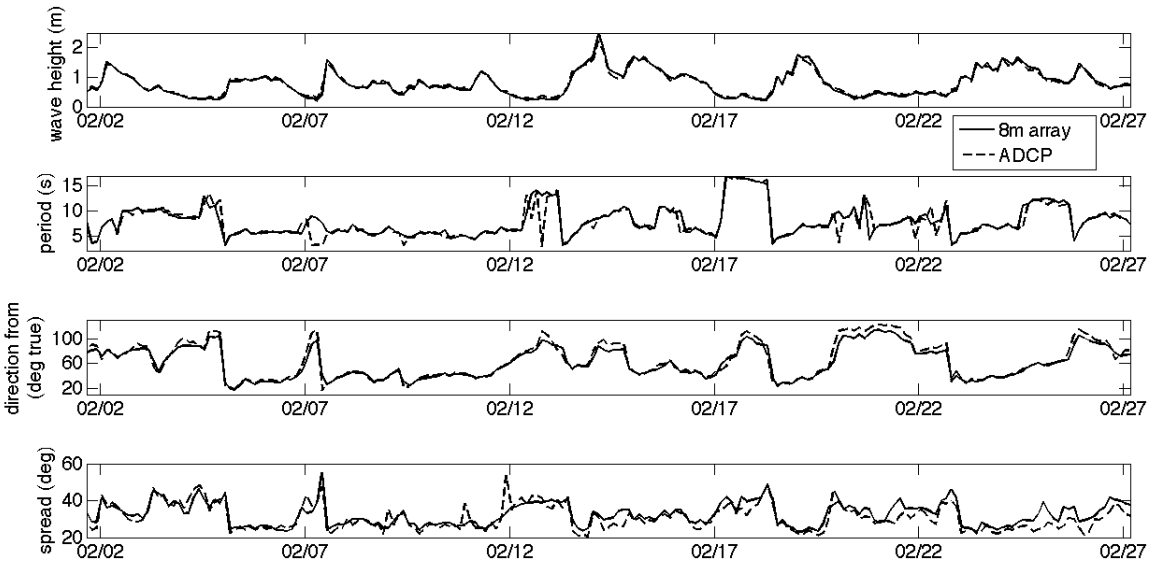

Figure 2.6 Time series plots showing a data comparison between the 8m array data processed by DPWP and co-located ADCP data processed by DPWP using the IMLM with radial velocity inputs. From top to bottom the plots are: significant wave height, peak period, mean direction and directional spread. The significant wave height for the 8m array and ADCP spectra are always within the 95% confidence limits of each other (not drawn due to clarity).

2.4 Extending the toolbox to the Nortek AWAC

To examine the applicability of the toolbox to the Nortek AWAC a test was performed at Bogue Pier located at Bogue Banks, NC. A Nortek AWAC was installed near a permanent ADCP for about 1 month beginning on 2 August 2007. The AWAC data was processed with both DPWP and the Nortek Quickwave software and a portion of the data was compared to spectra generated from the ADCP output.

The Nortek AWAC collects data for wave spectra in much the same way as the ADCP. The notable difference is that the AWAC uses three angled beams to collect radial velocity data, and one vertical beam used for a range-to-surface measurement or what Nortek refers to as Acoustic Surface Tracking (AST) (Nortek AS, 2004). The AWAC and ADCP configuration is documented in Table 2.1. The AWAC data is processed through DPWP using both the EMEP and IMLM estimation methods and using

the Nortek Quickwave software. For the comparison ADCP data is processed using the IMLM and radial velocity data. The first step of this analysis is to perform a statistical comparison of the AWAC data processed using the DPWP toolbox to the data processed through Nortek Quickwave. Then, the AWAC data processed through DPWP will be compared to the ADCP data processed through DPWP via the IMLM radial velocity options.

2.4.1 AWAC data processed through Nortek Quickwave and DPWP

The significant wave height, peak period and mean direction formed using the DPWP processing compares favorably with those formed using Nortek Quickwave processed spectra (Figure 2.7). The significant wave height measurements for DPWP and Quickwave are nearly identical and always within the 95% confidence limits. The peak period also compares well with the exception of a small number of instances where there are bimodal seas similar to those shown previously in ADCP spectra. The mean direction from the IMLM and EMEP methods visually compare closely with Quickwave, although the EMEP method shows slightly more deviation from the Quickwave data than the IMLM method. The directional spread displays the most variability between processing methods as the DPWP EMEP spread is greater than both the IMLM and Quickwave spread throughout almost the entire time period. The DPWP IMLM method generally has a tighter spread than Quickwave suggesting superior performance.

A statistical analysis confirms the visual assessment of close agreement between the data types with the exception of the directional spread. Using the Nortek Quickwave data as truth, the significant wave height measurements demonstrate negligible bias of

less than 0.01 m with an RMS error of 0.02 m and SI of 0.02. As expected, the bias, RMS error and SI values are all larger for the peak period due to the instances of a bimodal wave field with multiple spectral peaks similar in magnitude. For the 589 data points in this record, there are 25 instances of a bimodal wave field where the DPWP processing indicates a different peak than Quickwave. When these values are removed, the normalized RMS error and SI values of .80 and .79 respectively improve to 0.94 and 0.94 for DPWP compared to Quickwave.

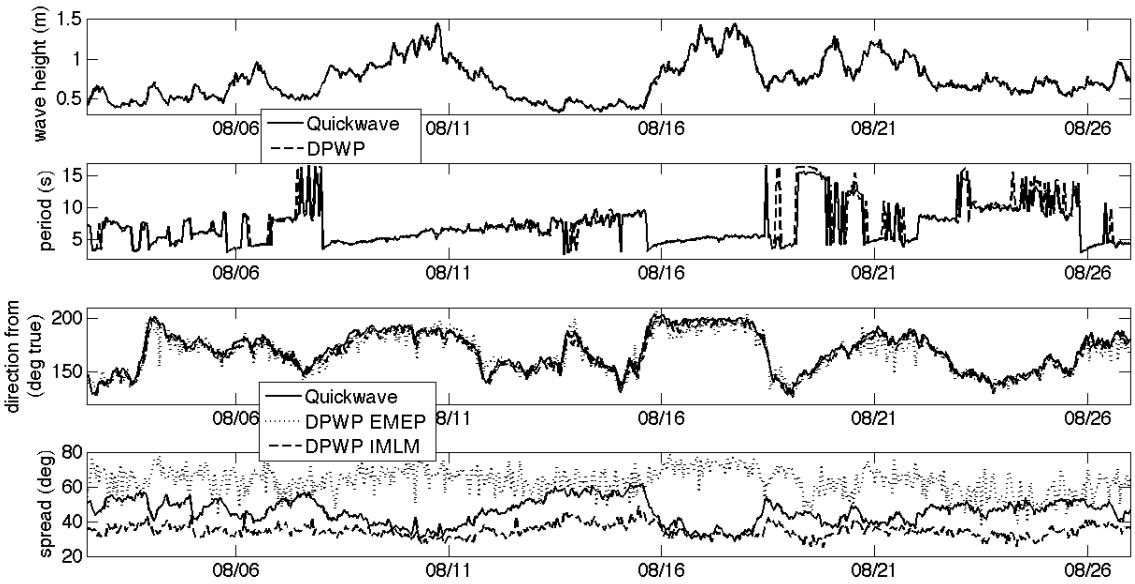

Figure 2.7 Time series plots showing a data comparison between the Nortek AWAC data processed by Quickwave and DPWP. From top to bottom the plots are: significant wave height, peak period, mean direction and directional spread. The significant wave height for the Quickwave spectra is always within the 95% confidence limits of the DPWP measurement (not drawn due to clarity).

The values of mean wave direction and directional spread for the EMEP and IMLM method are somewhat different. Similar to the ADCP comparison, the IMLM method appears to give a better indication of mean direction and directional spread with the AWAC data. The angular bias of -2.52 degrees for the IMLM is slightly better than

the -3.21 degrees calculated for the EMEP, and can be considered negligible due to the 4 degree directional resolution used by Quickwave. The circular correlation of 0.98 calculated for the IMLM is also slightly better than the value of 0.92 for the EMEP. Additionally, the directional spread measurements show the largest difference between the two methods as the IMLM is 11 degrees biased low (more constrained than Quickwave) while the EMEP is 17.6 degrees biased high (less constrained than Quickwave). These facts are also demonstrated in the plots of the individual spectra (Figure 2.8). The directional spectra generated through the IMLM method are generally more constrained directionally than that of the EMEP method.

The statistical analysis performed shows that both the EMEP and IMLM methods compare favorably to the Nortek Quickwave software. However, due to the improved directional spread of the IMLM method, we have chosen this method as the default for the AWAC.

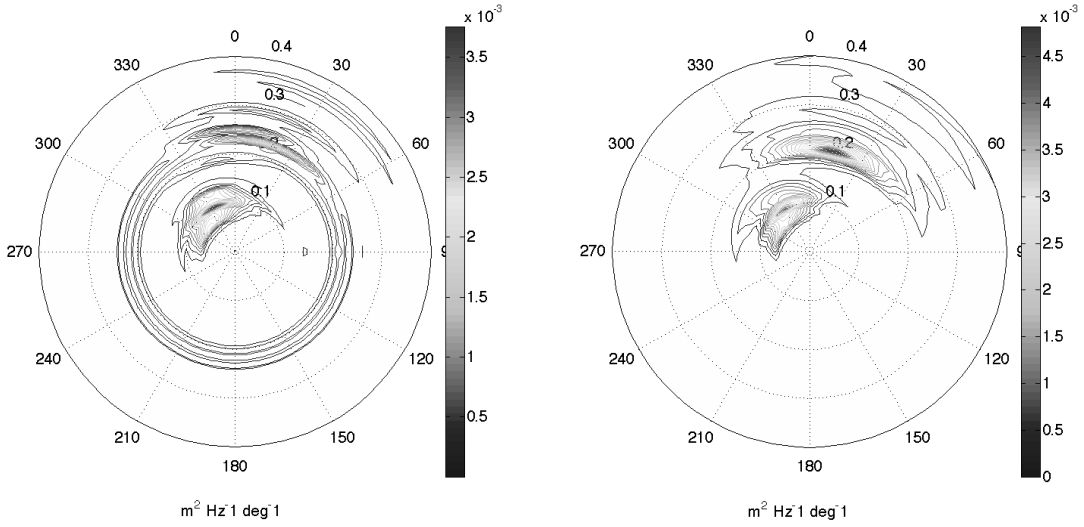

Figure 2.8 Plots of the 2-d directional spectra generated from a 17 minute AWAC record at Bogue Banks, NC in August 2007. Shown are polar plots from the DPWP EMEP method (left) and the DPWP IMLM method (right).

2.4.2 The AWAC vs. the ADCP

The close proximity of the AWAC to an ADCP at Bogue Pier made it desirable to compare the output spectra of each instrument given the settings and processing methods chosen previously in this paper. However, during the month deployment of the AWAC, a portion of the ADCP data is contaminated with bad data making it un-usable for a comparison. The reason for the abnormal amount of bad data during this month is unknown, but is likely related to lightning damage sustained at the shore-cabled installation. Still, there is enough good data in the record to allow for a reasonable comparison. For this comparison we have used approximately 3 days or 71 hours of data starting on August 16, 2007. When performing the statistical analysis, the AWAC data was chosen as the "truth" data, thus a positive metric indicates a positive deviation of the ADCP data from the AWAC data.

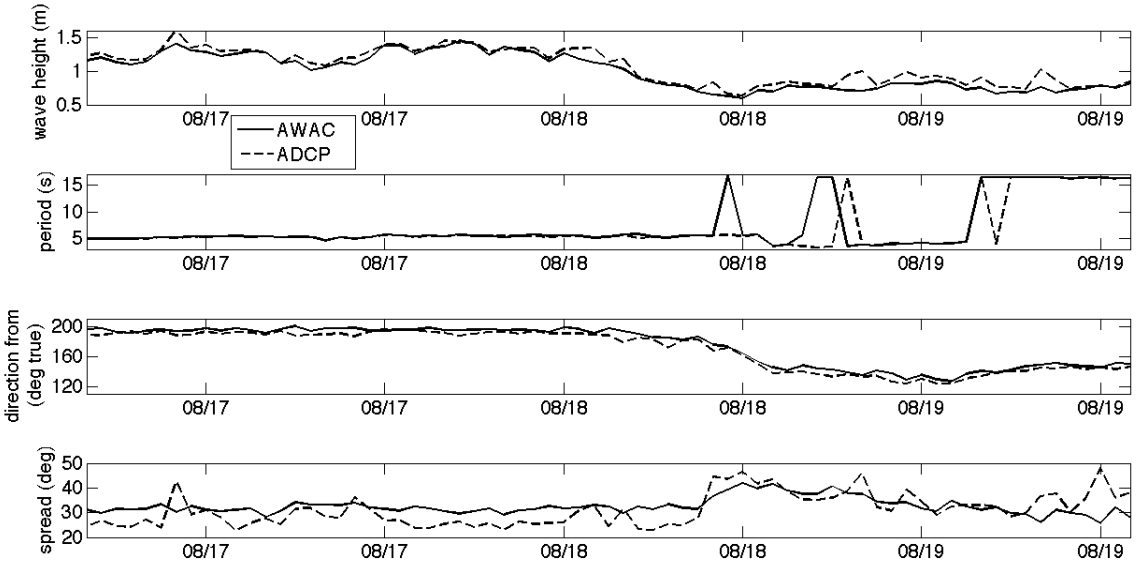

Figure 2.9 Time series plots showing a data comparison between the Nortek AWAC data and TRDI ADCP data processed via DPWP IMLM. From top to bottom the plots are: significant wave height, peak period, mean direction and directional spread. The significant wave height measurements from the AWAC and ADCP are always within the 95% confidence limits of each other (not drawn due to clarity).

A visual comparison of the significant wave height, peak period, mean direction and directional spread time series show that in general the spectra of both the AWAC and ADCP are very similar (Figure 2.9). The significant wave height is fairly close, however the bias is 0.07 m (Table 2.4). There is one time period that accounts for a portion of this bias on August 18 where the ADCP wave height is 0.29 m higher than the AWAC. This deviation represents an instance where a large number of bad data points create inaccuracies in the ADCP directional spectrum, however the measurements are still within the 95% confidence limits of each other. Despite this instance, normalized RMS error and SI values are high at 0.91 and 0.94 and compare favorably with the values calculated in the analyses of the prior data comparisons. The peak period plot clearly demonstrates an instance where there is a bimodal wave field causing differences in the spectral peak for each data type. When the six instances of this are removed from the statistical analysis, the normalized values of 0.99 for the bias and 0.98 for the RMS error and SI indicate that the ADCP and AWAC have nearly identical peak period measurements during this time period. Mean direction and directional spread also indicate a very close comparison. The bias of the mean direction is -4.88 degrees and circular correlation is 0.99, while the bias of the spread is only -1.42 degrees and the Normalized RMS error and SI values are 0.82 and 0.81 which are fairly high values for the spread compared to the previous analyses.

This comparison of the ADCP to the AWAC shows that the directional wave measurements collected by each instrument are very closely related. The significant wave height, peak period, mean direction and directional spread all compare well for

each instrument, giving confidence that either instrument can be used effectively with the DPWP software to provide quality directional spectral estimates.

Table 2.4 Frequency and Directional spectra error metrics resulting from the comparative statistical analysis of the Nortek AWAC and TRDI ADCP at Bogue Banks, NC.

	EMEP vs Nortek	**IMLM vs Nortek**	**Nortek IMLM vs ADCP IMLM**
Sig Wave Height			
bias	< 0.01		0.70
RMS error	0.02		0.10
SI	0.02		0.06
Norm bias	> 0.99		0.93
Norm RMS error	0.98		0.91
Norm SI	0.98		0.94
Peak Period			
bias	0.29		-0.58
RMS error	1.54		3.32
SI	0.21		0.49
Norm bias	0.96		0.93
Norm RMS error	0.80		0.61
Norm SI	0.79		0.51
Peak Period (with bi-modal points removed)			
bias	0.13		-0.04
RMS error	0.48		0.13
SI	0.06		0.02
Norm bias	0.98		> 0.99
Norm RMS error	0.94		0.98
Norm SI	0.94		0.98
Direction			
angular bias	-3.21	-2.52	-4.88
Norm angular b	0.98	0.99	0.97
Circular Correlation	0.92	0.98	> 0.99
Directional Spread			
bias	17.6	-11.01	-1.42
RMS error	21.48	12.41	5.99
SI	0.2	0.17	0.19
Norm bias	0.62	0.76	0.96
Norm RMS error	0.53	0.73	0.82
Norm SI	0.8	0.83	0.81

2.5 Discussion and Conclusions

Two intercomparison studies have been used to validate the ability of the DPWP toolbox to correctly process data from both Teledyne RDI ADCP and Nortek AWAC Doppler profilers and to determine the optimal data types and directional estimation methods to be used for the DPWP. Mean direction estimates using IMLM and EMEP are similar, however the IMLM method nearly always provides a directional spectrum with reduced directional spread. For this reason, the IMLM is the preferred method for the DPWP toolbox.

For 8m array data, the DPWP IMLM spectra and the FRF spectra are within 0.02 m RMS error for significant wave height, 0.4 seconds RMS error for peak period, and exhibit a correlation of 0.99 for the mean direction and an RMS error of 1.99 degrees for the directional spread. When using DPWP to process the ADCP data the radial velocity inputs with the IMLM estimation method produced results most consistent with the FRF 8m array spectra. The ADCP DPWP spectra and the 8m array spectra are within an RMS error of 0.07 m for significant wave height, within 0.5 seconds RMS error for peak period, and exhibit a correlation of 0.98 for the mean direction and an RMS error of 4.11 degrees for the spread. For each measurement, the bias was minimal. Additionally, the spectra generated with DPWP IMLM compared very favorably to Quickwave spectra when processing the Nortek AWAC data. In this case the RMS error was 0.02 m for significant wave height and under 0.5 seconds for peak period. The circular correlation was 0.98 for the mean direction and the bias of the directional spread was -11 degrees indicating DPWP generated more constrained directional spectra than Quickwave. For the significant wave height, peak period and mean direction bias was minimal.

Among the main benefits of DPWP is that the toolbox is operating system independent and that users have the ability to view and edit any of the processing steps. This enables the user to better understand the results obtained and to adjust options as needed for a particular type of location or wave environment. The advantages of this ability are most apparent in instances when the proprietary software packages provide poor or questionable results. Additionally, DPWP can utilize three different data sources from an ADCP or AWAC, which include the radial velocity data, pressure and *u*-*v*-*w* velocities and the range to surface measurements. Although the radial velocity data was chosen as the default option for DPWP, the flexibility to utilize the other data types can be invaluable in cases of poor or questionable data quality. Specific wave fields or locations may dictate when either the range data or the *p*-*u*-*v*-*w* will be preferred for spectral estimation of the wave field.

One factor that will influence the effectiveness of a particular measurement type is the instrument's depth. The range data was shown to be most effective for relatively short period (or wavelength) waves (< 12 s) when the ADCP was located at 8 m depth. It was estimated that the range data would be effective when the depth of the instrument is about 11% of the wavelength or less. The FRF wave data record shows that peak wave periods of swell waves rarely exceed 18 seconds at this location. Given this period, there will be a ratio of depth to wavelength of .11 when the wavelength is about 300 m and the depth is about 33 m. Thus, this would be roughly the minimum depth the ADCP should be placed in to directionally resolve the longest wavelength waves in this particular wave climate using range inputs.

Conversely, at this depth there will also be limitations on how well very short wavelength waves can be directionally resolved. At 33 m depth, the aperture of the range beams at the surface will be about 24 m. Thus, in theory, the minimum wavelength that would be resolvable would be 48 m, or a wave with about a 5.5 second period. Similar limitations will exist for both the *p-u-v-w* and radial velocity inputs, however since the aperture of the radial velocity bins will always be smaller than the range aperture (since the radial aperture reduces in size with bin depths closer to the transducer), using the radial inputs will allow for shorter period waves to be resolved directionally out to a greater depth. Although seemingly trivial, this analysis demonstrates how the depth and wave climate can influence the effectiveness of using a particular data type as the input into DPWP and also highlights a strength of the DPWP toolbox: the ability to choose the data input(s) that are most desirable for a given deployment.

This flexibility is further enhanced by instances when an ADCP may lack a pressure sensor. The TRDI Wavesmon software does not support waves measurements for this type of instrument configuration, yet DPWP can be easily configured to process radial velocity data if the sampling rate is sufficient. Similarly, since the code is open-source, end users could adjust DPWP to support additional Doppler Profiler configurations or to calculate the directional spectra using alternative methods similar to those developed by Hoitink et al. (2007) or Herbers and Lentz (2010).

Although confidence intervals are calculated for all frequency spectra and significant wave height measurements, the challenge of replicating this in the directional spectra still remains. It is worth noting that neither Wavesmon nor Quickwave inherently includes a calculation of the spectral error in either frequency or direction, hence the

confidence intervals formed within DWDP are a step towards quantifying wave statistic errors. A visual comparison of the directional spectra generated with DPWP with those of Wavesmon and Quickwave suggest the approaches yield similar results. A comparison of the spectral properties such as mean direction and directional spread has shown that spectra generated through DPWP compare closely to the proprietary software in most instances. Despite this, a quantitative measure of directional spectral accuracy needs to be developed.

The toolbox will benefit from being thoroughly tested under different environmental conditions such as increased water depth. The aperture size has a significant effect on the quality of the spectra, especially when using range data. A study in deeper water (20m or greater) to evaluate the performance of DPWP and determine any weaknesses that may exist under these conditions would be appropriate. We also envision that the toolbox will eventually be coded entirely in Python to maximize its portability and utility in a variety of configurations. Pursuit of these objectives can result in a reliable, open-source alternative to processing directional wave data from Doppler profilers that should benefit the community as a whole.

CHAPTER 3

AN ANALYSIS OF RIP CURRENT RESCUES AT KILL DEVIL HILLS, NORTH CAROLINA[1]

3.1 Introduction

According to the U.S. Lifesaving Association, rip currents are the number one cause for rescues and loss of life at the beach each year in the United States. In 2007 alone, 40,810 of the 74,463 rescues reported at US beaches were rip related. Similarly, from a reported 109 drownings, 53 were rip related (www.usla.org). The status as the number one beach safety hazard has garnered rip currents significant attention in the scientific research community. There has been a plethora of rip current related research over the past decade focusing on a variety of topics including observations of entire rip systems (MacMahan et al., 2005), rip current morphodynamics (Brander, 1999; Brander and Short, 2000; Calvete et al., 2005), rip current modeling (Garnier et al., 2008; Johnson and Pattiaratchi, 2006; Svendsen et al., 2000), surf zone bar behavior (van Enckevort and Ruessink, 2003; vanEnckevort et al., 2004) and the relationship of rip currents with variability in the local wave field (Johnson and Pattiaratchi, 2004; MacMahan et al., 2004).

Despite the increase in rip current research, there has been little investigation of the large scale alongshore (> 1km) and temporal (> 1 month) variability of rip current activity. The likely reason for this research void is the difficulty in obtaining accurate observations of rip currents over large scales in time and space due to the complexity and cost of instrument deployment. As an alternative to instrument collected observations, it is possible to use lifeguard rescue data as a relative indicator of hazardous rip current occurrence (Lushine, 1991; Lascody, 1998; Engle et al., 2002; Scott et al., 2007; Scott et al., 2009). This study utilizes a data set of 741 rip current rescues recorded at Kill Devil Hills, NC. Each rescue is identified in both time and alongshore location, which provides a unique opportunity to analyze the large scale variability in rip current activity. Concurrent with the rescue data, directional wave data, tidal height and weather observations have been collected at the nearby Army Corps of Engineers Field Research Facility in Duck, NC. Additionally, cross-shore bathymetry profiles were collected along the length of Kill Devil Hills in 2008 and 2009. This paper focuses on a statistical analysis in which rip current rescues are correlated with tidal elevation and the directional wave spectra to determine what factors most influence periods of increased hazardous rip current activity. Furthermore, analyses are performed to determine what factors influence variability in rip current activity both temporally and alongshore. This paper is organized as follows. First, background information is provided along with previous research utilizing rip rescues, and the field site located at Kill Devil Hills, NC is described. Next, the research methods used in the data analysis are introduced, followed by a presentation of the results of the wave spectral analysis, temporal variability in rip

current rescues and alongshore variability in rip current rescues. In the final two sections, the discussion and summary are presented.

3.2 Research Utilizing Rip Rescues

There have been multiple studies performed using lifeguard rescue or drowning data as a proxy for rip current occurrence. The three studies discussed in more detail below all focus on predicting rip current occurrence through a statistical analysis of rip current rescues with other physical factors. Lushine (1991) was the first to attempt rip prediction when he analyzed the relationship of rip drownings in southeast Florida to a variety of meteorological and oceanographic data. Lushine determined that rip current drownings were correlated with increasing wind speed, shore-normal wind direction, increasing wave height and low tide. He used his results to aid in the creation of an empirical rip current forecasting or prediction index called LURCS (LUshine Rip Current Scale), in which various inputs (wind speed and direction, wave height, tide) were assigned a numerical value and added together resulting in a rip current risk assessment. For example, 15 kt onshore winds, a 3 ft wave height and low tide would result in a category 5 risk, or a high likelihood for strong rip currents. Lascody (1998) performed a similar analysis as Lushine, but in east central Florida and with rip current lifeguard rescues instead of drownings, thus providing a much larger data set. In addition to re-affirming that rip currents were correlated to the wave height, low tide, wind speed and wind direction, Lascody found that wave period was also a factor and that rip currents were more likely during instances of long period swell (> 12 s). Lascody formulated the ECFL (east central Florida) LURCS index, which followed a similar method as Lushine's

LURCS, but with the addition of swell period as a factor. Four years later, Engle et al. (2002) performed additional analysis of lifeguard rescue data in east central Florida and made further changes to the ECFL LURCS index. Engle et al. found that wind speed and direction were not an important factor in determining rip current likelihood, but rather that the wave field (peak period, peak direction and height) and the tide were the most accurate indicators of hazardous rip activity. Thus, a modified ECFL LURCS index utilizing these factors was created and successfully back tested. The modified ECFL LURCS index (or a slight variation) is the rip current forecasting method predominantly used today by National Weather Service Weather Forecast Offices (WFOs; Pers. Comm. – WFO Morehead City / Newport).

The statistical relationship between the tide, the wave field and rip current activity seen in the studies utilizing rip rescues has a physical basis identified in observational and numerical model studies. Previous observational studies (e.g. Brander and Short, 2000; MacMahan et al., 2005) have determined that rip current intensity and activity is highest at low tide. This increase is due to increased breaking over the surf zone bar at low water leading to increased alongshore radiation stress gradients, as well as greater current speeds as water is forced through rip channels due to decreased water depth over the bar. Numerous observational studies find increasing rip current velocity with increasing wave height (Brander, 1999; Brander and Short, 2000; MacMahan et al., 2005), reflecting increased set-up and increased radiation stress gradients alongshore. Additionally, it is generally accepted that shore-normal wave incidence will lead to greater rip current activity (MacMahan et al., 2005), in that highly oblique waves will tend to drive stronger longshore currents that can suppress rip current formation (Svendsen et al., 2000).

However, there has been relatively little observational research or numerical model research (Svendsen et al., 2000) demonstrating how rip activity will vary with wave direction. Although some statistical analyses utilizing rip rescues have shown that there is an increase in rip current activity with relatively long wave periods (Engle et al., 2002; Lascody, 1998; Scott et al., 2009), the relationship between rip activity and wave period is otherwise relatively unaddressed in the literature.

3.3 Field Site

This study was performed at Kill Devil Hills, NC, a 7.5 km stretch of beach located on the northern Outer Banks of eastern North Carolina (Figure 3.1). The shoreline at the study site is generally straight and it faces to the east-northeast with a shore-normal direction of 63 ($\pm$ 2) degrees true. The beaches of the northern Outer Banks are generally characterized by a relatively steep foreshore (1:10) and more gradual slope offshore (1:500) and the existence of shore-parallel bars (Schupp et al., 2006). The nearshore is often double-barred, one bar in the surf zone (1-2 m depth) and an outer storm bar (~4.5 m depth) (www.frf.usace.army.mil) although depending on the location alongshore and time of year there can be one or no significant bars. The mean annual significant wave height is 0.9 m (McNinch, 2004), however the wave climate is variable throughout the year. The climate in the summer months, based on the observations used in this study, generally consists of a low energy swell of 0.4 to 0.6 m significant wave height (Hs) out of the southeast punctuated by storm events (1.0 to 3.0 m Hs), predominantly from the northeast. The tides are semi-diurnal and classified as microtidal as the mean range is 0.97 m (Birkemeier et al., 1985).

Figure 3.1 The study location at Kill Devil Hills, NC. The points show the location of the 18 lifeguard chairs. Points with a black dot mark locations where surf zone bathymetry was monitored in 2008 and 2009. The black cross-shore line indicates the break between the northern nine chairs and the southern nine chairs.

Kill Devil Hills (KDH) was chosen as the study site primarily due to the availability of the nine summers of rescue data and the willingness of Kill Devil Hills Ocean Rescue to aid in the research. KDH Ocean Rescue occupies 18-19 lifeguard stands located between 200-800m apart along KDH beach. The stands are occupied from 10am to 5:30pm, seven days a week from late May until early September each summer.

Dating back to the summer of 2001 there is a complete record of every lifeguard rescue made over the course of each summer. For each rescue made at the beach there is a record indicating the type of rescue as well as the time and location along the beach of the rescue (to the nearest lifeguard chair). Over the course of the nine summers of data collected, there were 741 rescues classified as rip current related.

3.4 Methods

3.4.1 Data collection

This study is performed under the assumption that for a rip current rescue to occur there must be a hazardous rip current present at that particular location and time. In this case, hazardous is defined as a rip current of sufficient strength to cause a swimmer distress. It is important to note that little can be inferred from instances when no rescues were made. The fact that no rescues were made does not mean there were no rip currents present. To the contrary, days of large surf conditions are likely to have rip currents, although these instances rarely have rescues because most people won't go into the water or beaches may be closed to swimming. Similarly, stormy weather and cold water temperatures keep swimmers out of the water and these days will be poorly represented in the rescue record.

Directional wave data, tidal heights and bathymetry data have been collected for correlation with the rescue data. Directional wave data were collected from a Waverider buoy maintained by the US Army Corps of Engineers Field Research Facility (FRF). The buoy is located 15 km to the north of the study site at 17 m depth and sampled hourly throughout the data period. During some time periods, back-up wave data were available

from an FRF maintained Teledyne RD Instruments ADCP (Acoustic Doppler Current Profiler) located at the northern extent of the study area at 12 m depth. These data were only used as a reference and not included in any of the statistical analysis due to the lack of a complete data record. Predominantly the data from the ADCP was used to supplement the significant wave height time series from 2006 since there were missing Waverider data from that summer. Tidal heights were observed from the pier located at the FRF onshore of the Waverider buoy.

Bathymetry data have been collected at KDH in the surf zone and in the outer nearshore, where the surf zone is defined as the region from the beach seaward to just beyond the extent of breaking waves (~ 2 m depth) and the outer nearshore is the region beginning just outside of the surf zone and extending 2-3 km offshore. Surf zone bathymetry data consist of profile lines at seven different locations along KDH. Each profile line begins at a location slightly seaward of the dune line and transects at a shore-normal direction to about 2 m depth. The profile lines were re-occupied a number of times over the summer. Each line began at the same location and followed the same transect as closely as possible. In 2008 data were collected along each profile line five times during the summer via a level and level rod at seven different lifeguard chair locations. At each location one transect was performed. In 2009, bathymetry data were collected on four separate instances using a Trimble RTK GPS system at the same seven locations as in 2008. While using the GPS system, two profile lines were surveyed, 50 m apart, at each location. The vertical accuracy for the level and level rod is dependent on the distance from the level with the upper extent of the error at near 10 cm. The vertical accuracy of the RTK GPS system has a maximum error of 5 cm. Bathymetry data

collected in the outer nearshore region consist of a swath bathymetry survey performed by the FRF in 2006. These data are considered to be a reasonable estimate of the bathymetry over the study time period as the region's large-scale morphological features demonstrate relatively little short-term temporal variability (Schupp et al., 2006).

3.4.2 Statistical analysis

Directional wave data

Data from the Waverider buoy are radio-telemetered to shore on a continuous basis. Spectral coefficients are computed onboard the buoy using the Fourier coefficient method (Longuet-Higgins et al., 1963) from contiguous 30-minute records sampled at 1.28 Hz. The Iterative Maximum Likelihood Method (IMLM; Pawka, 1983) method is used to convert these observations to two-dimensional (2d) directional wave spectra. The significant wave height, peak period and peak wave direction is then calculated from the 2d wave spectra. Additional processing is performed on the wave spectra by the MATLAB® toolbox XWaves (www.WaveForceTechnologies.com). XWaves partitions the 2d directional wave spectra into individual spectral components through identification of spectral peaks and breaks by treating the spectra as an inverted topographic domain and applying a watershed delineation transform. For a complete description see Hanson and Phillips (2001), Hanson et al. (2009) and Tracy et al. (2006). The classification of each component (e.g. wind sea or swell) is determined by the frequency and direction of each component relative to the local wind speed and direction. User options selected within XWaves determine how many spectral partitions are identified and how they are classified. For the Waverider wave data, a maximum of three partitions were allowed

(wind sea, dominant swell, secondary swell) and a minimum significant wave height of 0.2 m was required to identify a component. The significant wave height, peak period, mean wave direction and directional spread were then calculated for each wave component.

Rescue data analysis

In prior studies utilizing rip current rescues to determine rip occurrence (Lushine, 1991; Lascody, 1998; Engle et al., 2002), histograms were used to compare overall conditions to conditions when rip rescues occurred. That same method of analysis is followed here with some adjustments and with further quantification of results.

For each data type, distributions are formed of the entire data record and of the rip rescue record. The entire data record consists of the observations made every hour from late May until early September from 2001-2009. The rip rescue record consists of observations made during rip rescues, and if multiple rescues were made in an hour those instances were counted accordingly (e.g. if three rescues occurred at 1 pm when the significant wave height was 1 m, then that 1 m wave height was counted three times in the rip rescue distribution). It is important to note that the entire data record includes both daylight and evening hours, while the rescue record is by its nature only daylight hours since no lifeguards are on the beach in the evening. Although wind sea can vary between daytime and evening hours due to the sea breeze / land breeze cycle, this variability was found to be slight when compiling the data for all nine summers and did not significantly alter the interpretation of the results. Thus, to maintain data consistency

and to utilize as much of the data record as possible, both daylight and evening hours are included in the data analysis presented.

For visual analysis each distribution is plotted as a normalized histogram. If a particular physical property (e.g. peak period) has no impact on rip current activity it would be expected that the histogram representing the rip rescue distribution would be similar to the entire data record distribution. Any significant deviation suggests that property has some impact on rip occurrence. Additionally, where the deviation between histograms occurs suggests how that physical property impacts rip occurrence. Since rip current activity is often dependent on multiple wave spectral properties, and since wave direction, height and period are often correlated, contour plots have also been created to visually represent and compare two-dimensional distributions of the data.

To test for significant differences between the entire data distribution and the rip rescue record distribution for each data type, the Kolmogorov-Smirnov statistical test (KS-test) has been applied. The KS-test, when applied to two empirical non-parametric distributions, can determine at a particular confidence level or p-value, if two distributions are from the same underlying distribution (Conover, 1999). The KS-test can be displayed graphically as confidence limits on two side-by-side cumulative distribution functions (CDF) (Figure 3.2). In this case, the sample distribution for each CDF can be said to represent the ensemble CDF within the confidence bounds with an X % certainty (99% as shown). If the confidence limits of the two distributions do not everywhere intersect we can say within that level of certainty that the distributions are different. The

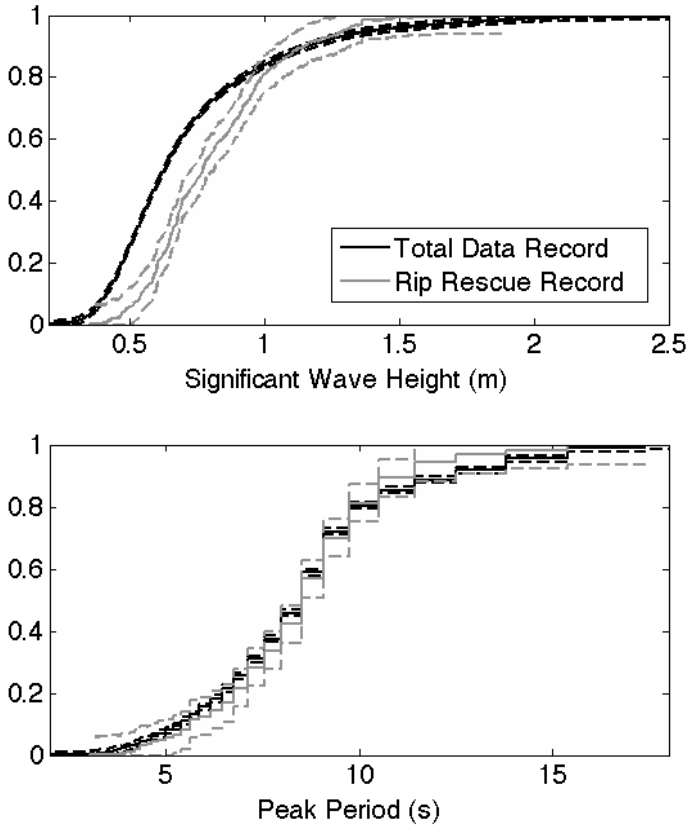

Figure 3.2 The cumulative distribution functions for significant wave height (top) and peak period (bottom) with both the entire data record (black line) and rip rescue record (grey line) shown. The 99% confidence intervals (dashed) are shown for each distribution.

test can also be shown numerically via the two-sample KS-test. In this case the test will result in a minimum p-value, or maximum confidence level (100x(1-p)) for which the two distributions can be said to be different (Table 3.1). This method allows for the variability of the distributions to be characterized with more detail and goes beyond a pass-fail for a set confidence level. For example, a KS-test with a p-value of .03 and one with a p-value of $3x10^{-20}$ would both be said to be different at a p-value of .05 or the 95% confidence level, however the test resulting in the much smaller p-value can be said to be

Table 3.1 The p-values for the two sample KS-test between the rip rescue record and the entire data record for the named variable

Measurement	**p-value**
Tidal Elevation	3×10^{-33}
Entire 2d Spectrum	
Significant Wave Height	3×10^{-53}
Peak Period	0.021
Peak Direction	5×10^{-57}
One Swell	
Significant Wave Height	9×10^{-45}
Peak Period	0.003
Mean Direction	6×10^{-83}
Directional Spread	4×10^{-22}
Two Swells (Dominant)	
Significant Wave Height	2×10^{-10}
Peak Period	0.052
Mean Direction	3×10^{-17}
Directional Spread	2×10^{-5}
Two Swells (Secondary)	
Significant Wave Height	8×10^{-10}
Peak Period	9×10^{-6}
Mean Direction	0.002
Mean Direction (> 7s PP)	2×10^{-6}
Directional Spread	2×10^{-6}
Wind Sea	
Significant Wave Height	0.030
Peak Period	0.078
Mean Direction	5×10^{-10}
Directional Spread	0.099

different with significantly more certainty (18 orders of magnitude). This information would be lost with just a pass-fail measure of confidence.

3.5 Results

3.5.1 Influence of tidal elevation and the wave field on rip current activity

Tidal elevation

A comparison of the distributions from the KDH study shows evidence of increased rip activity at low tide levels (Figure 3.3). This result corresponds well to previous observational (Brander and Short, 2000; MacMahan et al., 2005) and statistical studies (Engle et al., 2002; Lascody, 1998; Lushine, 1991). For tidal elevations of 0 m National Geodetic Vertical Datum (NGVD) and below, 58% of all rip rescues occurred, while only 36% of the entire data record was in this range (Table 3.2). Additionally, the p-value of the KS-test is $3x10^{-33}$ essentially assuring that the two distributions are different (Table 3.1).

Bulk measurements of the wave field

Previous research has shown that rip activity increases with increasing wave height and as wave direction is close to shore-normal (e.g. Engle et al., 2002; MacMahan et al., 2005; Svendsen et al., 2000). The histograms of significant wave height and peak direction from the KDH data set agree with previous research (Figure 3.4). Between significant wave heights of 0.6 m and 1.4 m there is a substantial increase in rip current rescues when compared to the entire data record (Table 3.2). This result suggests a

strong relationship between wave height and hazardous rip current activity. At wave heights greater than 1.5 m there is a slight decrease in the number of rescues, which can

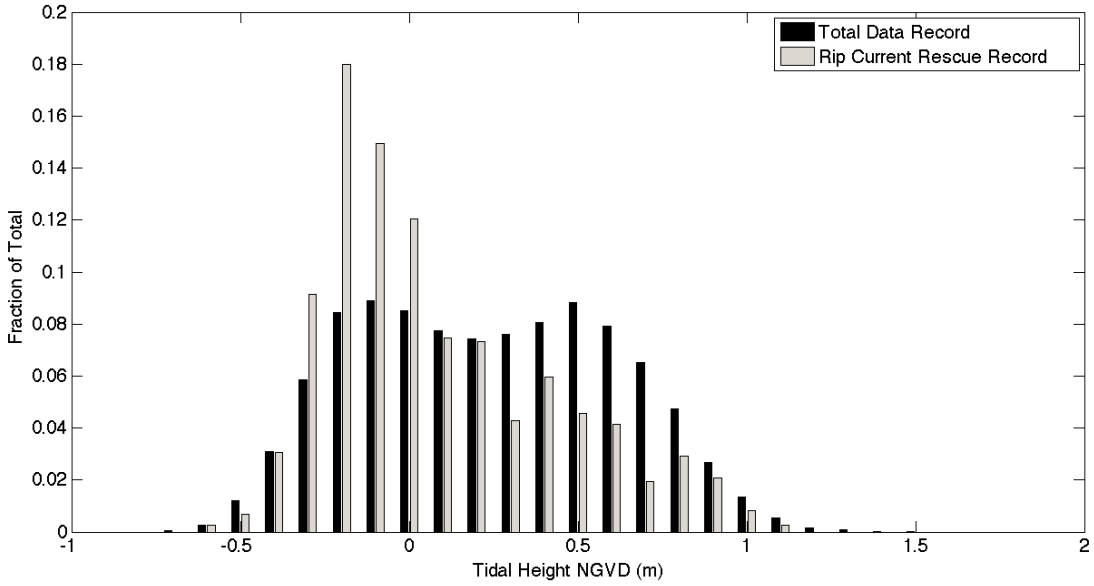

Figure 3.3 Distributions of the tidal height for the entire data record (black) and rip current rescue record (grey) represented as normalized histograms.

Table 3.2 The percent of occurrence of various factors in the rip rescue record compared to the entire record

Measurement	Rip Record	Entire Record
Water level (< 0 m NGVD)	58%	36%
Bulk Spectral Statistics		
Significant wave height (.6 m < Hs < 1.4 m)	79%	49%
Peak dir within 25 deg of shore-normal	58%	30%
Partitioned Spectra		
Only 1 or 2 swells present	77.2%	64.9%
Wind sea present	22.8%	35.1%
Event Related Rescues		
72 hours following northerly event	40%	19%

be attributed to adverse surf conditions and people unwilling or unable to go into the water. The difference between the two distributions is almost certainly significant as the

p-value is only 3 x 10^{-53} (Table 3.1). The histogram of the peak direction shows that a majority of the wave energy arrives out of the southeast (> 25 degrees south of shore-normal) during the summer months, while a majority of rescues (58%) occur when the peak direction is within 25 degrees of shore-normal (Table 3.2). The p-value of 3 x 10^{-57} assures that the two distributions are different within a very high level of confidence. The histogram of peak period shows less variability between the two distributions as there is a maximum difference of only 4.9% at a period of 11 seconds. Contrary to previous research, this suggests that period may not be an important factor when determining rip current activity at KDH. Additionally, the KS-test resulted in a p-value of .021, which provides relatively low certainty that the two distributions are different.

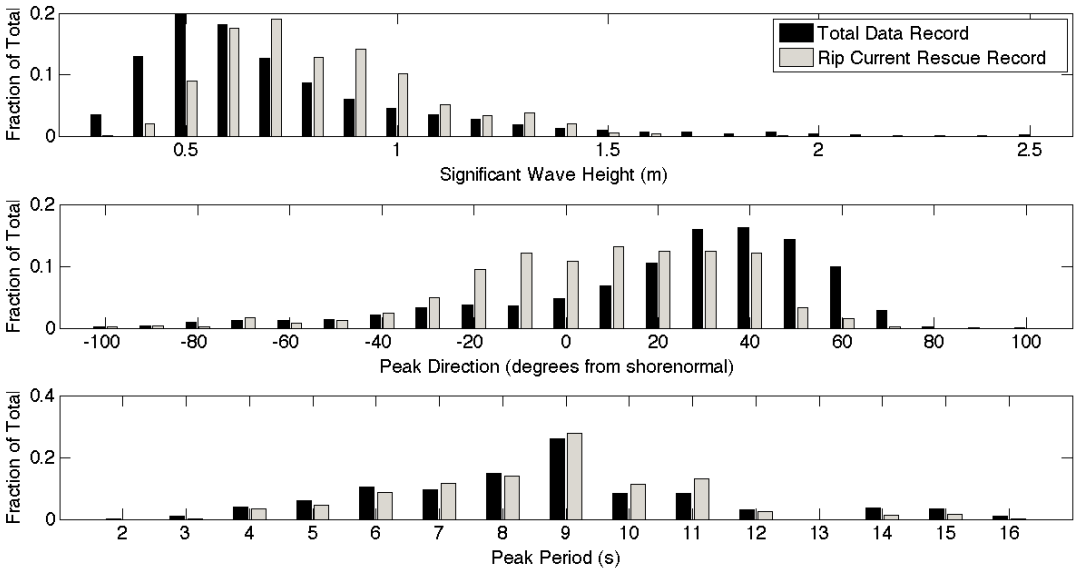

Figure 3.4 Distributions of the significant wave height (top), peak direction (middle) and the peak period (bottom) for both the entire data record (black) and rip rescue record (grey). In each plot the distributions are shown as normalized histograms.

The partitioned wave spectrum

Once the wave spectral data are partitioned into individual components, there is evidence that some components may play a larger role than others in hazardous rip current activity. Instances of either one or two swells and no measureable wind sea occurs 64.9% of the time for the entire data record, but occurs 77.2% of the time for the rip current rescue record. Conversely, a wind sea is present 35.1% of the time in the entire record but is present only 22.8% of the time in the rip rescue record (Table 3.2). Although a lack of rescues does not necessarily indicate a lack of rip current activity, this disparity suggests that hazardous rip currents are more likely to occur during swell dominated periods and not as likely when wind sea is more significant. The p-values corresponding to the wind sea significant wave height and period are relatively large (Table 3.1), which provides additional evidence that for the wind sea component the rip rescue distributions are relatively similar to the distributions for the entire data record. The p-value for the distributions of the wind sea mean direction is much smaller which nearly assures that the directional distributions are different. This may be because wind sea can have potentially large oblique angles of incidence, which can be unfavorable for rip current development (MacMahan et al., 2006). Thus, the presence of wind sea at oblique angles may tend to suppress rip current activity due to the increased likelihood of a stronger alongshore current. This may further explain why fewer rescues occur when wind sea is present in the wave field.

Analysis of the swell components provides additional insight into potential wave field mechanisms for increased rip current activity. When only a single swell is present, hazardous rip currents are more likely to occur with higher significant wave heights and

when the mean direction is closer to shore-normal (Figure 3.5). A wave vector time series from 2008 provides an example of increased rip current activity due to shore-normal single-swell conditions (Figure 3.6). In addition, the p-values for each statistic are extremely small (Table 3.1) which affirms that the rip rescue distribution is different than the entire data set distribution at a confidence level well over 99%. This result correlates well with the analysis of the bulk spectral measurements. Similarities between the distributions of the single swell measurements and bulk spectral measurements are expected since in every instance when there is just a single swell, the properties of the single swell component will be the same as the properties of the total spectrum.

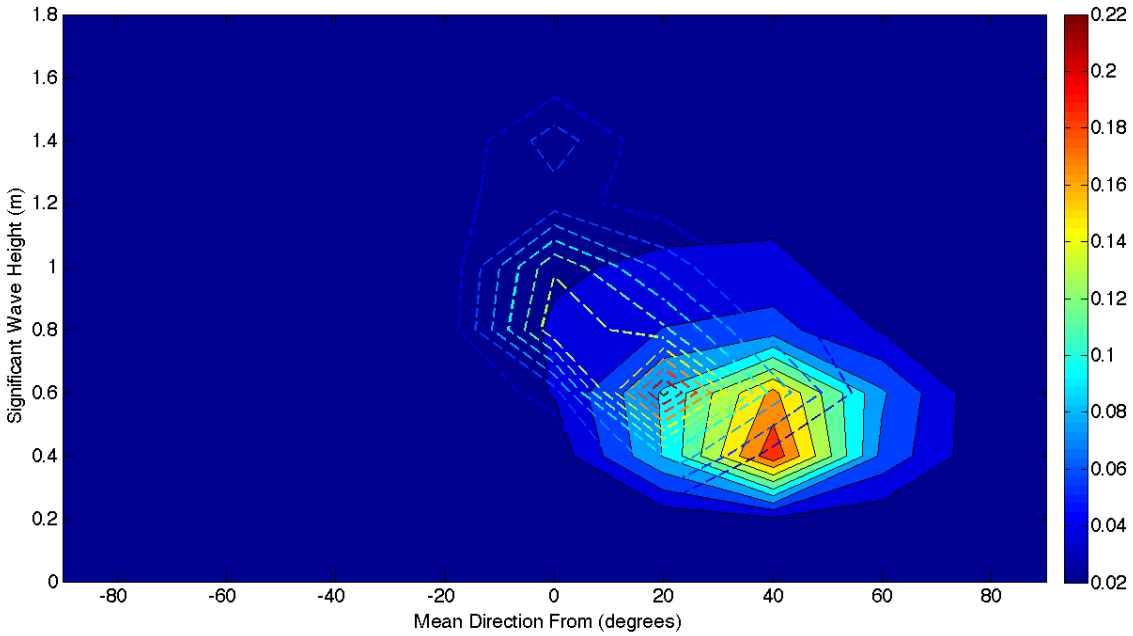

Figure 3.5 Contour plots showing the bivariate distribution of significant wave height and mean direction of the swell when only this partition is present for the entire data record (solid) and rip rescue record (dashed). A mean direction from 0 represents shore-normal incidence where negative degrees is north of shore-normal and positive degrees is south of shore-normal. Contour values are the fraction of the total for each distribution.

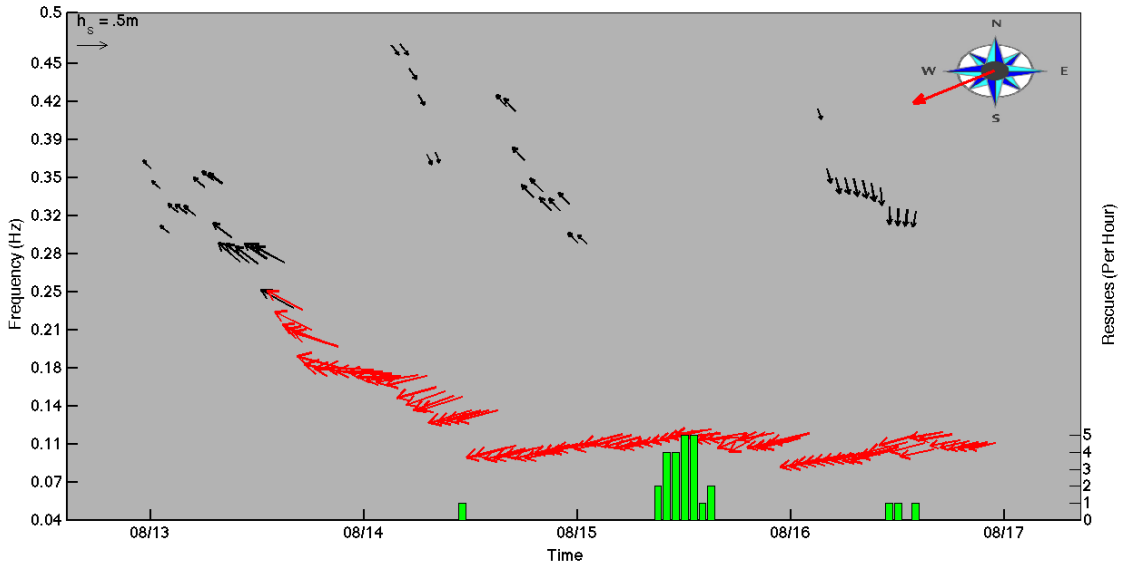

Figure 3.6 A wave vector plot over four days in 2008 showing an example of a single-swell shore-normal wave field leading to increased rip current activity. Each vector represents the frequency (vector origin), significant wave height (vector length) and wave direction (vector azimuth) of a spectral component for each hour. In this case light shaded vectors represent swell and the dark vectors represent wind sea. A vector length equating to 0.5 m Hs is shown in the upper left and the direction of shore-normal is shown by the arrow on the compass rose in the upper right. The right y-axis shows the number of rip rescues per hour, which are displayed as bars on the bottom of the plot.

The directional spread of each swell component may also be a contributing factor to increased rip current activity. There is a noticeable increase in the relative number of rip rescues as the directional spread of the dominant swell decreases (Figure 3.7), and the very small p-value confirms that the distributions are different in this instance (Table 3.1). This increase in rescues is at least in part due to the relatively higher significant wave heights associated with smaller spread values (Figure 3.8). Despite this fact, the contour plots of the distributions suggest that the smaller spread plays at least a partial role in the increase in rescues. In the instances of multiple swells, rescues also increase

with decreasing directional spread of each component, and this relationship appears to be of significant importance in this case as well (Table 3.1).

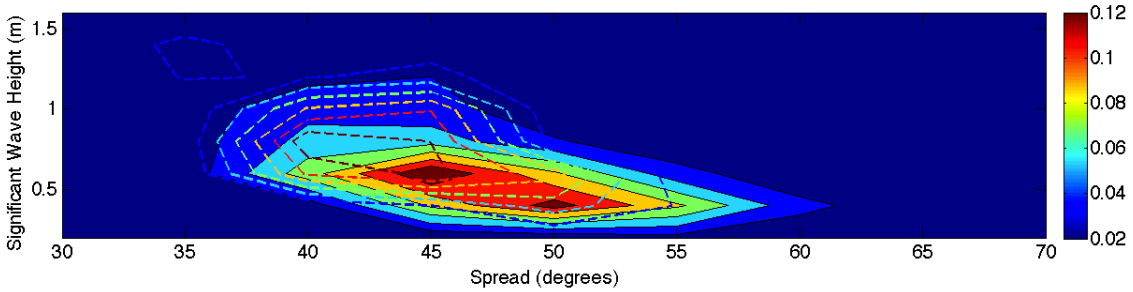

Figure 3.7 The bivariate distribution of directional spread and significant wave height of the dominant swell for the entire data record (solid) and rip rescue record (dashed). Contour values are the fraction of total for each distribution.

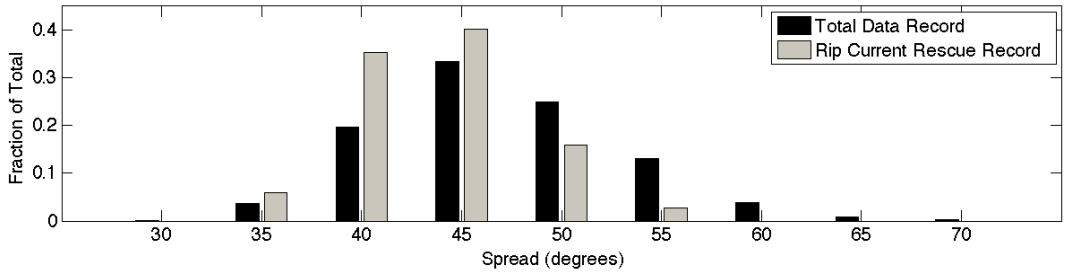

Figure 3.8 The normalized histograms representing the distribution of the directional spread for the entire data record (black) and the rip rescue record (grey) of the dominant swell.

For instances with two swells the distribution of the rip rescue data looks quite different than the entire data distribution (Figure 3.9). In the case of the dominant swell the p-values for Hs and mean direction are extremely low (Table 3.1) indicating high levels of confidence that the rip rescue distributions are different than the entire data distributions. For the secondary swell the p-value for the significant wave height is very small (8×10^{-10}), but the p-value for the mean direction, while small, is relatively larger at 0.002. This is due to the secondary swell consisting of two different sources: long period

swell from the southeast and short period swell, often from the northeast and with very small significant wave height, resulting from local wind sea that is no longer wind forced. Once the short period secondary swell (< 7 s) is removed the p-value decreases by three orders of magnitude (Table 3.1).

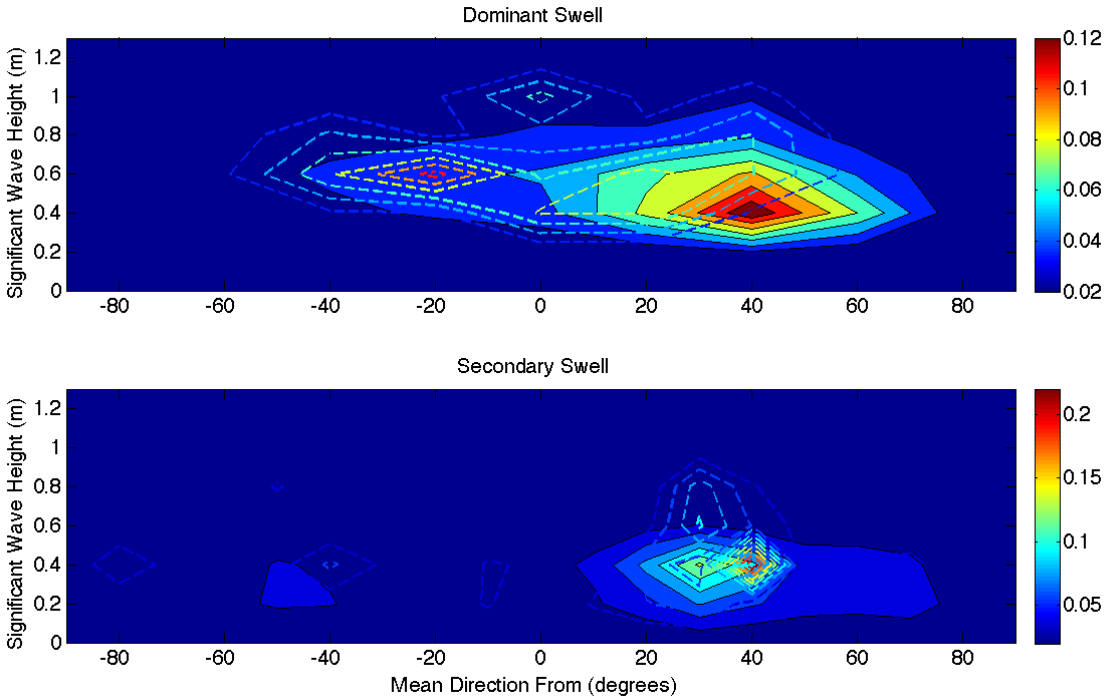

Figure 3.9 The top contour plot shows the bivariate distribution of significant wave height and mean direction for the dominant swell component. The bottom contour represents the secondary swell component. In both cases the entire data record (solid) and rip rescue record (dashed) are shown and for the mean direction 0 represents shore-normal. This data is only for times when two swells are present and with no measureable wind sea.

The mean direction distributions of the rip rescue record for the instances of two swells are very different from the mean direction distributions of the rip rescue record when only one swell is present. For the two swell case the rip rescue distribution for the dominant swell is shifted towards more northerly directions and increased wave height, while the rip rescue distribution for the secondary swell is shifted towards more southerly

directions and increased wave heights (Figure 3.9). The directional differences imply that rip activity increases when the dominant and secondary swells arrive at oblique angles with a large directional difference between them. A histogram of the swell direction difference confirms this, as there is a large increase in rip rescues when the difference of direction is between 60 and 100 degrees (Figure 3.10). This result suggests that a bi-directional spectrum, representing crossing wave trains may be a mechanism for rip current generation and an example of this can be seen clearly from a wave vector plot from 2004 (Figure 3.11). This possibility has been hypothesized (Dalrymple, 1979; Kennedy, 2005) and realized in numerical model (Johnson and Pattiaratchi, 2006) and lab studies (Fowler and Dalrymple ,1990), however observational studies of the influence of multi-directional waves have been limited to instances of shore-normal wave incidence (Johnson and Pattiaratchi, 2004), and lack a full analysis of the directional spectra.

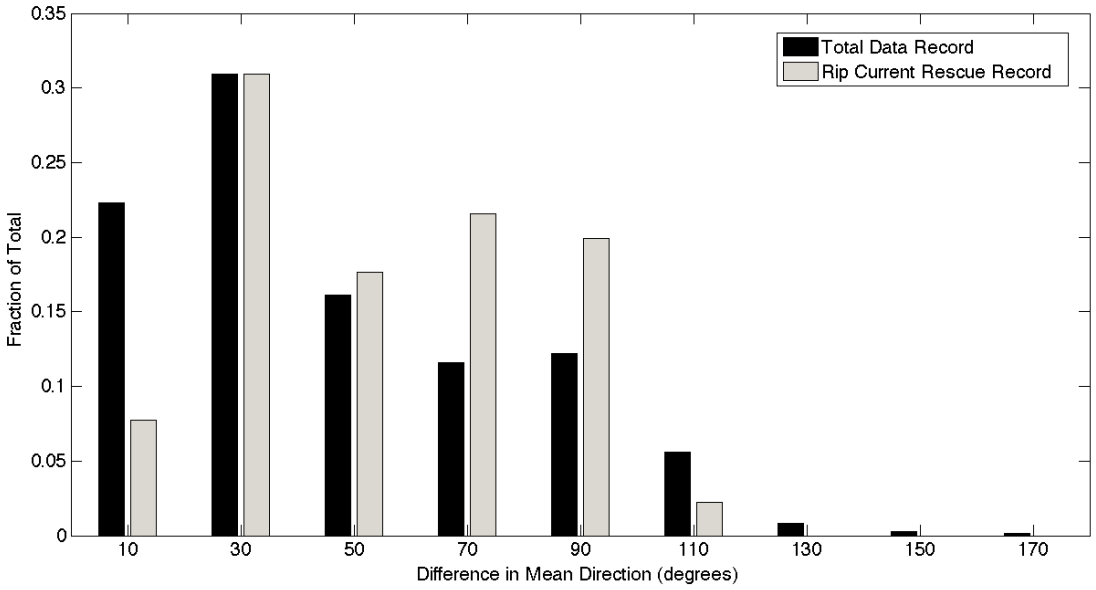

Figure 3.10 Normalized histograms representing the distributions of the swell mean direction difference for instances when two swells are present. The direction difference is defined as the absolute value of the difference in the mean direction of the dominant and secondary swell components. Both the entire data record (black) and rip rescue record (grey) are shown.

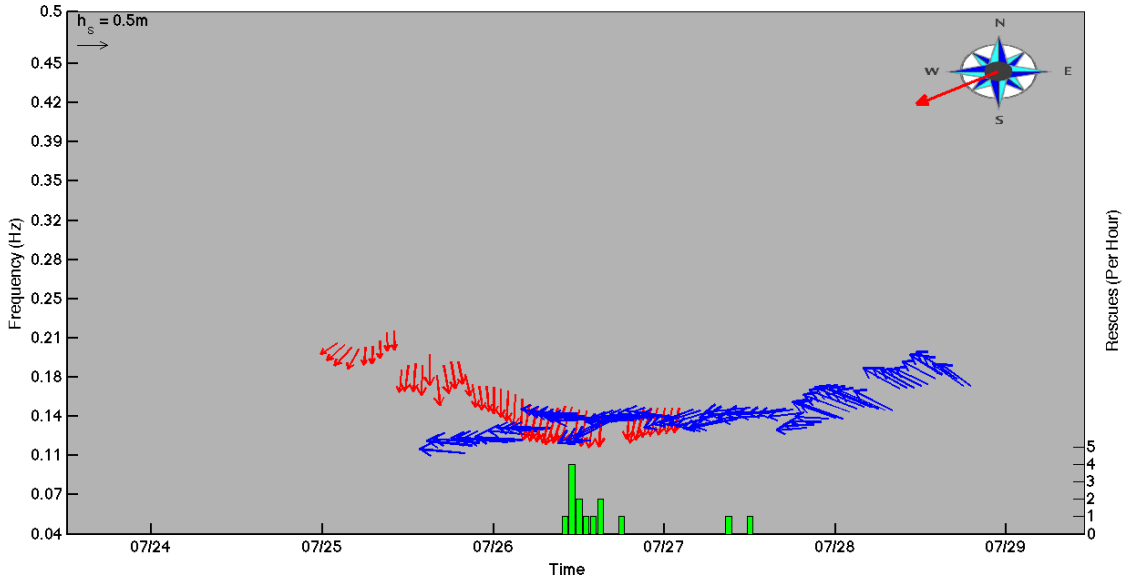

Figure 3.11 A wave vector plot over four days in 2004 showing an example of a bi-modal wave field leading to increased rip current activity. Each vector represents the frequency (vector origin), significant wave height (vector length) and wave direction (vector azimuth) of a spectral component for each hour. In this case light shaded vectors represent swell 1 and dark vectors represent swell 2. A vector length equating to 0.5 m Hs is shown in the upper left and the direction of shore-normal is shown by the arrow on the compass rose in the upper right. The right y-axis shows the number of rip rescues per hour, which are displayed as bars on the bottom of the plot.

3.5.2 Temporal variability in rip rescues

The summer wave climate at KDH can be described as predominantly low energy swell (0.4 to 0.6 m Hs) out of the southeast punctuated by storm events (1.0 to 3.0 m Hs), mostly from the northeast. The punctuated nature of the wave climate encourages a more detailed analysis of the effect of large wave events on rip current activity. For this analysis wave events are identified throughout the data record. The rescues that occur following each event are compared with the event characteristics to determine the influence of large wave events on hazardous rip current occurrence.

Event classification

Based on the summer wave climatology, an event was identified when the significant wave height reached at least 1 m and lasted for a minimum of 4 hours in duration. If the significant wave height dropped below 1 m for less than 4 hours before increasing to over 1 m again, that would constitute the same event. There were a total of 115 events identified over the nine summers, or 23,279 total hours of data collected. This averages to about 13 events per year, or roughly one event every 8.5 days. Events were classified as either predominantly northerly or southerly relative to shore-normal. A total of 64 events had an average peak wave direction from north of shore-normal and 51 events were from the south. Events out of the north were typically front or storm-related and thus begin as wind sea events and transitioned into swell events following passage of the storm system. Events from the south were more often dominated by longer period swell. Event length ranged from the minimum 4 hours to a maximum length of 129 hours. The average event length was 28.8 hours in duration. The maximum significant wave height of an event varied from 1.02 m to a maximum of 3.45 m and averaged 1.56 m. The rescue period for each event consisted of the 72-hour window following the peak wave height of a particular event. In the cases when a rescue period overlapped with another event, the rescue period from the first event was cut short as to not overlap with the rescue period of the second event.

Event related rip rescues

In many instances there were a significant number of rescues in the 72-hour period following events. This is especially apparent in 2006 when each group of multiple

rescue days follows shortly after a high-energy wave event (Figure 3.12). A total of 412 out of the 741 rip rescues made over nine summers, or 56% of all rescues, occur during a 72-hour window following wave events. When a cross correlation is made between the significant wave height and the hourly record of rip rescues over the entire data record, the maximum normalized value occurs when rescues are at a 21 hour lag from the significant wave height and the second and third highest values occur at a 45 hour and 68 hour lag respectively. These lags essentially represent one, two and three days following an event. It is important to note that the break in rescues between days does not represent a physical change in rip current activity but rather a zero in bather load during the evening hours (6 pm to 8 am). When considering the average peak wave direction of each event, 301 rescues, or 73% of the 412 rescues following events occur in the rescue period following events from north of shore-normal. The 72-hour rescue periods following northerly events account for a total of 4344 hours of observations. Thus 40% of all rescues occur during only 19% of all observations (Table 3.2).

The increase in rip rescues following wave events may be wave field dependent, topographically controlled or a combination of both as the typical characteristics of the wave field following an event are favorable to both rip current activity (MacMahan et al., 2005) and the development of an alongshore-variable bar system (Calvete et al., 2005; Garnier et al., 2008; Lippmann and Holman, 1990). Following an event the wave field is typically characterized as having relatively high significant wave heights and close to shore-normal wave direction. Wave height, although steadily decreasing following the peak of the events, is still on average higher than during other time periods (0.92 m compared to 0.62 m). The dominant swell following wave events out of the north

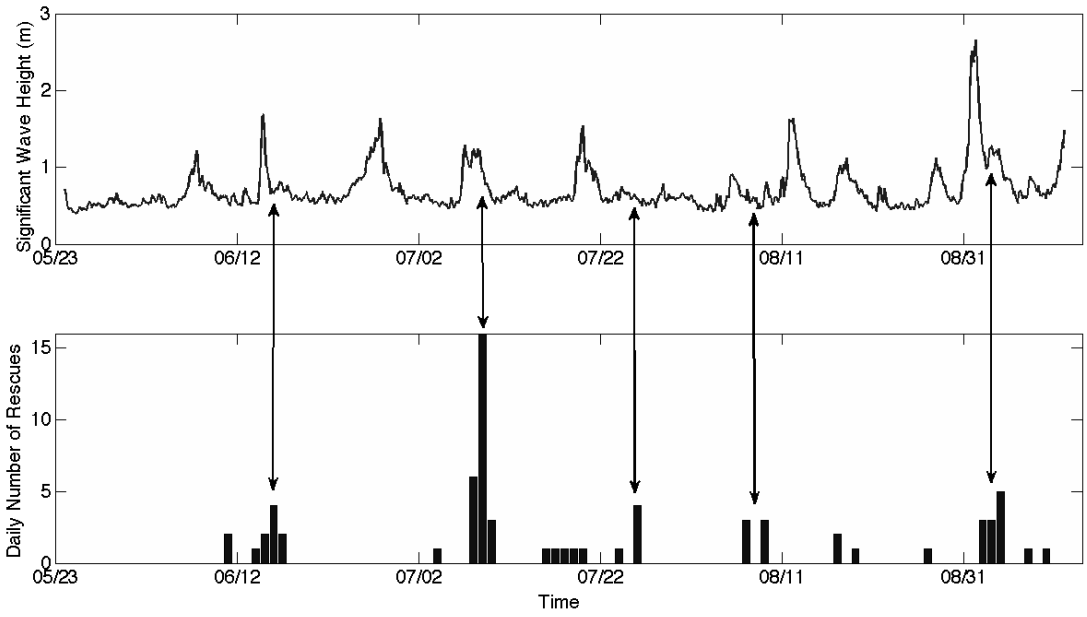

Figure 3.12 The top plot shows the hourly record of the significant wave height at KDH for the summer of 2006. The bottom plot shows the corresponding number of daily rip rescues made at KDH. Arrows are used to show instances where high rescue days follow large significant wave height events.

generally begins at a significant oblique angle from the north, trends towards shore-normal as wave energy decreases following the peak of the event and eventually arrives from a slightly southerly direction (Figure 3.13). Thus, a majority (63%) of the time immediately following a northerly wave event, the dominant swell is within 25 degrees of shore-normal.

3.5.3 Alongshore variability

Variability in the number of rip related rescues

Each of the 741 rescues recorded from 2001-2009 includes the location of the rescue to the nearest lifeguard chair and enables an analysis of the alongshore variability in the number of rip rescues at each chair location. From 2001-2008 there was a

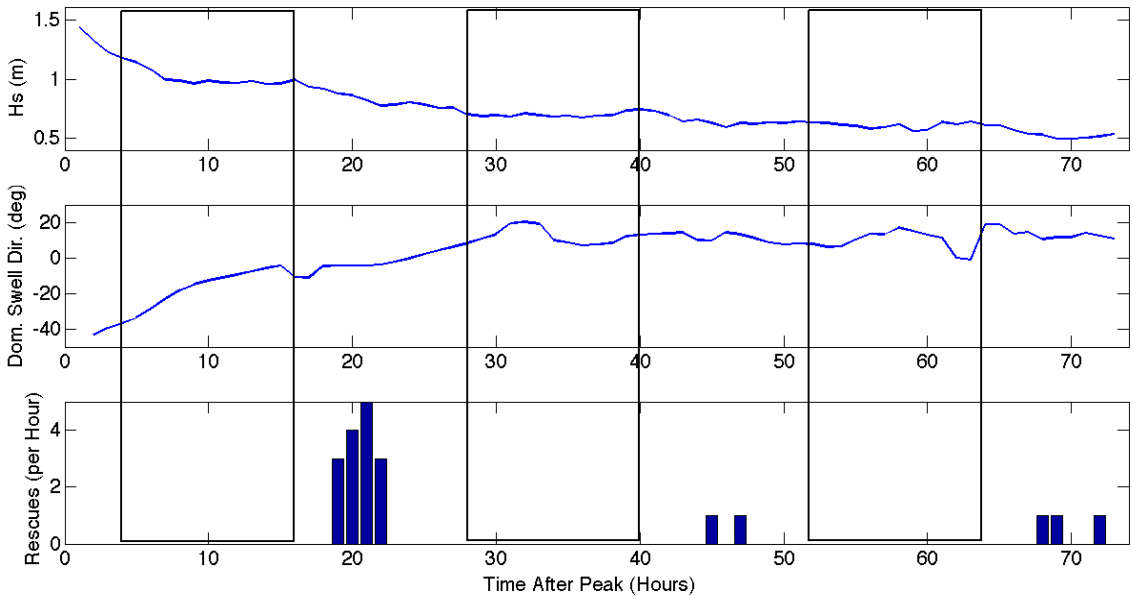

Figure 3.13 The plots show the significant wave height (top) and mean direction of the dominant swell relative to shore-normal (middle) and rip rescues per hour (bottom) for a 72 hour period following a large wave height event out of the northeast. The x-axis is the number of hours following the peak of the event and the rectangles represent the evening hours from 1900 to 0600 EST when rescues will not occur.

significant difference in the number of rescues made alongshore (Figure 3.14). If the beach is divided into the northernmost nine chairs (~4 km) and the nine chairs to the south (~3 km) (Figure 3.1), there were a total of 177 rescues made in the northern half of KDH compared to 339 rescues made in the southern half. In 2009, this disparity between north and south changed dramatically as there was 117 rescues made in the northern half of KDH compared to 118 rescues in the southern half. Average daily beach counts were recorded in 2009 and they show that beach attendance is relatively consistent alongshore, with the exception of Ocean Bay, which is the main beach access point in KDH. Although detailed beach count data are not available for other years, according to KDH Ocean Rescue personnel, beach attendance is usually fairly uniform throughout KDH (Pers. Comm.). Since rescues are dependent on the number of people in the water, this

demonstrates that beach attendance is not the primary reason for the variability in rescues alongshore. The number of rescues in 2009 and the distribution of these rescues alongshore appears to be relatively unique when looking at the annual variability of the northern and southern portions of KDH (Figure 3.15). From 2004 to 2008, the southern half of KDH consistently has more rescues than the northern half of KDH, but this significantly changes in 2009. This result suggests that annual alongshore variability in the surf zone bathymetry may determine areas of increased hazardous rip current activity.

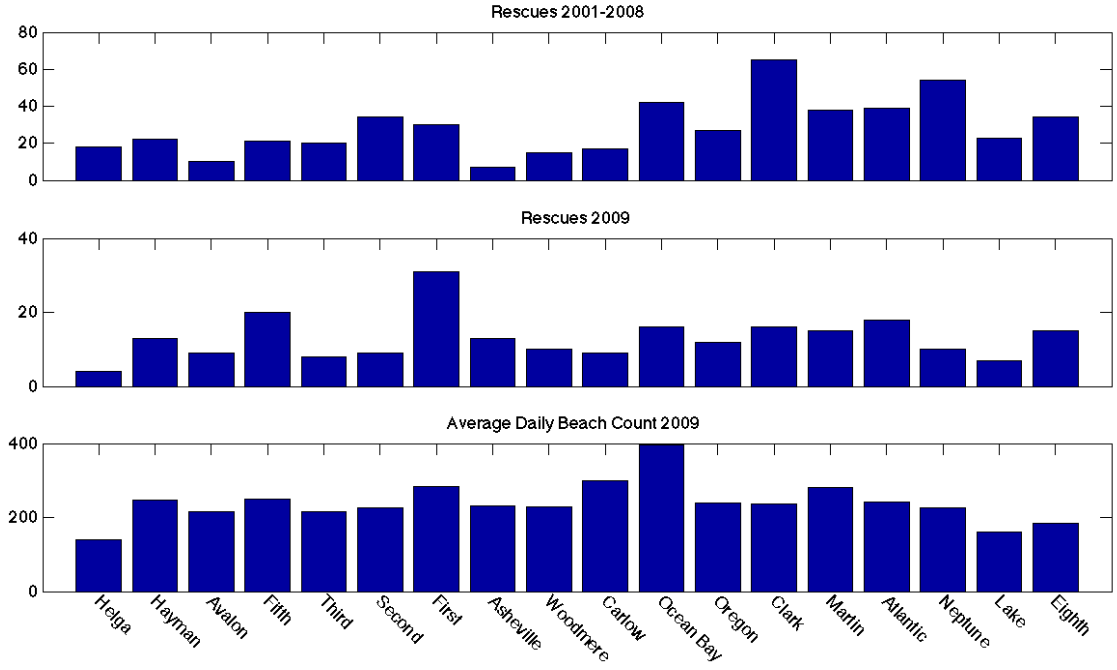

Figure 3.14 The top plot shows the total number of rip rescues made for each lifeguard chair (from North to South) at KDH from 2001-2008. The middle plot is the total number of rip rescues made for each chair in 2009. The bottom plot shows the average estimated daily beach count for each chair in 2009.

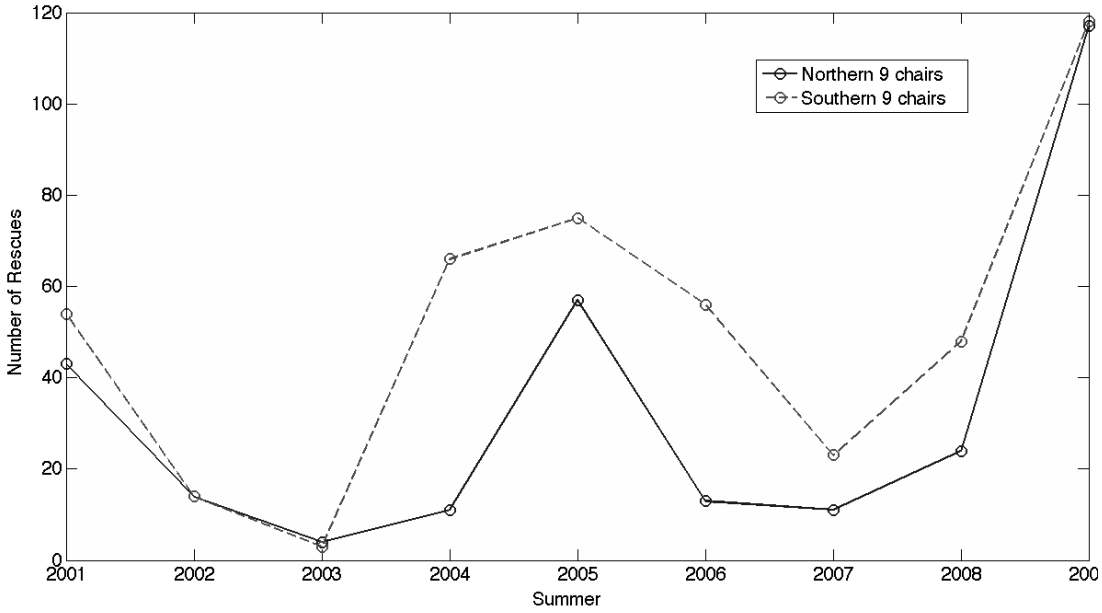

Figure 3.15 The number of rip rescues made at KDH for each summer from 2001 to 2009. The dashed plot is the yearly total rip rescues for the nine northern lifeguard chairs and the solid plot is yearly total for the southern nine chairs.

The role of the surf zone bathymetry

Surf zone bathymetry data are not available for the summers from 2001-2007 in the study area. However, cross-shore transects were performed at seven different chair locations five and four times in the summers of 2008 and 2009 respectively. The generation of strong rip currents is closely tied to the surf zone morphology and more specifically to the extent of the surf zone bar system (Brander, 1999; Brander and Short, 2000; Haller et al., 2002; MacMahan et al., 2005). Thus, the expectation is that from 2004-2008 (Figure 3.15), there would be more significant surf zone bar formation in the southern half of KDH compared to the northern half and that in 2009 bar formation would be evident in most locations along KDH due to the large number of rescues recorded at nearly every chair location. Using the simple measure of bar presence in the profile lines recorded in 2008 and 2009 supports this expectation. It is important to note

that the KDH region is often double-barred, with an inner surf zone bar (1-2 m depth), and an outer storm bar (~4.5 m depth) (www.frf.usace.army.mil). This analysis is only of the inner surf zone bar, as bathymetry data of the outer bar was not available and the outer bar is outside of the surf zone region.

In 2008, the profiles recorded for the northern chairs (Hayman, Third, First and Asheville) rarely show any evidence of a surf zone bar in the measured region (Table 3.3). Ocean Bay, which is counted among the nine southern chairs, also shows no evidence of a surf zone bar. However, the profiles recorded in the southernmost two chairs (Clark and Neptune) show evidence of a bar in four out of the five dates data were collected. Comparing the profile lines recorded at First Street and Clark Street in 2008 demonstrates the significant difference in the surf zone bathymetry in the northern and southern extents of KDH (Figure 3.16). While First Street has very linear profiles with no evidence of bar formation in the measured region, Clark Street shows a significant trough and bar for four out of the five dates profiles were performed.

Table 3.3 The fraction of profiles in which a bar is visibly present for each chair location at KDH beach

	Fraction of profiles with bar	
Street	2008	2009
Hayman	0	0.75
Third	0.2	1
First	0	1
Asheville	0	1
Ocean Bay	0	1
Clark	0.8	1
Neptune	0.8	0.66

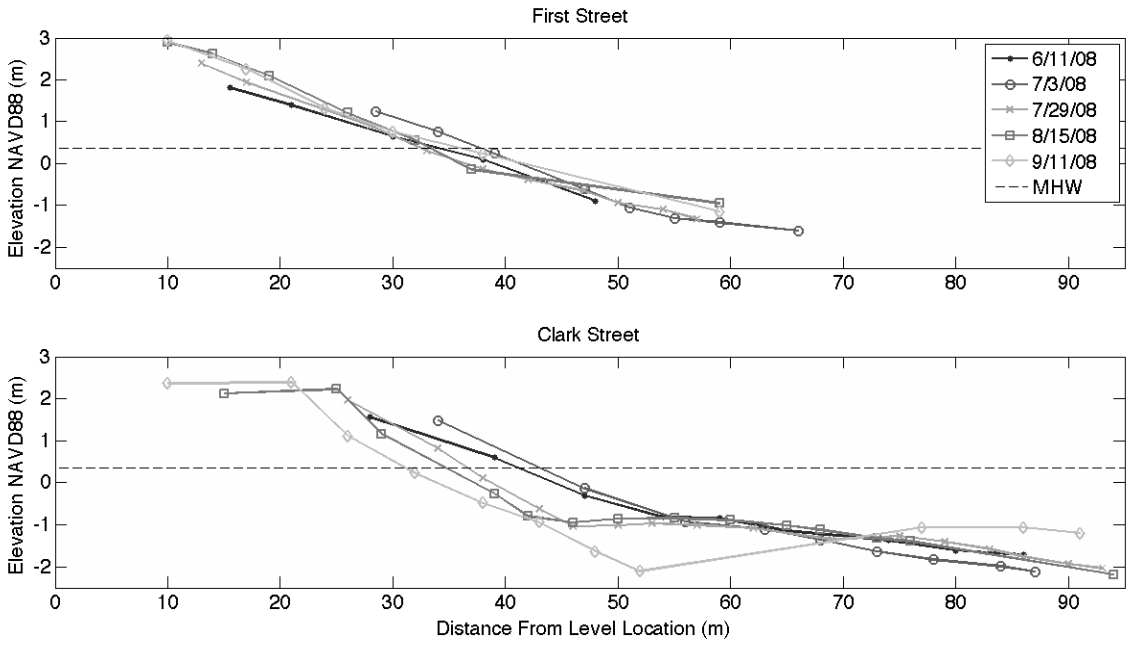

Figure 3.16 Cross-shore profiles made on five different instances in 2008 at both the First Street (top) and Clark Street (bottom) lifeguard chair locations. The x-axis is the cross-shore distance from the starting location, which was kept constant for each profile. The mean high water elevation of 0.36 m is shown (horizontal dashed) for each plot.

In 2009, the profiles recorded at every location along the beach nearly always show evidence of a surf zone bar (Table 3.3). Comparing First Street and Clark Street for the profiles performed in 2009 shows very different results from 2008 (Figure 3.17). The bathymetry at First Street is different than in 2008 and shows a significant trough and bar at every profile date. Clark Street is similar to 2008 in that a significant bar system is evident at all four profile dates. Consequently, in 2009 the bathymetry at First Street now shows strong similarities to the data collected at Clark Street. At both locations the most significant trough and bar is depicted on June 25, with a change to a more subtle surf zone bar by July 15. This also suggests that, contrary to 2008, for the summer of 2009 the changes in the bar system alongshore at KDH are correlated in time.

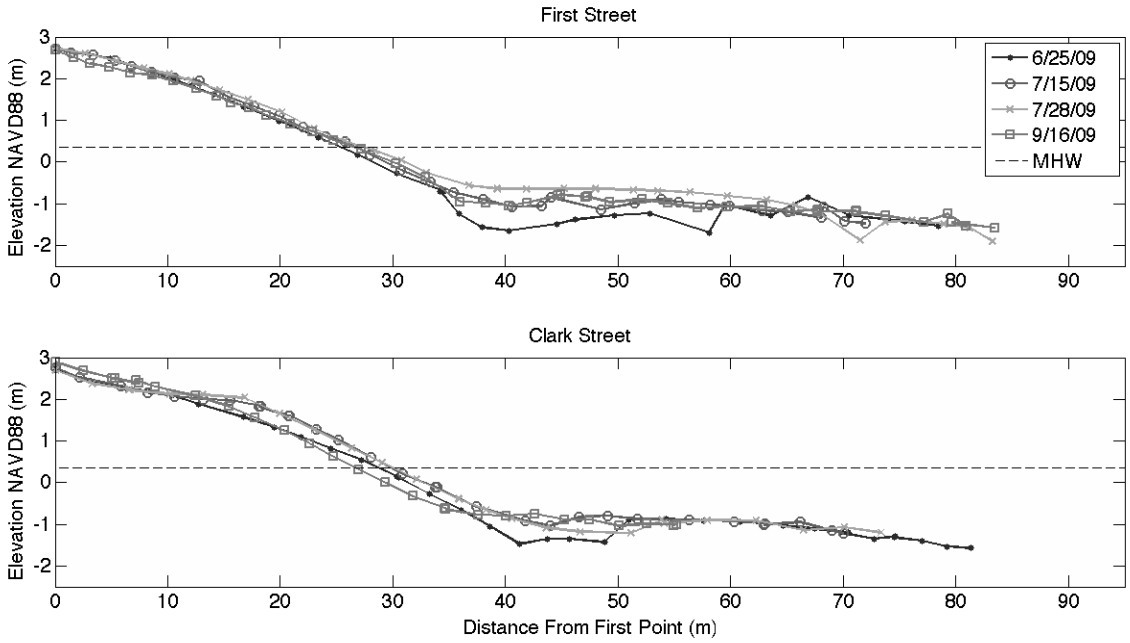

Figure 3.17 Cross-shore profiles made on four different instances in 2009 at both the First Street (top) and Clark Street (bottom) lifeguard chair locations. The x-axis is the cross-shore distance from the starting GPS location, which was kept constant for each profile and is the same starting location used in 2008. Cross-shore distances are not equivalent for First and Clark Street so the mean high water elevation of 0.36 m is shown (horizontal dashed) for each plot.

It is evident that the surf zone bathymetry at KDH is fairly dynamic in both time and space, however it is also apparent that there is some alongshore persistence in the presence of the surf zone bar system. From the bathymetry data in 2008 and 2009, it can be inferred that the alongshore variability in the number of rip current rescues is related to the presence of a significant surf zone bar relatively near shore. The rescue record then suggests that while a strong bar system likely persisted in the southern portion of KDH in the summers from 2004 to 2008, there most likely was not consistent surf zone bar formation in the northern portion of KDH over the same time period. In 2009, there was significant bar formation along most of KDH for most of the summer. From 2001-

2003 rescue numbers were similar in both portions of KDH, implying that bathymetric conditions were not as varied alongshore.

3.6 Discussion

3.6.1 Rip favorable wave conditions

An analysis of the partitioned wave data has suggested that there are two characteristic wave fields when hazardous rip currents are most favorable: A single swell with relatively high significant wave height and shore-normal incidence; and two distinct swells at highly opposing angles (> 60 degrees) approaching at oblique incidence. The single swell case has been shown to be rip favorable in previous studies (Engle et al., 2002; Svendsen et al., 2000) and describes the wave forcing often applied to numerical model (Calvete, et al., 2005; Svendsen et al., 2000) and lab studies (Haller et al., 2002). The bi-modal case has received much less attention. Crossing wave trains have been shown to be a potential mechanism for rip currents in lab studies (Fowler and Dalrymple, 1990), but have never been documented observationally. The importance of recognizing a bi-modal wave field as a potential mechanism for hazardous rip currents is two-fold. First, rip currents of this nature are forced hydrodynamically and thus do not rely on the surf zone bathymetry (Johnson and Pattiaratchi, 2006). This fact may be especially significant in terms of rip current prediction, as rips forced from a bi-modal wave field will not be constrained spatially and thus could occur anywhere alongshore. Second, during instances of two swells with highly opposing angles the bulk statistics of the wave field will often represent a single wave direction at a highly oblique incidence. Thus, the present rip current forecast index, if it takes into account the wave direction, would

predict low rip hazard conditions and be inaccurate in these instances as it relies on bulk spectral statistics like peak direction (Engle et al., 2002), and would not identify the secondary spectral peak.

3.6.2 Surf zone response to wave events

The temporal analysis of wave event related rip rescues found that 40% of all rescues were made within 72 hours following wave events out of the northeast. It was shown that the wave field following these events consists of moderately high swell close to shore-normal, which are wave conditions that are dynamically favorable for rip current activity (MacMahan et al., 2005). High energy and shore-normal swell conditions along with decreasing wave energy are also favorable for the development of an alongshore-variable surf zone bar system (Calvete et al., 2005; Garnier et al., 2008; Lippmann and Holman, 1990). As rip currents are highly dependent on the surf zone bathymetry (Brander, 1999; Haller et al., 2002; MacMahan et al., 2008), an alongshore-variable surf zone bar system will be morphodynamically associated with rip currents (Wright and Short, 1984). Thus, the increase in hazardous rip activity following these events is most likely due to wave conditions that are both favorable for rip current activity and for generating rip favorable surf zone bathymetry. The occurrence of hazardous rip activity within three days following these events is also consistent with previous morphodynamic research.

It has been shown that immediately following a large wave event a relatively alongshore-uniform bar is developed on the outer boundary of the surf zone (van Enckevort and Ruessink, 2003; van Enckevort et al., 2004). As wave energy decreases,

the bar moves towards shore, developing alongshore non-uniformities on roughly weeklong time scales (van Enckevort et al., 2004). However, under moderate wave conditions a partial reset is possible (vanEnckevort et al., 2004), with such an event resulting in alongshore non-uniformities immediately following or within days following the moderate wave event (Garnier et al., 2008). This result corresponds well to the rip rescue record at KDH as wave events can typically be characterized as "moderate" (Hs of 1 – 2 m) and the majority of rescues occur one to three days following the event. Additionally, since the surf zone bathymetry is closely tied to wave events it is possible that wave events of similar magnitude and direction might result in a similar surf zone morphology following each instance. This hypothesis is especially significant to rip current forecasting, as often little information is available regarding the surf zone bathymetry. If certain wave events force the surf zone bathymetry in such a manner that rip currents are more likely after these types of wave events, this factor could be included to improve the accuracy of rip current forecasts.

3.6.3 Nearshore controls on the surf zone bathymetry

An analysis of the alongshore variability in rip rescues has determined that an increase in rip current activity is correlated to the presence of a surf zone bar. However, it is uncertain why the surf zone bar system varies alongshore at KDH. One possible explanation is the difference in the outer nearshore bathymetry (seaward of the surf zone) and underlying geology between the southern and northern portions of KDH. The nearshore of the northern Outer Banks is characterized by several regions of gravel outcrops and shore-oblique bars (McNinch, 2004), and these regions are typically

correlated with paleo-river channels (Browder and McNinch, 2006). One such region begins north of KDH in Kitty Hawk and extends southward to near the location of First Street, covering over 3 km of KDH (Figure 3.18). The oblique bars extend at a northward angle from shore-normal and vary in size and scale. They can be found as shallow as 2 m depth and reach beyond 1 km from shore (McNinch, 2004). Additionally, the oblique-bars and gravel outcrops are relatively stationary in both location and time, showing essentially no variation following large wave events (Schupp et al., 2006).

Although the bars do not extend into the surf zone, thus not directly influencing surf zone processes, the morphological characteristics of this region are very different from southern KDH and may be influencing the behavior of the alongshore bar system. The northern region of KDH is characterized by a steeper and more variable cross-shore bathymetry gradient than in southern KDH (Figure 3.18). The northern region is also an area of relatively high rates of both short-term (1974-2002) and long-term (1933-1998) shoreline erosion and high rates of shoreline variability, while most of the southern portion of KDH has a relatively stable shoreline, is experiencing short-term accretion and the entire region from First Street southward has net long-term accretion (Schupp et al., 2006). Furthermore, much of the northern region has a relatively thin and presumably active layer of sand compared to the southern region, which has a thicker and more uniform sand layer (Schupp et al., 2006).

These factors might all be contributing to the variability in the alongshore (surf zone) bar system from northern to southern KDH. The steeper cross-shore slope in the northern portion of KDH presents a slightly more reflective beach state, which results in

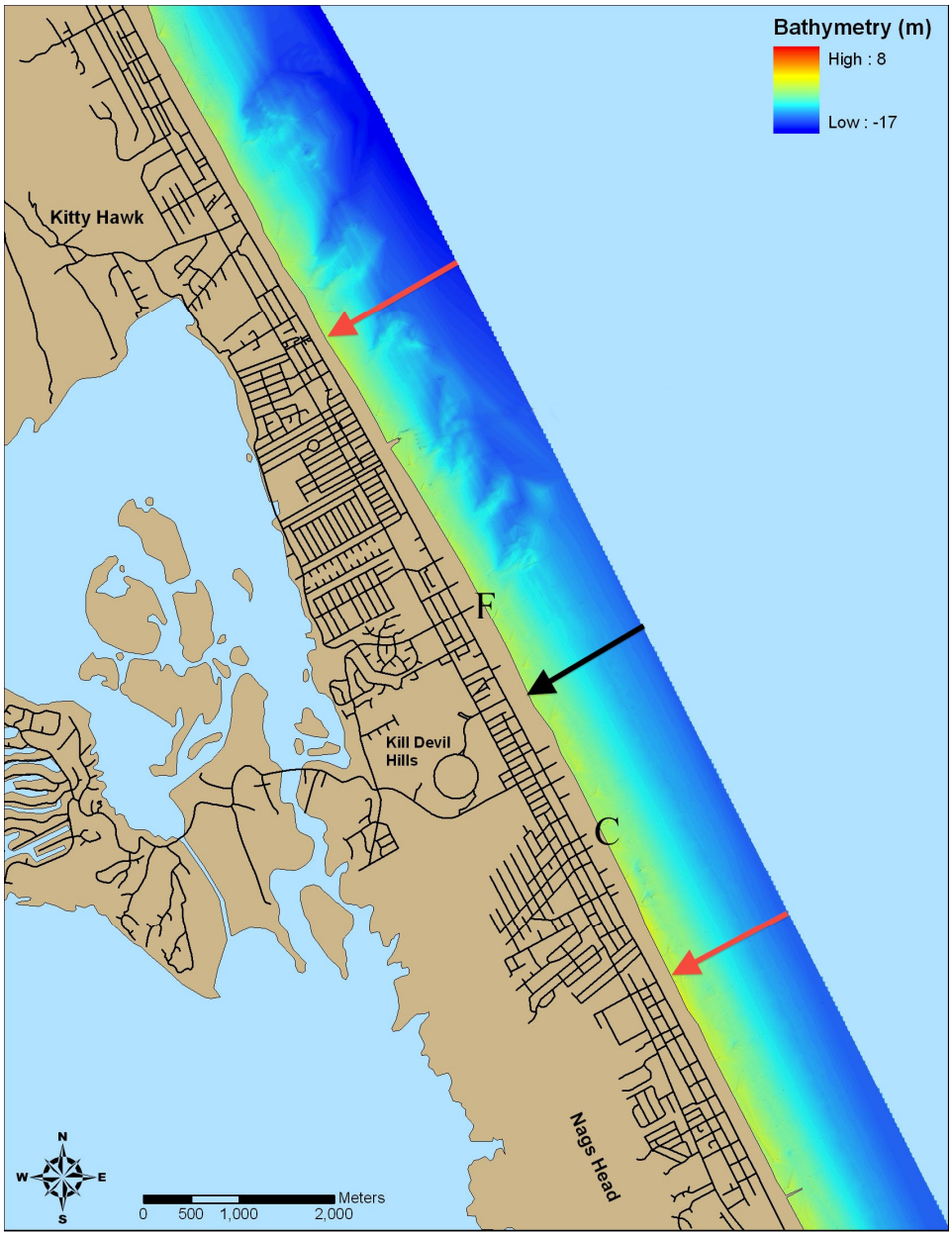

Figure 3.18 Bathymetry data resulting from a swath bathymetry survey performed by the US Army Corps of Engineers FRF in 2006. Vertical scale is in meters NAVD88 and the northern and southern extents of KDH are shown (light shaded arrows). Additionally, the locations of First Street (F) and Clark Street (C) are labeled. The northern nine chairs fall to the north of the dark shaded arrow while the southern nine chairs are located to south of the black arrow.

an increase in wave energy in the surf zone and is less favorable to bar formation in general (Wright and Short, 1984). The relatively thin layer of sand and the erosion rates in northern KDH suggest a small sediment supply compared to southern KDH. A small sediment supply is also a characteristic of a more reflective beach state, and can also hinder surf zone bar formation. The reason for the sudden presence of a strong surf zone bar along essentially the entirety of KDH is more difficult to explain, however the hypothesis posed by Schupp et al. (2006) that the upper sand layer in the northern portion is highly active supports the possibility of forming a significant bar system under optimal wave conditions.

3.7 Summary

The distribution of rip current rescues at Kill Devil Hills in both time and space suggests that rip current activity is dependent on the wave field and tide, previous wave conditions, and the surf zone bathymetry. In general these results conform well to previous research. The results of this study demonstrate that rip activity increases with increasing significant wave height, shore-normal wave incidence and lower tidal elevation. These three factors have been shown repeatedly in previous research to impact rip activity and intensity (Brander, 1999; Brander and Short, 2000; Engle et al., 2002; MacMahan et al., 2005; Svendsen et al., 2000). It is also shown that rip currents are highly dependent on the surf zone bathymetry, which has been demonstrated in multiple publications as well (Brander, 1999; Brander and Short, 2000; Haller et al., 2002; MacMahan et al., 2005; MacMahan et al., 2008). However, the alongshore resolution and temporal extent of the rescue data combined with the availability of directional wave

data and surf zone and nearshore bathymetry data have enabled a more detailed analysis of the contributions of these physical factors to rip current activity.

The analysis of the individual spectral components has shown that rip rescues are more likely to occur during swell conditions than when wind sea is present, however there is not a very significant relationship between rescues and the peak period of either the entire spectrum or the individual components. When just a single swell is present in the spectrum, rip activity increases with increasing wave height, smaller directional spread and with wave incidence near shore-normal. When two swells are present, rip activity is most prevalent when the difference in the mean direction of each swell is between 60 and 100 degrees, which suggests that a bi-modal wave field causing crossing wave trains nearshore may be an important mechanism for hazardous rip current occurrence.

The temporal analysis performed in this paper has demonstrated that rip currents are especially likely about a day after relatively large wave events from the northeast. The characteristics of the wave field following these events may be the primary reason for this increase in hazardous rip currents. The wave field within 72 hours following a northeasterly event generally consists of relatively large shore-normal swell. A wave field with these characteristics is not only dynamically favorable to rip current activity, but is also likely to generate alongshore variable surf zone bathymetry, which itself increases the likelihood of hazardous rip activity.

Comparing the number of rip rescues alongshore at Kill Devil Hills suggests that rip currents are generally more likely in the southern half of KDH than in the northern half, but that this relationship can occasionally vary. From 2004-2008 there are a

relatively high number of rip current rescues made at KDH and for each of those summers, there are significantly more rescues made in the southern half than in the northern half. In 2009 the number of rescues is well above average along the entirety of KDH. An analysis of the surf zone profiles recorded at KDH in 2008 shows that the southern half of KDH had surf zone bar formation throughout the summer, consistent with the high number of rip rescues, while the northern half did not. Since rip rescue records from 2008 are consistent with the previous four years, this is presumed to be the normal mode of surf zone bathymetry alongshore at KDH. However, this mode is subject to variability for a particular summer and in 2009 the bathymetry varied dramatically. Additionally, the presence or lack of surf zone bar morphology at a particular location alongshore appears to be consistent over the course of one summer.

Although the results of this study provide valuable insight into how hazardous rip current activity is influenced, it is important to note the limitations of using rescue data as the primary rip current observational resource. As mentioned previously, not having a rip current rescue at a particular location and time indicates very little regarding whether or not a hazardous rip current exists at that location and time. Rip rescues are closely tied to bather load, and if bather load is low due to bad weather, cold water temperatures or beach closures there will be few or no rescues even if hazardous rip currents are present. To address this concern, lifeguard observations of rip current activity and intensity were made in 2008 and 2009 and these will be included in a future study to verify the current results.

CHAPTER 4

THE INFLUENCE OF THE WAVE FIELD AND SURF ZONE BATHYMETRY ON DAILY VARIATIONS IN RIP CURRENT INTENSITY

4.1 Introduction

Rip currents have become an increasingly well-researched surf zone process. Recent work has ranged from detailed observations of rip current circulation (Austin et al., 2010; MacMahan et al., 2010) to modeling of rip current morphodynamics (Garnier et al., 2008). Although significant advances have been made regarding the understanding of rip currents, the majority of research has focused on rip current behavior over relatively small scales (< 1 km and ~ days). There has been comparably little focus on large-scale (days to years and > 1 km) variations in rip current presence and intensity. Understanding variations in rip current intensity over large scales is essential to rip current forecasting.

Rip currents are the number one safety risk for beachgoers in the United States (www.usla.org). The National Weather Service (NWS) rip current forecast serves as a primary safety and awareness mechanism for the public. However, the accuracy and functionality of the NWS forecast system is limited. There has been increased focus on improving the present rip forecast method through application of a wave current model in the surf zone (Voulgaris et al., 2011), yet a similar focus utilizing observations has not

been realized. Critical to the creation of an operational rip current forecast model is an understanding of large-scale rip current variability. However, a primary challenge in studying rip currents over large-scales is data collection. Surf zone instrument deployment over long time periods and large distances is difficult and costly. Although using camera systems like the Argus system has enabled long-term (~ years) kilometer scale surf zone observations (e.g. Holman et al., 2006; Turner et al., 2007) these observations are dependent on the amount of wave breaking and have thus far been limited to rip current presence. They provide no information regarding rip current intensity.

Lifeguard rip current rescues have been used as an alternative to instrument observations with some success. Assuming that a rip current rescue indicates the presence of a hazardous rip current, rip rescues can be correlated with wave and bathymetry data to determine the conditions that favor hazardous rip current occurrence. There have been multiple studies utilizing rescues in the United States (Lascody, 1998; Engle et al., 2002) and United Kingdom (Scott et al., 2007; 2009). However, all of these studies lack the alongshore position of each rescue, nor is surf zone bathymetry data available. Dusek et al. (2011; see also Chapter 3) compiled a data set of 741 rip rescues made over 9 summers, which included the time and alongshore location of each rescue. The factors that most influenced the occurrence of rip rescues (or hazardous rip currents) were determined through correlation with tidal, wave and bathymetry data. Yet there remains some uncertainty when utilizing rip rescues as an indicator for hazardous rip current occurrence. Bather load determines whether or not rip rescues occur. If people are not in the water due to weather, water temperature or large surf conditions there will

not be any rescues even if rip currents are present. Thus, the rescue record provides no information on the presence of rip currents when no rescues are made. Rescues also fail to provide any rip current intensity information.

Lifeguards at Kill Devil Hills, NC (KDH) have performed daily observations of rip current intensity to provide more detailed rip current information. Lifeguards estimated daily rip current intensity from 0 (no rip currents) to 3 (very strong rip currents) for 19 lifeguard chairs covering about 7.5 km of beachfront. Directional wave measurements were collected by two Acoustic Doppler Current Profilers (ADCPs) located just offshore of the study area. Bathymetric features were measured from cross-shore profiles collected at multiple locations alongshore at KDH.

In this paper statistical analyses are performed to determine how the wave field influences rip intensity, and what surf zone bathymetric features are responsible for alongshore variations in rip intensity. To accomplish these analyses the rip intensity observations are organized in two ways: first as a beach-wide average for comparison with the wave field, and then as a sub-sampled record at individual alongshore locations for comparison with bathymetric surveys.

4.2 Field Site

The study was performed at Kill Devil Hills on the northern Outer Banks of North Carolina (Figure 4.1). The 7.5 km stretch of beach faces the northeast (63$\pm$ 2 degrees true), is relatively straight and is often characterized as double-barred with one bar in the surf zone at 1-2 m depth and one outer storm bar at 4-5 m depth (www.frf.usace.army.mil/survey/frfsurvey.html). The nearshore region of the Outer

Banks generally slopes at about 1:10 in the foreshore region and transitions to a more gradual offshore slope of 1:500 (Schupp et al., 2006). The nearshore bathymetry (from the surf zone to about 10 m depth) at KDH varies from south to north. The southern portion of KDH is characterized by shore-parallel isobaths in the nearshore region, while large, semi-permanent shore oblique bars from 2 to 10 m depth characterize the northern portion of KDH (Figure 4.2; McNinch, 2004).

Figure 4.1 The study location at Kill Devil Hills, NC. The green marks show the location of the 19 lifeguard chairs, and black stars indicate the locations where surf zone bathymetry was monitored in 2008 and 2009. The red lines indicate the offshore extent of the RTK GPS (solid) and FRF (dashed) profiles. The white marks show the location of the 2 ADCPs deployed at roughly 12 m depth from June to December in 2008 and 2009.

The region is wave dominated with a mean annual significant wave height (Hs) of 0.9 m (McNinch, 2004), although wave height ranges vary with events and season. The

wave climate in the summer months consists of low energy swell (Hs = 0.4 - 0.6 m) generally out of the southeast, punctuated by storm events (Hs > 1m) on average every 8.5 days (Chapter 3). The tides are semi-diurnal with the mean tidal range of about 1 m (Birkemeier et al., 1985).

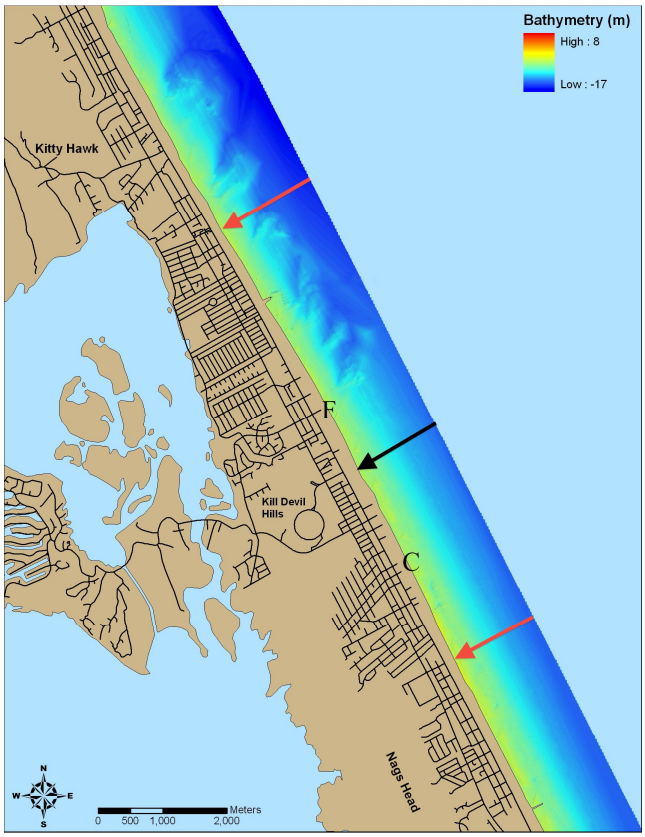

Figure 4.2 Bathymetry data resulting from a swath bathymetry survey performed by the US Army Corps of Engineers FRF in 2006. Vertical scale is in meters NAVD88 and the northern and southern extents of KDH are shown (red arrows). Additionally, the locations of First Street (F) and Clark Street (C) are labeled. The northern nine chairs fall to the north of the black arrow while the southern ten chairs are located to the south of the black arrow.

4.3 Methods

4.3.1 Data collection

Wave data

Two Teledyne RDI 600 kHz ADCPs were deployed at KDH during the summer of 2008 and 2009. The ADCPs were located in the northern and southern extent of KDH at approximately 11 m to 12 m depth (Figure 4.1). They both sampled every 2 hours for 20 minutes at 2 Hz and they were deployed from 20 June through December of 2008 and from 10 June through December of 2009. The records utilized for the analysis are limited to the days that both wave field and lifeguard observations were performed, 20 June to 31 August in 2008 and 10 June to 5 September in 2009. For comparison with bathymetric survey data, the wave record is extended up to 20 September for both summers.

The binary ADCP data were processed into two-dimensional (2d) directional wave spectra using the open-source waves toolbox DPWP (Doppler Profiler Waves Processing Toolbox; Chapter 2). Processing utilized the default DPWP options, which include the along-beam radial velocity data input and the IMLM (Iterative Maximum Likelihood Method; Pawka, 1983; Oltman-Shay and Guza, 1984) estimation method. The bulk statistical measurements of significant wave height, peak period, vector mean wave direction and directional spread (Kuik et al., 1988) were calculated.

Following the analysis in Chapter 3, the 2d directional spectra were partitioned into wave components using the MATLAB® toolbox XWaves (www.WaveForceTechnologies.com). XWaves identifies peaks and valleys in the 2d spectra and utilizes local wind data to identify wind sea and swell components in the spectra (Hanson and Phillps, 2001; Hanson et al., 2009; Tracy et al., 2006). A maximum

of two partitions were allowed (wind sea and up to two swells) with a minimum significant wave height of 0.2 m required for a component to be identified. Wind sea is defined as surface gravity waves forced by the local wind field and swell is defined as surface gravity waves without a local wind forcing. The significant wave height, peak period, vector mean wave direction and directional spread are calculated for each component.

The refracted mean wave direction and the refracted and shoaled significant wave height are considered as an alternative to the observed wave statistics. Rip currents are forced by the wave field at the point of wave breaking, so obtaining wave height and direction at the break-point provides the most physically significant wave measurements. A simple way to estimate the refracted wave direction is to assume parallel and monotonically decreasing depth contours and estimate the change in wave direction and height from the ADCP measurement location (~12 m depth) to some shoreward location. Although the point of wave breaking would be the ideal shoreward location, complex surf zone bathymetry both cross-shore and alongshore complicate this calculation. Thus, a point just outside the surf zone (3m depth; just seaward of the deepest surf zone bar found in surf zone survey data of KDH) is used as the shoreward location. Snell's law is used to compute the refracted wave direction. The change in wave height due to shoaling and refraction is calculated using the following relationship (Dean and Dalrymple, 2002):

$$H_{3m} = H_{12m} K_s K_r , \quad (4.1)$$

where H_{12m} is the observed significant wave height at 12 m depth, K_s is the shoaling coefficient defined as:

$$K_s = \sqrt{\frac{C_{g_{12m}}}{C_{g_{3m}}}}$$

where C_g is the wave group velocity at 12 m or 3 m depth (calculated using the peak period). K_r is the refraction coefficient defined as:

$$K_r = \sqrt{\frac{\cos\theta_{12m}}{\cos\theta_{3m}}}$$

where θ is the observed angle of incidence at 12 m depth and the Snell's law refracted angle of incidence at 3 m depth. There are some limitations in this simplistic approach. The assumption of parallel and monotonic depth contours may oversimplify the nearshore bathymetry of KDH given the complex bathymetry in northern KDH and common presence of a secondary nearshore bar at about 4 – 5 m depth. Additionally, the computations above are most appropriate for a monochromatic wave field. Variations in spectral shape may decrease the accuracy of these estimations. However, applying these transformations to the wave height and direction can provide a general view of what the wave forcing is at the outer edge of the surf zone. The transformation also provides a means to standardize the wave height and direction with measurement depth, which potentially allows for portability of the results to other locations. The height and direction transformation is considered for the bulk spectral measurements.

Tidal elevation

Measurements of tidal elevation were collected at the Army Corps of Engineers Field Research Facility (FRF) located about 15 km north of the study area. The tide has clearly been shown to influence rip currents at KDH (Chapter 3) and elsewhere (Brander, 1999, MacMahan et al., 2005). However, the temporal resolution of lifeguard observations (1 day) hinder the possible identification of a tidal relationship. No

discernable influence of the tide was found on the observed daily-averaged rip current intensity and thus no further tidal analysis is included.

Surf zone and nearshore bathymetry data

Bathymetry data collected includes surveys of the beach and surf zone performed over the summers of 2008 and 2009 as well as nearshore surveys completed by the FRF in 2004 and 2006. The surveys performed in 2008 and 2009 consist of profile lines sampled at seven different locations along KDH (Figure 4.1). Each profile transect follows an approximately shore-normal direction from just seaward of the dune line out to about 2 m depth MHW. The profile lines were re-occupied a number of times each summer and capture the bathymetry of the surf zone (from the beach seaward to just beyond the extent of breaking waves). In 2008 one profile transect was collected at each alongshore location using a level and level rod. The same locations were re-sampled five times that summer. In 2009 two profile transects about 50 m apart were collected at the same alongshore locations using a Trimble RTK GPS system. There was poor GPS reception at the most southern location (Neptune Street) due to the distance from the permanent RTK base station. The poor reception resulted in unacceptably high vertical error levels and so data from this location has not been included. The vertical accuracy for the level and level rod is dependent on the distance from the level with the upper bound of the error at about 10 cm. The vertical accuracy of the RTK GPS system has a maximum error of about 5 cm.

There were two types of surveys completed by the FRF. Cross-shore transects were performed using the Lighter Amphibious Resupply Cargo (LARC) Survey System

in August of 2004, and in April and September of 2006 (USACE-ERDC-CHL, 2007). Each transect begins just landward of the dune line and extends seaward to about 10 m depth (Figure 4.1). The transect lines are about 300 m apart alongshore and the same lines are re-sampled for each survey. Since the 2006 surveys were completed in the spring and fall, they are only used to characterize typical bar location. The survey from August 2004 is analyzed in greater detail. The two transect lines closest to each profile location sampled in 2009 were chosen for analysis. A SWATH bathymetry survey was also performed at KDH (from the surf zone out to about 15 m depth) in 2006 that provides a high-resolution depiction of the nearshore region (Figure 4.2).

Rip current observations

KDH Ocean Rescue lifeguards recorded daily observations at 19 lifeguard chair locations to determine the presence and intensity of rip currents throughout the study area (Figure 4.1). The chairs are located between 200 m and 800 m apart along KDH and are occupied from 10 am to 5:30 pm, 7 days a week throughout the summer. The lifeguards performed daily observations to estimate rip intensity as 0 to 3 relative to the potential risk to swimmers. Each level of rip intensity is described as follows:

- 0 - No rip currents present
- 1 - Some low intensity rip currents present, may be hazardous to some swimmers
- 2 - Medium to strong rip currents present, will likely be hazardous to swimmers
- 3 - Very strong rip currents present, hazardous conditions

Each lifeguard recorded daily observations in the late afternoon to represent the conditions occurring at their location throughout the day. Observations were made from

June 1 to August 31 in 2008 and from May 31 to September 5 in 2009. On some occasions the observations were limited to a few chairs or missing altogether.

Previous research using ocean rescue observations has primarily utilized drownings (Lushine, 1991) or lifeguard rescues (Lascody, 1998; Engle et al., 2002; Scott et al., 2009; Chapter 3) to provide an indication of hazardous rip current occurrence. However, since rescues are dependent on swimmers being in the water and swimmer competency, a lack of rescues provides no information regarding rip current presence or absence. Lifeguard observations provide an estimate of rip intensity regardless of bather load. However, since the intensity observations are subjective they are validated against the rip current rescue record from the summer of 2009.

A binary analysis is made assuming that a rip intensity observation of 0 indicates no risk of hazardous rip currents occurring and an observation of 1,2 or 3 indicate some risk for hazardous rip currents occurring. When rescues occurred, the lifeguards observed a 1, 2 or 3 rip intensity 92% of the time. Assuming that all rescues indicate hazardous rip current occurrence, the lifeguard rip intensity observations can be estimated as 92% accurate in identifying hazardous rip conditions. The accuracy of lifeguard observations can be verified further by calculating the percentage of rescues and observations that occur for each level of rip intensity (0,1,2 or 3; Figure 4.3). Few rescues occur when there is a 0 rip intensity observation, while more rescues occur (24%) when there is a 1 rip intensity observation. When there is a level 2 or 3 rip intensity, significantly more rescues occur relative to the percentage of observations (68% of all rescues compared to 20% of all observations). This analysis shows that lifeguard observations are a reasonable estimate of the rip intensity within a relatively small margin of error. The

principle advantage of using rip intensity observations is the consistent data record of rip current observations, compared to the inherently discontinuous nature of rip current rescues.

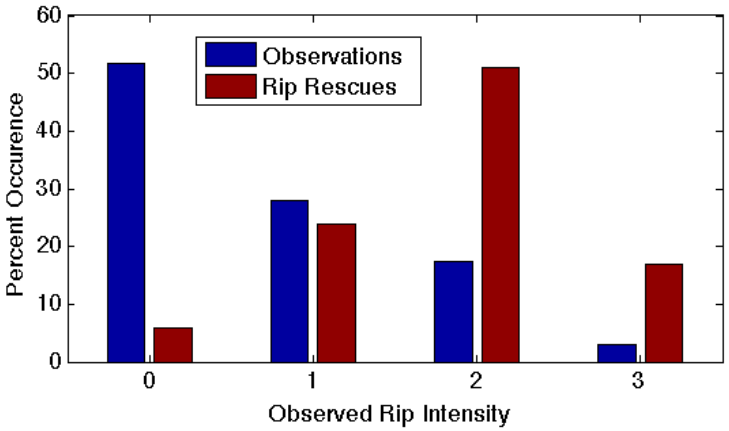

Figure 4.3 The percent occurrence of lifeguard rip intensity observations and rip current rescues for the summer of 2009. Each is normalized such that the value is the percent of the total observations or rescues.

4.3.2 Statistical analysis

The directional wave field

Statistical analyses are performed to determine the influence of daily average wave measurements on the daily beach-wide average rip intensity. Spectral measurements (e.g. significant wave height, peak period, mean direction) collected while lifeguards are on the beach (bi-hourly samples between 10 am and 5 pm) are temporally averaged. The wave field can change significantly over the course of the day and there is the concern that the average conditions might not be representative of all 7 hours guards are present. To address this concern the standard deviation is calculated for each wave statistic over the 4 bi-hourly samples each day (Table 4.1). Although there are a handful of instances when the standard deviations are large (typically if the onset of a large storm event falls during the day), the mean values indicate relatively small variations (Table

4.1). As such, it is reasonable to utilize the average wave statistic over the 4 bi-hourly samples. Results were similar using spectral component statistics and thus these data are averaged in the same manner. For a spectral component (e.g. wind sea or swell) to be included in the daily averages, it has to be present for at least two time samples.

Table 4.1 The average and maximum standard deviations of the daily averaged wave data. The standard deviation is calculated for the 4 bi-hourly bursts taken by the Northern ADCP between 10am and 5pm each day.

Measurement	Average STD	Max STD
Significant Wave Height	0.05 m	0.47 m
Mean Direction	6.2 deg	38.4 deg
Directional Spread	3.1 deg	11.1
Peak Period	0.9 sec	6.2 sec

The analysis of the wave field and rip intensity does not consider alongshore variability in the wave field. An analysis of the wave measurements from the northern and southern ADCP indicate that there are only slight differences in the wave field measured at each location, and that the differences in significant wave height are nearly always insignificant at the 95% confidence limits. Thus, the spectral statistics from both ADCPs are averaged together. When averaging statistics of spectral components (i.e., wind sea, dominant and secondary swell), care is taken to ensure that the same components are included.

The influence of wave spectral statistics on rip intensity is assessed through correlations and a comparison of distributions. The Kolmogorov-Smirnov statistical test (KS-test) is applied to identify significant differences between the rip intensity distributions relative to various spectral measurements (Chapter 3). The KS-test applied to two empirical non-parametric distributions can determine if the two distributions are

from the same underlying distribution within a certain confidence level or p-value (Conover, 1999). The KS-test will result in a minimum p-value for which the two distributions can be said to be different. For example, a KS-test resulting in a p-value of 0.02 would signify that the two distributions are different at the 98% confidence level.

The surf zone bathymetry

Significant alongshore variations in rip current intensity were observed at KDH. The wave field showed little variation between the two ADCP locations. Absent significant alongshore variations in the wave field at the ADCP locations, it is likely that bathymetry variations shoreward of the ADCPs influence the presence and intensity of rip currents at different locations alongshore. Bathymetry features between the surf zone and the ADCP location might induce alongshore variations in the wave field and thus contribute to the differences in rip intensity between north and south KDH. However, accurately assessing the wave field transformation in this region requires a computationally intensive phase resolving wave model, and is beyond the scope of this project. Surf zone bathymetry features are often the primary driver of rip current circulation (MacMahan et al., 2008), and an analysis of these features may explain alongshore variations in rip intensity. There are two phases of analysis. First, determine if profile features from each alongshore location vary in a similar manner throughout the summer. The variability between profile lines over the entirety of KDH will be referred to as large-scale variability (> 1 km). Second, determine if rip intensity is influenced locally by any surf zone features represented in the profiles.

A number of geometric features have been identified for each profile from 2008 and 2009 (Figure 4.4). These include: the average beach slope from 0.5 m above and below Mean High Water (MHW); the distance from where MHW intersects the profile line to the bar crest; the bar and trough depth from MWH; the difference between the bar and trough depth (from this point forward referred to as the bar-trough depth difference); and the trough volume (similar to Larson and Kraus, 1994). Trough volume is the cross-sectional volume (m^3/m) of water contained in the trough up to the bar crest. For instances when no bar is present in the profile the bar-trough depth difference and the trough volume are 0. In 2009 there were two profile lines collected at each chair location. The maximum, mean and difference between the geometric features are calculated for each profile pair in this instance. Most significant of these calculations is the bar depth difference between profile pairs. This value gives an indication of alongshore variability in the surf zone bar, which can drive rip current circulation (MacMahan et al., 2008). The variability seen between profile pairs will be referred to as small-scale alongshore variability (~ 50 m). For instances when only one profile of a pair has a bar, a proxy for bar depth (E_B or bottom elevation) is used for the non-barred profile so that the alongshore bar depth difference can be calculated. This proxy assumes the non-barred profile will have a bar depth,

$$E_B = D_B + 0.5(D_T - D_B), \quad (4.2)$$

where D_B is the bar depth and D_T is the trough depth of the barred profile.

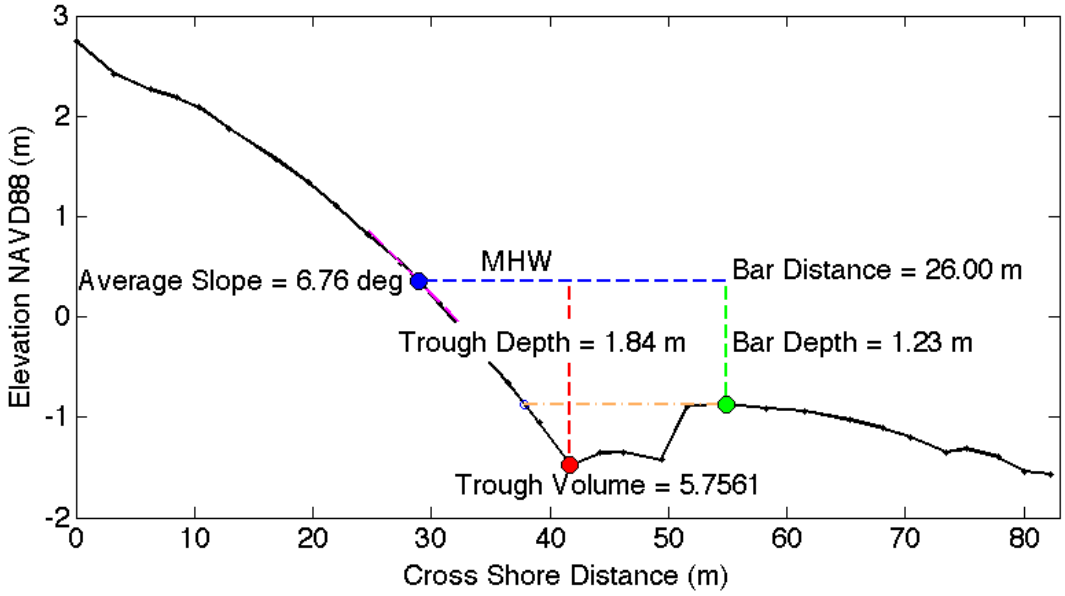

Figure 4.4 An example GPS profile from Clark Street on June 25, 2009. Cross-shore distance is measured from the initial sample point, which was kept constant for all profiles. Shown are the Mean High Water level and bar distance (blue-dashed), trough depth (red-dashed), bar depth (green-dashed), average slope at MHW (magenta-dashed) and trough volume (orange-dashed).

Three FRF surveys are utilized to determine if the GPS profiles extend far enough offshore to capture the surf zone bar features. The broader-scale FRF surveys completed in 2004 and 2006 serve as an additional reference for large-scale bathymetric variability. Many of the FRF profiles show the presence of two bars, a surf zone bar typically less than 50 m from the MHW location and an outer storm bar that is at least 90 m from MHW (Figure 4.5). The presence of two bars is fairly typical of this region (Larson and Kraus, 1994; Lippmann and Holman, 1990). The level rod and GPS surveys completed in 2008 and 2009 do not extend far enough offshore to capture the outer bar. However, the FRF surveys show that the surf zone bar is generally within the offshore range of the 2008 and 2009 surveys. The outer bar can have an influence on the wave field and on nearshore processes, but due to the aforementioned data limitations only the surf zone bar will be considered in this analysis.

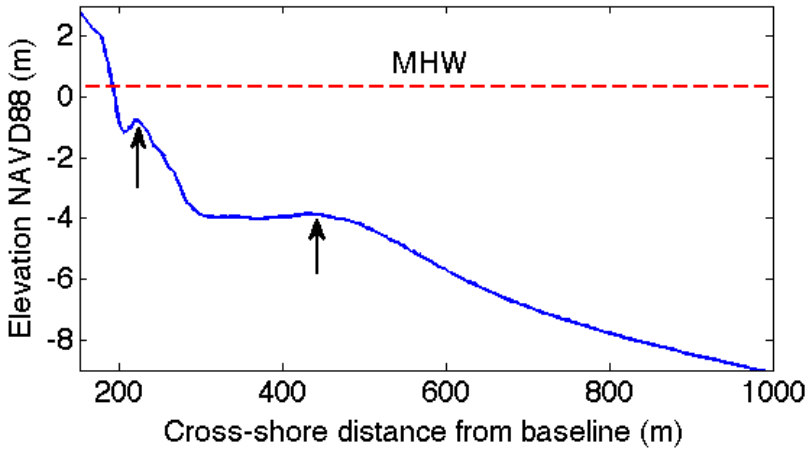

Figure 4.5 An example FRF LARC profile from Neptune Street in October, 2004. The surf zone and outer bars are shown (black arrows) along with Mean High Water (red dashed).

It is necessary to place the profiles within the context of wave field induced morphological change. Specifically, it is desirable to determine the most common morphology of KDH and the likelihood of significantly altering this morphology. The non-dimensional fall velocity, Ω, is used to determine modal beach states and as an indicator of sand bar permanence (Wright and Short, 1984; van Enckevort et al., 2004). The non-dimensional fall velocity is defined as:

$$\Omega = \frac{H_b}{T_p \omega_s}, \quad (4.3)$$

with H_b defined as the height of the breaking waves in the surf zone, T_p is the peak period and ω_s is the sediment fall velocity.

$$H_b = \left(\frac{\gamma}{g}\right)^{1/5} \left[H_{rms}^2 C_g \cos\theta\right]^{2/5}, \quad (4.4)$$

where γ is the breaker parameter set to 0.4 (van Enckevort et al., 2004), and θ is the angle of wave incidence at the breakpoint, which is set to 0 since that data is not available. H_{rms}

is the root-mean-square wave height, C_g is the group velocity and g is acceleration due to gravity.

$$\omega_s = \left[\left(\frac{\rho_s}{\rho_w - 1}\right) g\right]^{0.7} \frac{d_{50}^{1.1}}{6\nu^{0.4}} \quad , (4.5)$$

is the sediment fall velocity (Shore Protection Manual,1984), ρ_s is the density of the sediment and ρ_w is the density of seawater (2650 kg/m^3 and 1025 kg/m^3 respectively). The value d_{50} is the median grain size estimated at about 0.18 mm for this region (van Enckevort et al., 2004), and ν is the kinematic viscosity of seawater ($1x10^{-6}$ m^2/sec at 20° C).

The parameter Ω identifies a modal (most occupied) state for a particular beach, as well as temporal variations in that beach's state (Wright and Short, 1984). The beach state can be characterized as reflective ($\Omega < 1$), intermediate ($1 < \Omega < 6$) or dissipative ($\Omega > 6$). There typically will not be significant temporal changes in a beach state unless Ω crosses a threshold value (i.e. $\Omega = 1$ or 6). In the summer of 2009, KDH has an intermediate modal state (Ω between 3 and 4). This modal value corresponds to the intermediate state of rhythmic bar and beach (characterized by a deep trough and an alongshore-crescentic surf zone bar; Wright and Short, 1984). It is expected that KDH will maintain a rhythmic bar and beach morphology unless Ω varies. The most significant changes in the surf zone morphology of KDH will occur during relatively large wave events when Ω exceeds 6 and KDH becomes increasingly dissipative. At nearby Duck, NC it was found that a complete morphological reset of the surf zone bar system occurred when Ω exceeded 10 (van Enckevort et al., 2004). The rhythmic or alongshore variability in bar morphology was replaced with a more dissipative and

alongshore uniform morphology. Alongshore non-uniformities developed and the morphology took on an intermediate rhythmic bar and beach shape once wave energy decreased and Ω dropped back below 6. At nearby KDH significant changes in the surf zone morphology are expected when Ω exceeds 6, however a complete reset in alongshore variability is not expected until Ω reaches 10.

The second phase of the bathymetry analysis is to determine how differences in the surf zone bar system relate to rip intensity. Only data from 2009 have been used in this analysis because of higher quality bathymetry and lifeguard data. The rip intensity observations made at each profile location were analyzed over a seven-day period (three days prior to and after the profiles were collected). Rip intensities are taken as individual observations (in which case 0 = no rips or 1,2,3 = rips) or averaged over the seven-day period. There is a relatively small sample size of rip intensity observations, and slight biases may exist depending on the observer (e.g. differing observations of what constitutes a 1 or 2 rip rating). These biases could influence results for one particular chair. To address this concern, the analysis of the bathymetric influence is considered more robust when comparisons over multiple chair locations are utilized (i.e. comparing the rip intensity with bar features over the northern three chairs to that of the southern three chairs).

The rip intensity observations are compared to the mean, maximum and difference in the geometric features identified in the profile pairs. The profiles are assumed to be reasonably valid for three days before or after the survey date as this is a conservative estimate of the time required to affect significant changes in the surf zone bar system at this location during low wave energy (or $1 < \Omega < 6$) conditions (Larson and

Krauss, 1994; Lippman and Holman, 1990). The seven-day period was shortened on occasions when Ω exceeded 6 and more dramatic changes in the surf zone might occur.

4.4 Results

4.4.1 The influence of the wave field on rip intensity

Bulk spectral measurements

Rip intensity increases with significant wave height, when the mean direction is close to shore-normal and with narrower values of directional spread (Table 4.2). The measurements of peak period show little correlation with the average rip intensity. The significant wave height correlates with rip intensity at a relatively high normalized value of 0.67 at 0 lag (1 lag = 1 day), while the mean direction and spread are inversely correlated to rip intensity at values of -0.40 and -0.63 respectively. The peak period demonstrates no significant correlation. Additionally, the significant wave height and mean direction demonstrate correlation with rip intensity at 1 day lag (0.61 and -0.42 respectively) that is statistically equivalent to the 0 lag correlation. The shoaled and refracted wave height and direction correlate with rip intensity with about the same magnitude as the observed height and direction (the differences are insignificant at the 95% confidence level). Mean direction and spread also correlate fairly well with wave height, and thus at least part of their correlation with rip intensity may be due to this relationship. An attempt to isolate the relationship between spread and wave direction with wave height is presented later in this section.

Table 4.2 Correlation coefficient matrix for rip intensity and spectral statistics at 0 lag. Significant correlations at 95% confidence level are bolded.

Bulk Spectral Statistics

	Rip Int	Hs	Mean Dir	Spread	Peak Period	Hs 3m	Dir 3m
Rip Int	1.00	**0.67**	**-0.40**	**-0.63**	-0.05	**0.70**	**-0.34**
Hs	-	1.00	**-0.42**	**-0.77**	**-0.18**		
Mean Dir	-	-	1.00	0.11	**0.29**		
Spread	-	-	-	1.00	**0.20**		
Peak Period	-	-	-	-	1.00		

One Swell Spectral Statistics

	Rip Int	Hs	Mean Dir	Spread	Peak Period
Rip Int	1.00	**0.83**	**-0.53**	**-0.73**	-0.03
Hs	-	1.00	**-0.45**	**-0.83**	-0.11
Mean Dir	-	-	1.00	**0.37**	0.03
Spread	-	-	-	1.00	**0.29**
Peak Period	-	-	-	-	1.00

Distributions of the spectral measurements can be created by sub-sampling based on rip intensity. The distributions of spectral measurements of the 0, 1 and 2-3 rip intensity observations can be distinctly different depending on the spectral measurement against which they are compared (Figure 4.6). The significant wave height distribution shifts from reaching a maximum at 0.5 m for 0 rip intensity, to 0.6 m for 1 rip intensity to 0.8 m for 2 or 3 rip intensity (Figure 4.6 A). The distributions are statistically different at a high confidence-level (Table 4.3). The 1 and 2-3 rip intensity values have distributions that are much broader than the distribution for 0 rip intensity, which is narrow and highly peaked at low wave heights. This suggests that very little or no rip activity exists at low wave conditions, but that rip intensity values of 1,2 or 3 can occur over a wide range of wave heights. The shoaled and refracted wave height distributions show a very similar relationship, although with a slightly larger range of wave heights (Figure 4.6, C).

Table 4.3 The p-values for the two sample KS-test between the distributions of different rip intensity observations		
Measurement	**p-value**	
Entire 2d Spectrum	**0 and 1 RI**	**1 and 2-3 RI**
Significant Wave Height	$8x10^{-60}$	$8x10^{-32}$
Mean Direction	$2x10^{-42}$	$21x10^{-4}$
Directional Spread	$8x10^{-20}$	$5x10^{-28}$
Peak Period	$2x10^{-4}$	0.25
3m Significant Wave Height	$2x10^{-96}$	$6x10^{-39}$
3m Mean Direction	$2x10^{-39}$	$5x10^{-6}$
1 Swell Only		
Significant Wave Height	$1x10^{-40}$	$8x10^{-23}$
Mean Direction	$8x10^{-21}$	$2x10^{-10}$
Directional Spread	$4x10^{-22}$	$4x10^{-22}$
Peak Period	0.07	0.21
Wind Sea Dominated		
Significant Wave Height	$2x10^{-15}$	$2x10^{-4}$
Mean Direction	$2x10^{-4}$	0.08
Directional Spread	$1x10^{-5}$	0.01
Peak Period	$4x10^{-4}$	0.07

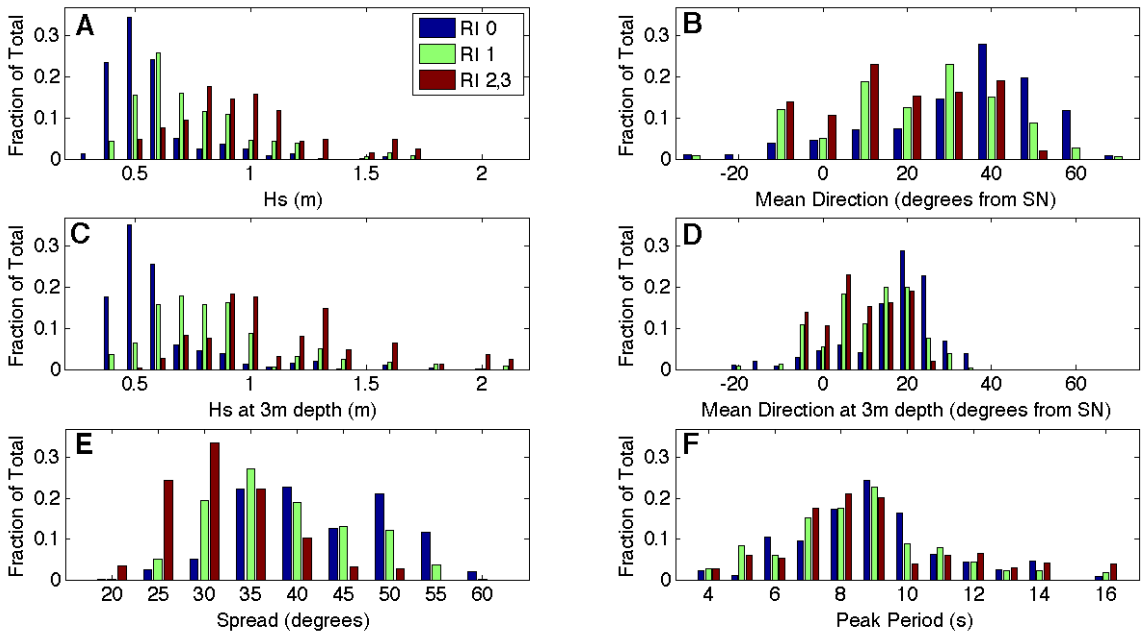

Figure 4.6 Normalized histograms representing the distributions of the 0, 1 and 2-3 rip intensity observations for each bulk spectral measurement. Each distribution represents all rip intensity observations made for each day and chair location over the course of the summers of 2008 and 2009. The plots are of the significant wave height (A), mean direction (B), the shoaled and refracted significant wave height to 3 m depth (C), the refracted wave direction at 3 m depth (D), directional spread (E) and peak period (F).

For the mean direction the 1 and 2-3 rip intensity distributions are both shifted toward shore-normal compared to the 0 rip intensity distribution (Figure 4.6 B). The refracted wave direction shows a similar shift, although the range of wave directions is tightened considerably (Figure 4.6 D). The mean direction distributions are also statistically different at a high level of confidence (Table 4.3). Similarly, the 1 and 2-3 rip intensity distributions are shifted toward narrower directional spread and are again different at a high level of confidence (Figure 4.6 E). Conversely, the peak period distributions are all very similar, suggesting that peak period does not significantly influence rip intensity (Figure 4.6 F).

The dataset can alternatively be viewed as average rip intensity values for a given spectral measurement. The average rip intensity values for each spectral measurement

are similar to the rip intensity distributions (Figure 4.7). An increase in significant wave height has a clear influence on the rip intensity. Average rip intensity increases dramatically between wave heights of 0.6 m and 0.8 m (Figure 4.7 A). The level of rip intensity for low wave heights is even lower when analyzing the shoaled and refracted wave height (Figure 4.7 C). Rip intensity for wave heights of less than 0.7 m are nearly 0 in this case, suggesting that smaller waves that also experience relatively little growth due to shoaling (e.g., shorter period and less energetic wind sea) rarely cause significant rip currents to occur.

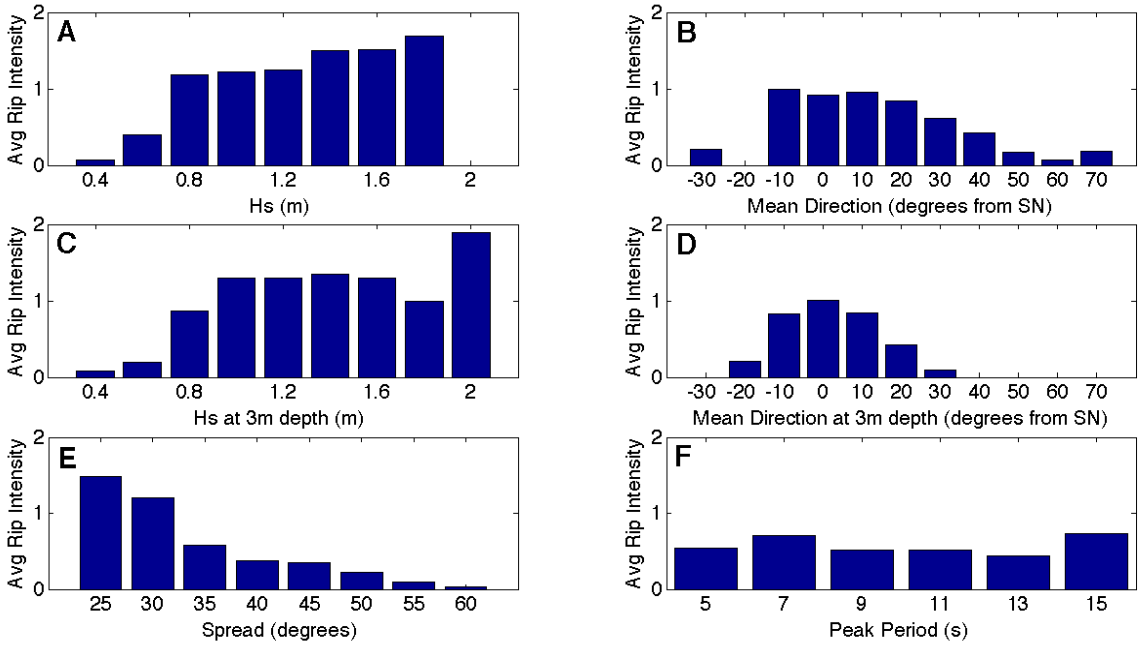

Figure 4.7 Plots of the beach wide rip intensity averaged for each bin width. Each value represents the average rip intensity made when the daily spectral measurements were in that bin range for the summer of 2008 and 2009. The bulk spectral measurements shown are of the significant wave height (A), mean direction (B), the shoaled and refracted significant wave height to 3 m depth (C), the refracted wave direction at 3 m depth (D), directional spread (E) and peak period (F).

The average rip intensity is highest with close to shore-normal mean wave direction (Figure 4.7 B). When the direction is refracted to 3m depth, this relationship is

even more evident as the histogram has a fairly normal shape, peaked at 0 degrees (Figure 4.7 D). The average rip intensity is also greatest when directional spread is minimal (Figure 4.7 E). Variations in the peak period again appear to be insignificant to rip intensity (Figure 4.7 F).

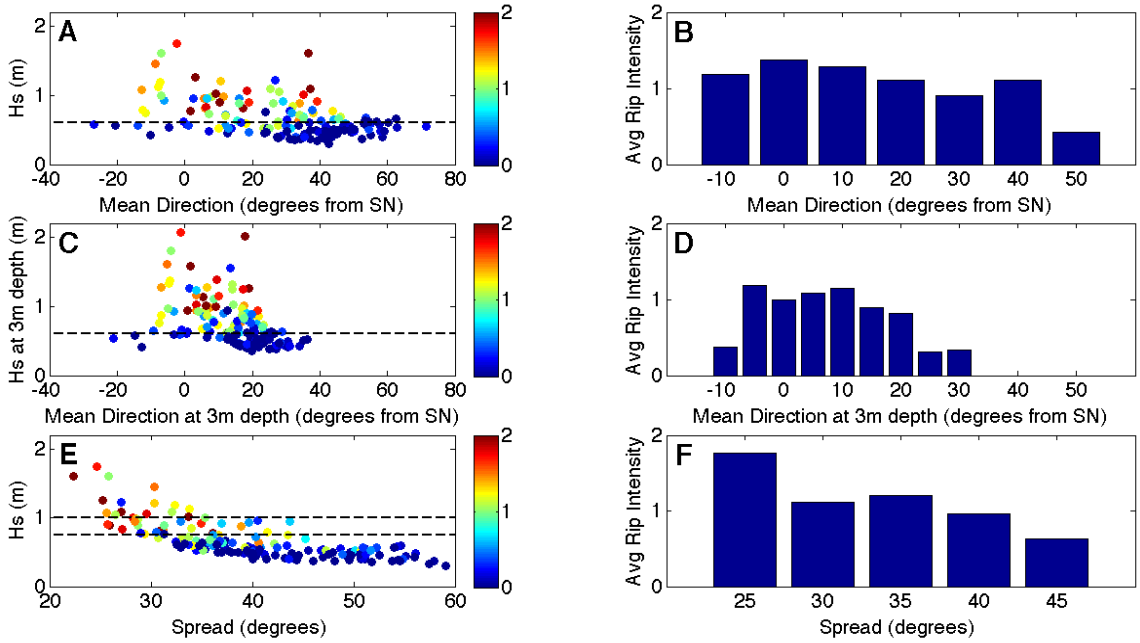

Figure 4.8 The left-most plots show scatter plots of the mean direction (A) and spread (E) against the significant wave height and mean direction against wave height at 3m depth (C). Each data pair represents the daily averaged measurements from the summer of 2008 or 2009. The magnitude of the beach wide averaged rip intensity for each data pair is shown with dark blue representing low rip intensity magnitudes and red representing high magnitudes. The dashed black lines indicate the portion of data plotted as a rip intensity bar plot to the right. For the mean direction and 3m refracted mean direction, all points with a significant wave height (or Hs at 3m) of 0.6 m or greater are plotted on the rip intensity plot to the right (B and D). For the spread, all points with a significant wave height between 0.75 m and 1.0 m are plotted on the rip intensity plot (F).

Wave height is significantly correlated to both directional spread and mean direction, which complicates determining the relative contribution of each variable. This correlation is shown through a 2d representation of the data (Figure 4.8 A, C, E). Average rip intensity plots are made for a sub-sampled portion of the data in an attempt to

minimize the correlation with wave height (Figure 4.8 B, D, F). For the mean direction and refracted direction, only heights over 0.60 m are included. For spread, only wave heights between 0.75 and 1.0 m are included. When these subsets are plotted as rip intensity averages, there remains an increase in rip intensity with shore-normal wave direction (Figure 4.8 B, D) and with narrower spread (Figure 4.8 E). However, both relationships are less pronounced than when the entire data set is plotted (Figure 4.7).

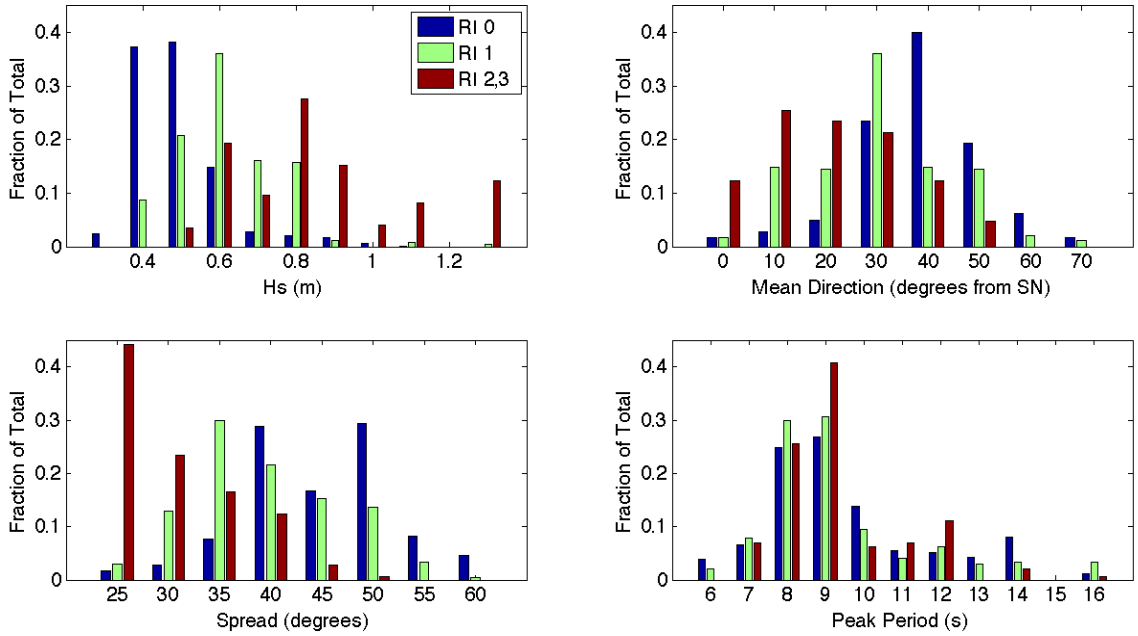

Figure 4.9 Normalized histograms representing the distributions of the 0, 1 and 2-3 rip intensity observations for each dominant swell component measurement. Each distribution represents the rip intensity observations made for each day and chair location over the course of the summers of 2008 and 2009 when the wave field constituted only a single dominant swell. The plots are of the significant wave height (top left), mean direction (top right), directional spread (bottom left) and peak period (bottom right).

The partitioned wave field

Analysis of wave field components (wind sea, dominant swell, secondary swell) yields similar results to the analysis of the bulk spectral measurements. Out of the 161 total days, 81 were characterized by only one dominant swell, 22 days by two swells and

58 days with wind sea present (28 of which were predominantly wind sea). A correlation between dominant swell statistics and rip intensity yields similar results to the correlation done with the bulk statistics. There is a slightly stronger correlation for significant wave height, spread and mean direction with rip intensity (0.83, -0.73 and -0.53 respectively). Again, the peak period shows no evidence of correlation with the rip intensity.

The distributions of the rip intensity observations, when one dominant swell is present, are also very similar to the distributions calculated for the bulk spectral measurements (Figure 4.9); rip intensity increases with significant wave height, shore-normal wave direction and narrower spread and is un-influenced by peak period. The similarities between the bulk spectral measurements and the one-swell measurements may not be surprising. When only one swell is present the swell component spectra will be essentially the same as the entire spectra. In addition, days with primarily only one swell present make up roughly half of all the days sampled (81 out of 161).

For the 28 days of predominantly wind sea the rip intensity distributions are slightly different (Figure 4.10). Rip intensity increases with significant wave height and as mean direction approaches shore-normal, however a relationship with the directional spread is not as clear. The peak for the 2-3 rip intensity distribution is at 30 degrees compared to 25 degrees for the one swell case and the statistical difference between each of the rip intensity distributions is not as evident (Table 4.3). Rip intensity also shows some dependence on the peak period. The 1 and 2-3 rip intensity distributions are shifted slightly towards longer period waves compared to the 0 distribution and have a higher confidence of statistical difference (Table 4.3).

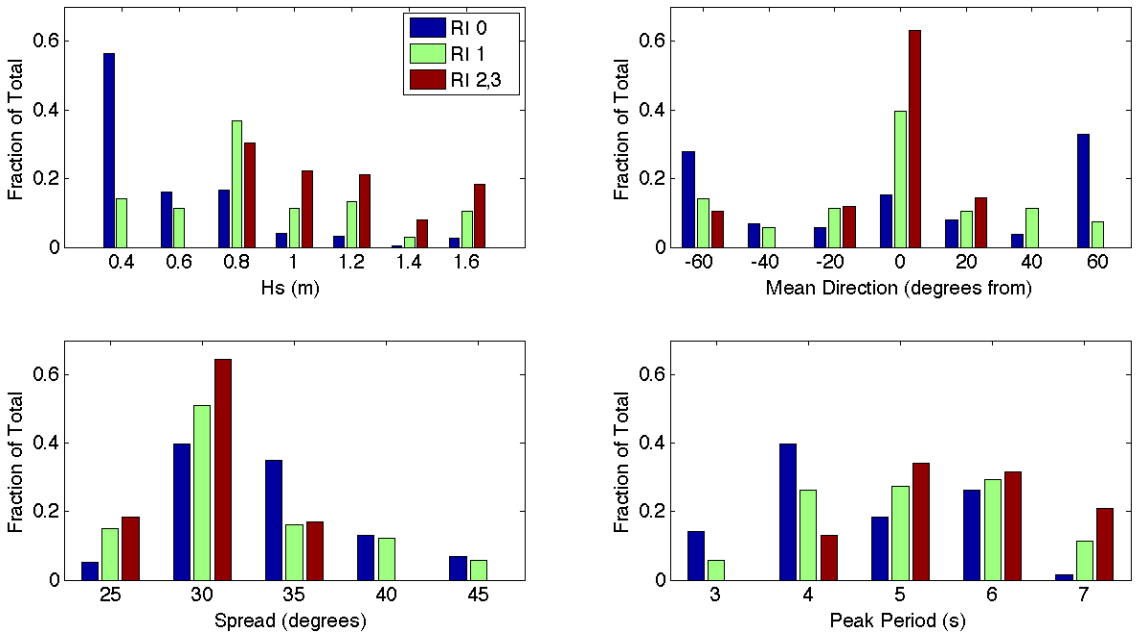

Figure 4.10 Normalized histograms representing the distributions of the 0, 1 and 2-3 rip intensity observations for each wind sea component measurement. Each distribution represents the rip intensity observations made for each day and chair location over the course of the summers of 2008 and 2009 when the wave field constituted primarily wind sea. The plots are of the significant wave height (top left), mean direction (top right), directional spread (bottom left) and peak period (bottom right).

A direct comparison between spectral measurements of the one-swell and wind sea conditions are made with the average rip intensity (Figure 4.11). The rip intensity for both components increases with larger significant wave heights, however under swell conditions rip intensity is higher from 0.5 m to 1.3 m (there are no average swell components with a wave height over 1.3 m). The rip intensity for mean direction is very similar for both wind sea and swell over the range of observations. The spread measurements show that rip intensity for swell components is nearly twice as high as the wind sea component intensity for the 22.5 to 27.5 degree range. The rip intensity for wind sea peak period shows a large increase from 7 to 9 seconds, while the swell component shows no relationship with period.

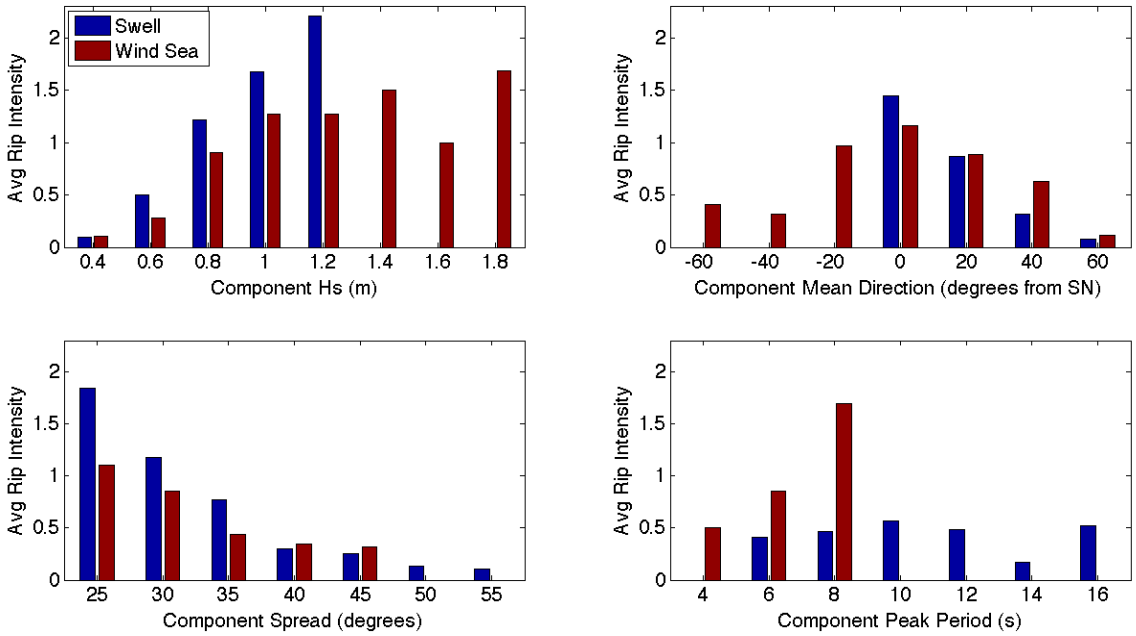

Figure 4.11 Plots of the beach wide rip intensity for either dominant swell (blue) or wind sea conditions (red). Each value represents the average rip intensity made when the daily spectral component measurements were in that bin range for the summer of 2008 and 2009. The bulk spectral measurements shown are significant wave height (top left), mean direction (top right), directional spread (bottom left) and peak period (bottom right). When there is no data plotted it is because that component measurement never reached those values.

Analysis of two-swell wave fields is complicated as the presence of two components makes using many of the prior analyses difficult. Prior research has suggested that when two swells are present, rip activity increases when the swells arrive from opposing oblique angles (Chapter 3). Although there are only 22 days when two swells are present, there is some evidence suggesting that swells at opposing angles do increase rip intensity. Two swells with mean directions from 50 to 90 degrees apart result in relatively higher levels of rip intensity than instances when both swells arrive from similar directions (Figure 4.12). However, the limited number of data points in each bin somewhat limits confidence in this result. Significant wave height is an

important consideration as low energy days (Hs < 0.6 m) rarely have high levels of rip intensity even when the swells are highly opposed. The one exception is an instance where the total wave height is 0.52 m yet the rip intensity average was a relatively high 1.2. The mean direction of the components is 80 degrees different in this case, lending credence to the notion that two opposing swells can create hazardous rip current conditions.

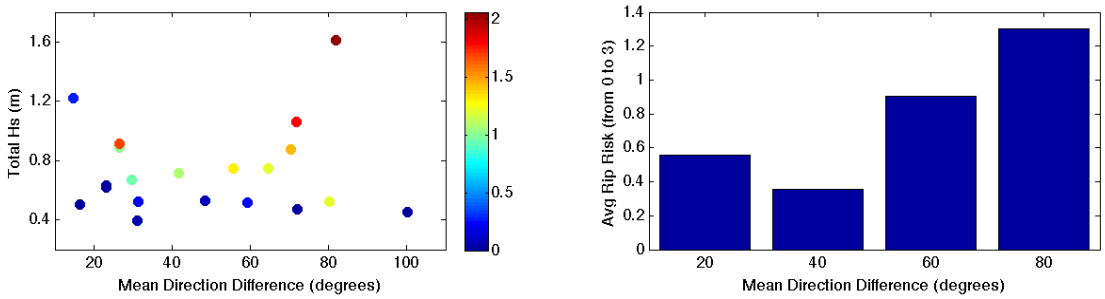

Figure 4.12 The left plot shows a scatter plot of the mean direction difference between two swell components against the total significant wave height. Each data pair represents the daily averaged measurements when two swells were present from the summer of 2008 or 2009. The magnitude of the beach wide averaged rip intensity for each data pair is shown with dark blue representing low rip intensity magnitudes and red representing high magnitudes. The same mean direction difference data is shown on the right plotted as average rip intensity.

4.4.2 The influence of the surf zone bathymetry on rip intensity

Large-scale alongshore variability

The bar-trough depth difference and the cross-sectional trough volume are two profile features that indicate how substantial the bar system is at a sample location. These features tend to co-vary and the alongshore variability of both features suggest how the surf zone of KDH develops over the summer. The first survey (June 25th, 2009) shows a relatively significant surf zone bar along all of KDH (Figures 4.13 and 4.14). There is some small- (~50 m) and large-scale (beach-wide) alongshore variability in the size of the

bar, however there is a bar evident at every sample location. Three weeks later (July 15th) there is no longer a measureable bar at one of the profile lines at Hayman and Third Street and the size of the bar has decreased at nearly every location. By the third survey (13 days later on July 28th) there is a significant alongshore shift in the development of the bar system. The bar over the three most northern locations is nearly gone, while each of the three southern locations has a large bar (Figures 4.13 and 4.14). By the last survey date on September 16, small bars are found in only a few profiles along all of KDH.

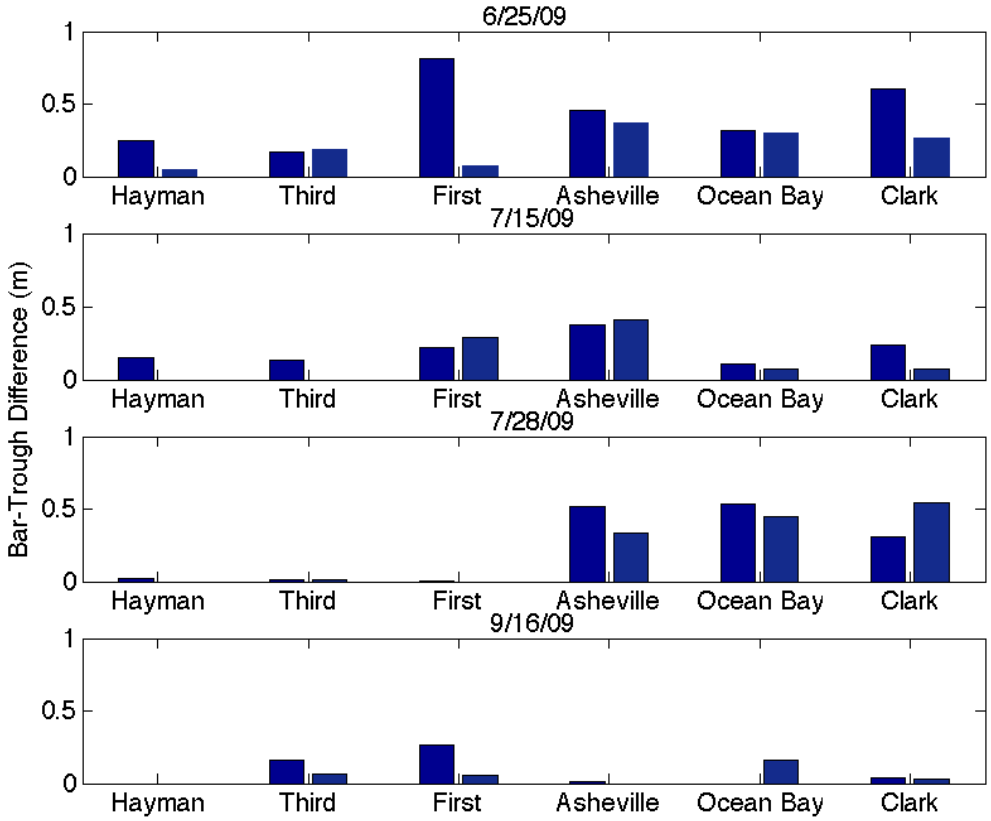

Figure 4.13 Bar plots showing the difference between the bar depth and trough depth along a particular profile from surveys in 2009. The date of collection is shown above each panel. For each location both the northern (leftmost) and southern (rightmost) profile lines are shown. Each profile pair is 50m apart.

Bars were less evident in 2008. Similar to 2009, the bar-trough depth difference shows a more significant bar in the south of KDH compared to the north in the latter half of the summer (Figure 4.15). There is only one FRF summertime survey from 2004, but the measures of bar-trough difference and trough volume also suggest a more significant bar in the southern half of KDH (Figure 4.16). These data suggest that late in the summer the southern portion of KDH often has a more substantial surf zone bar system than the northern portion of KDH.

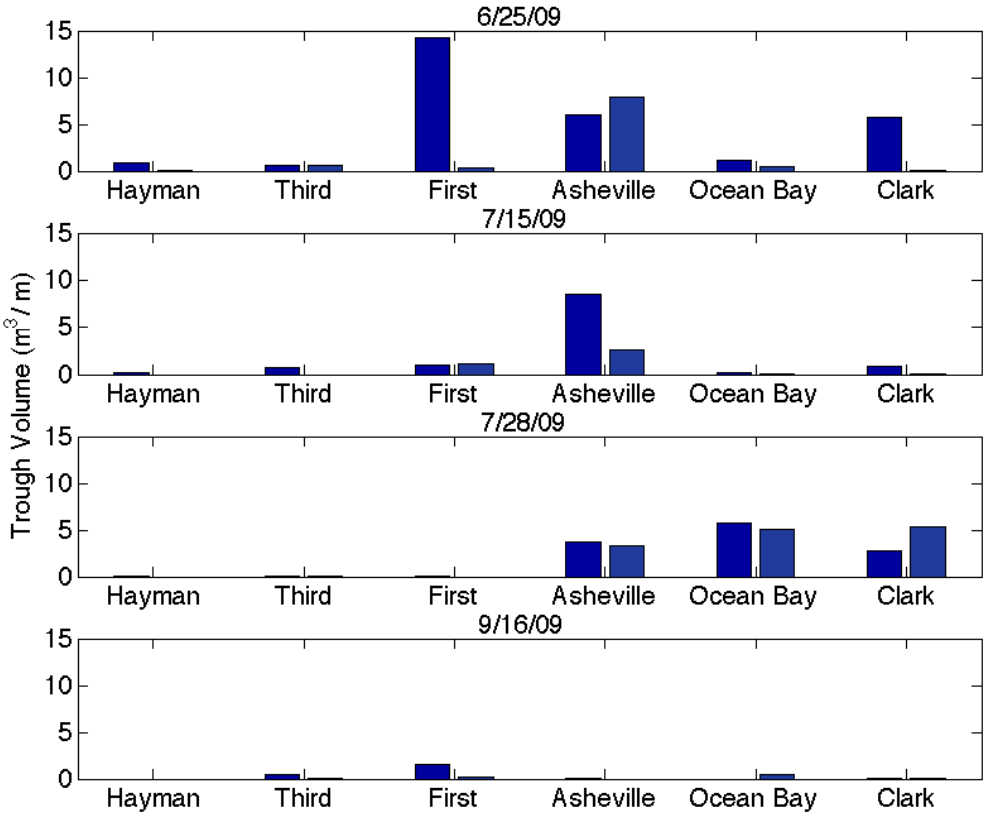

Figure 4.14 Bar plots showing the cross-sectional (two-dimensional) trough volume along a particular profile from surveys in 2009. The date of collection is shown above each panel. For each location both the northern (leftmost) and southern (rightmost) profile lines are shown. Each profile pair is 50m apart.

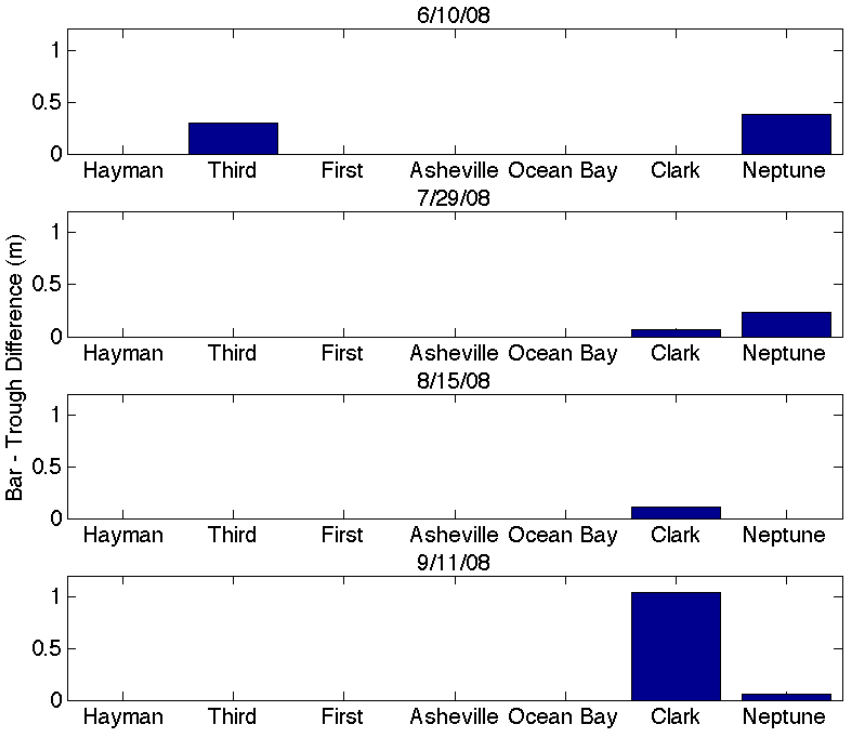

Figure 4.15 Four bar plots showing the difference between the bar depth and trough depth along a particular profile. Each plot runs north (left) to south (right). The profiles from the survey completed on 7/3/08 are excluded because none of the profiles had a surf zone bar present. Only a single value is plotted for each location, as in 2008 only a single profile line was collected at each location.

Temporal changes in the profile features suggest that the surf zone in the north and south of KDH develops differently over the course of the summer of 2009 (Figure 4.17). Over the last two survey dates of 2009 the trough volume and bar-trough difference of the northern and southern portions of KDH have opposite trends. The larger bar systems tend to be further from the MHW point. The bars tend to be furthest from shore early in the summer progressing to small bar features that are close to shore by the early fall, with bar distance trending to alongshore uniformity by the last survey. Conversely, the mean slope at MHW is relatively alongshore uniform early in the summer, and then varies dramatically alongshore by the final survey.

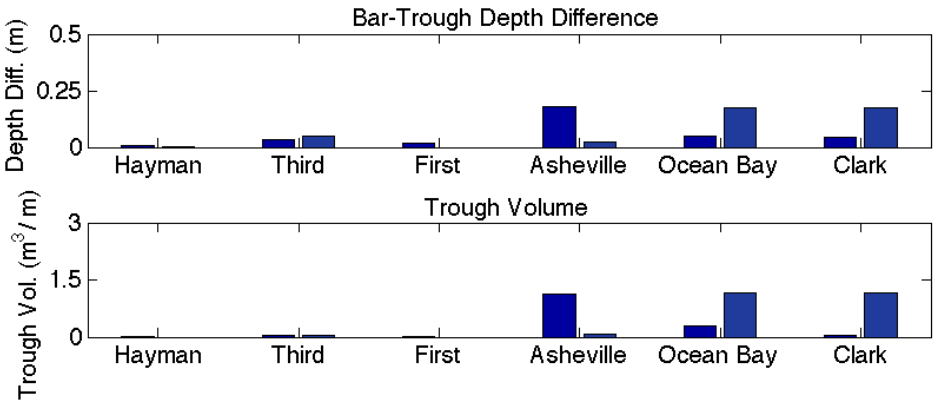

Figure 4.16 Plots resulting from a survey completed by the FRF LARC system on August 23 and 24, 2004. Shown are the difference between the bar depth and trough depth along a particular profile (upper) and the cross-sectional (two-dimensional) trough volume along a particular profile (lower). The two values shown for each location correspond to the FRF profile lines closest to the northern and southern profile lines sampled using the GPS in 2009. Each profile pair is about 300m apart.

The changing wave energy experienced at KDH throughout the summer provides a potential mechanism for the surf zone response. The early summer is characterized by low energy conditions (Hs of 0.4 m to 0.8 m) punctuated by several moderate wave energy events (Hs > 1 m; Figure 4.18). Each of the first three surveys was conducted a few days after one of these moderate wave events, and depicts the surf zone response to these events. Assuming Ω must exceed 10 to cause a full morphological reset in this region (Van Enckevort et al., 2004), none of the wave events immediately preceding the first three surveys is sufficient for this to occur (Figure 4.18). The wave event on June 17th has a maximum significant wave height of 1.49 m and Ω=11.1, and is followed by a short-lived wind sea event on June 21st that has a maximum Ω of 10.5, but the 10 threshold is only exceeded for a two-hour period. The next wave event, immediately preceding the first survey on June 25th has a maximum Ω of 7.9 and Ω=10 is not exceeded again until August 31st.

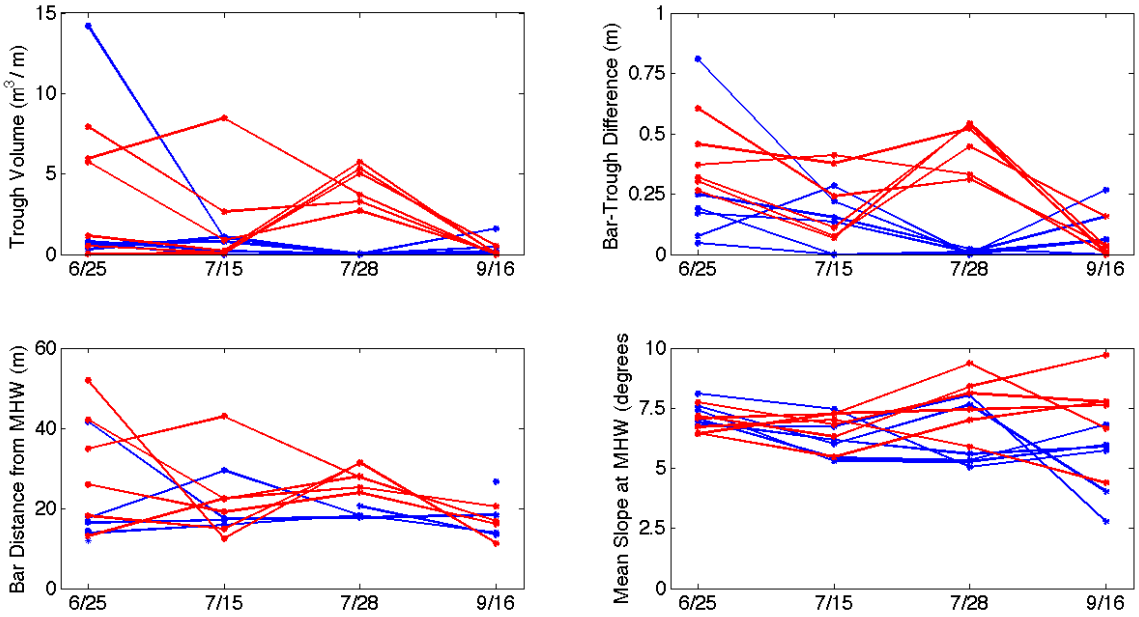

Figure 4.17 Shown are plots of the cross-sectional (two-dimensional) trough volume (top left), the difference between the bar and trough depth for a given profile (top right), the distance from the MHW line and the bar crest (bottom left), and the mean slope within .5 m of MHW (bottom right). The values correspond to the GPS surveys completed at KDH in 2009. Values from the southern three locations are shown in red and values from the northern three locations are shown in blue.

Comparison of the wave data and survey results suggest that the further removed a survey is from a wave event with $\Omega > 10$, the larger the bar system is in southern KDH compared to northern KDH. The survey on June 25th is only a few days following a threshold event, and the bar system is relatively large along all of KDH (Figures 4.13 and 4.14). The two surveys 25 and 38 days following the last wave event with $\Omega > 10$ reveal a more substantial bar system in the south compared to the north. The final survey on September 16th follows two high-energy wave events which both exceed the Ω threshold. The profiles illustrate a bar system that is more uniform alongshore although also less substantial than during the early summer.

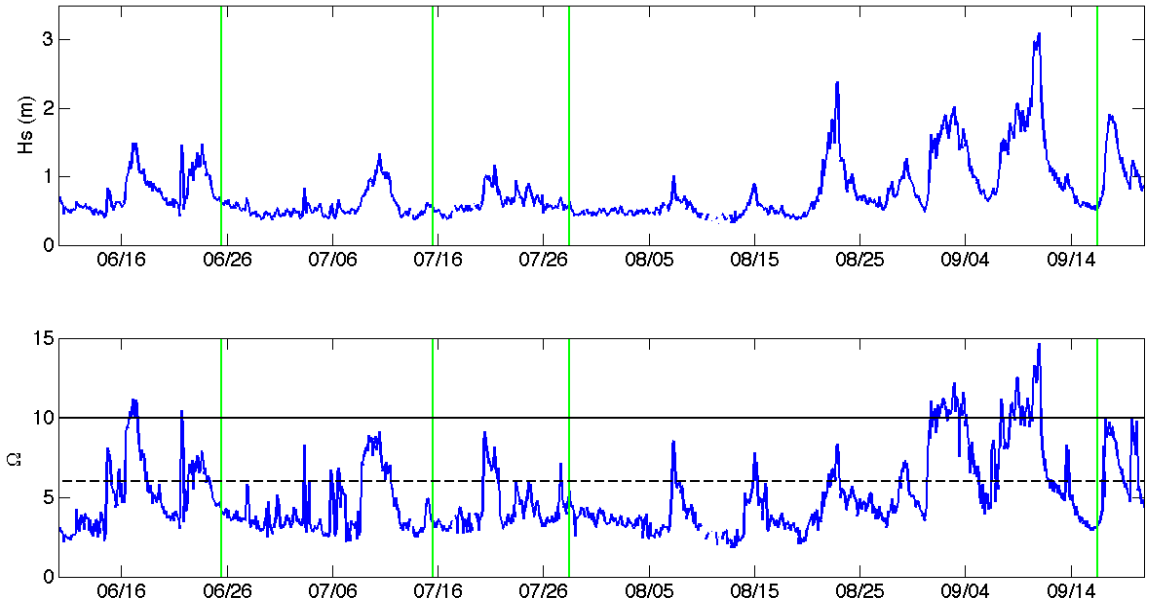

Figure 4.18 The bi-hourly record of significant wave height (top) and the non-dimensional fall velocity Ω (bottom) from the summer of 2009. The green vertical lines indentify the days when surf zone surveys were completed. The $\Omega = 6$ (black dashed) and the $\Omega = 10$ (black solid) thresholds are shown.

The summer of 2008 also experiences relatively low wave energy throughout, and the profiles suggest that bar formation is more significant in the south than the north (Figure 4.15). There is a large wave event with $\Omega > 10$ just before the survey on September 11th, and yet the surf zone bar system does not become uniform from northern to southern KDH as it does after a large wave event in 2009. This suggests that low wave energy may favor a mode in which the surf bar system is more substantial in the southern portion of KDH. However, a large morphological reset event ($\Omega > 10$) does not ensure a shift to similar surf zone bars along all of KDH.

Correlation of surf zone bathymetry with rip intensity

The three surveys from 2009 performed while the lifeguards recorded rip intensity observations enable a correlation of the surf zone profile features with rip intensity. For the surveys completed on July 15th and July 28th the rip intensity observations are averaged over a seven-day period, assuming that the profiles are valid estimates of the surf zone for three days prior to and after the surveys (Figure 4.19). For the survey completed on June 25th, the rip intensity observations are only averaged over a five-day period, since two and three days prior to the survey Ω was consistently > 6. Although Ω exceeded 6 on the day prior to the July 28th survey, it only exceeded 6 for one bi-hourly record, and thus the valid time period was not abbreviated.

The mean, maximum and difference of the geometric features identified in the two profile lines at each location are correlated with the average rip intensity. The only features that demonstrate a correlation with rip intensity are the maximum or mean bar-trough depth difference and the difference in bar depth for a profile line pair. The limited number of profiles available results in uncertainty regarding the precise influence of these features on rip intensity. However, when plotted against rip intensity the four highest average rip intensity instances correspond to the four largest measures of bar depth difference between profile pairs. Further, all four of these instances have relatively large mean bar-trough depth differences (Figure 4.20).

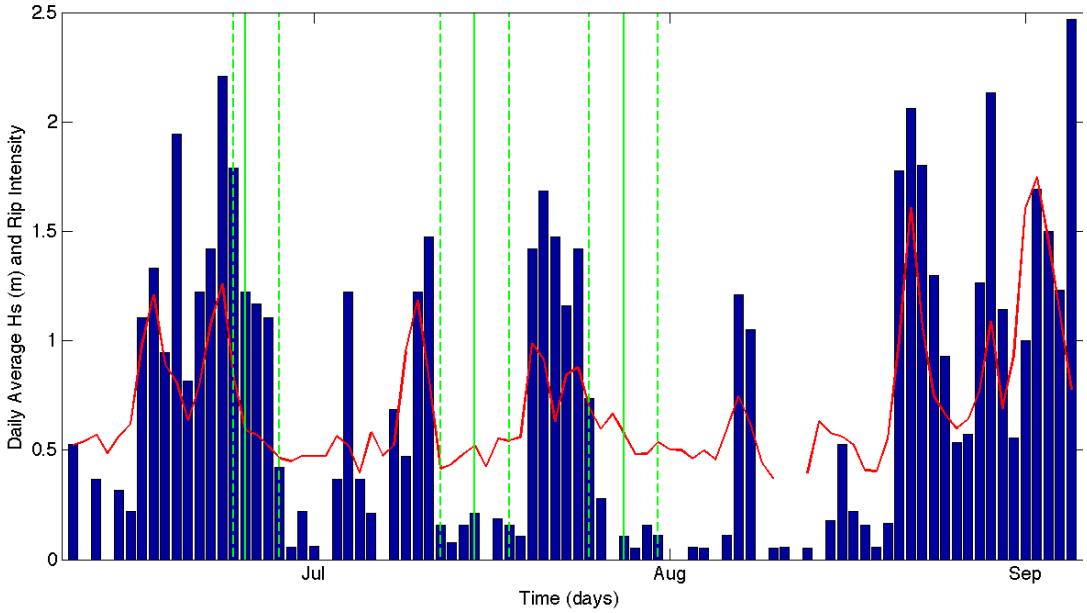

Figure 4.19 The daily averaged significant wave height observations (red line) and beach-wide averaged daily rip current intensity observations (blue bars) are shown. Also shown are the survey dates (green-solid) and valid rip intensity time periods for each survey (green-dashed). The significant wave height is averaged from the measurements of both the northern and southern ADCP from 10-5pm each day.

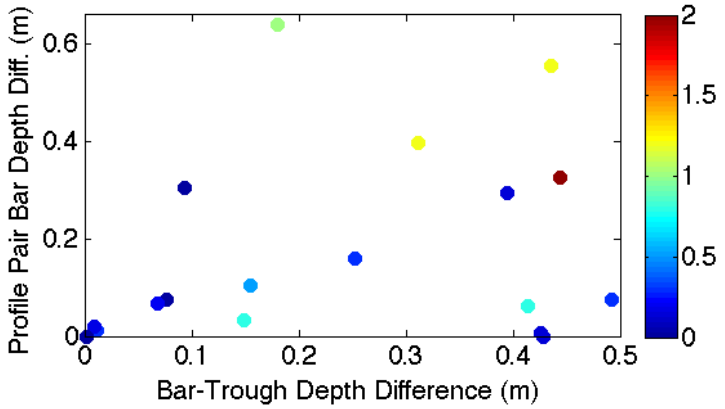

Figure 4.20 Scatter plot of the depth difference between the bar and trough of each profile (values from each profile pair are averaged) and the difference in bar depth between a profile pair. The colorbar represents the average rip current intensity observed at the profile location over the valid time period (ranging from 5 to 7 days). Data is from the three GPS surveys performed in June and July of 2009.

An additional consideration is the influence of the wave height on rip intensity levels; high levels of rip intensity are rare when the wave height is below about 0.7 m. Since wave heights are relatively low during surveys because these are the only times when data collection could be carried out safely, rip intensity will generally be lower during these periods. Wave height has been plotted against both the bar-trough depth difference and the difference in profile pair bar depth to assess the contribution of both wave height and bar features on rip intensity (Figure 4.21).

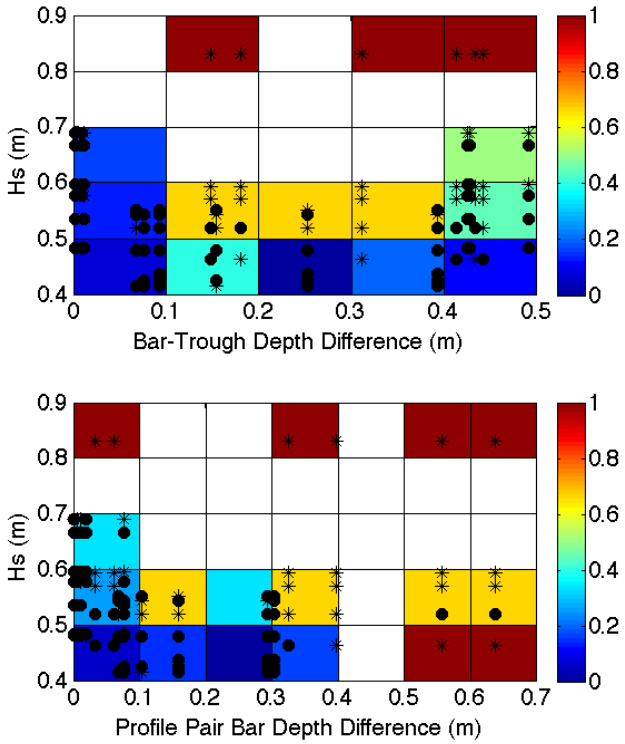

Figure 4.21 Binned and scatter plots of the depth difference between the bar and trough of each profile (values from each profile pair are averaged) vs. significant wave height (top) and of the difference in bar depth between a profile pair vs. significant wave height (bottom). Each black point represents the daily observation of each value at a particular profile location and is marked as rip currents observed (star) or not observed (circle). The binned color plot shows the fraction of observations in each bin that indicated a rip current was present. No observations were recorded for the white bins.

Although sparsely populated, the data comparison shows that rip currents are unlikely when both the wave height is low (< 0.7 m) and bar features are small (<0.1 m). The data suggests that rip likelihood will increase as these values increase. The effect of the bar features at a given wave height is especially important. Within the wave height range of 0.5 to 0.6 m rip currents occur fairly often when the bar-trough difference is at least 0.10 m and when there is some alongshore variation in the bar height (> 0.10 m). There are even two instances when the wave height is under 0.5 m and rip currents are observed, apparently because there was a substantial difference in the bar height alongshore (> 0.5 m). This instance provides an example of how a substantial alongshore variable bar can drive some rip circulation even when there is relatively low wave energy.

The influence of the bar-trough depth difference and profile pair bar depth difference can also be determined through a comparison of two surveys. The rip intensity observations made for the survey performed on July 15th are dominated by low wave energy levels (seven-day average of 0.48 m). These are wave height levels that generally do not produce much, if any, rip current activity. While the mean significant wave height during the June 25th and July 28th survey periods is still relatively low (0.60 m and 0.58 m respectively), the survey periods are energetic enough to lead to some rip intensity and are compared further.

The profiles from June 25th show a surf zone bar system with relatively large bars that vary significantly in depth alongshore over both small- (~50m) and large-scales (beach-wide; Figure 4.22). Average rip intensity exceeds 0.8 at every location and reaches a maximum of 2 at First Street. The profiles from the July 28th survey suggest a

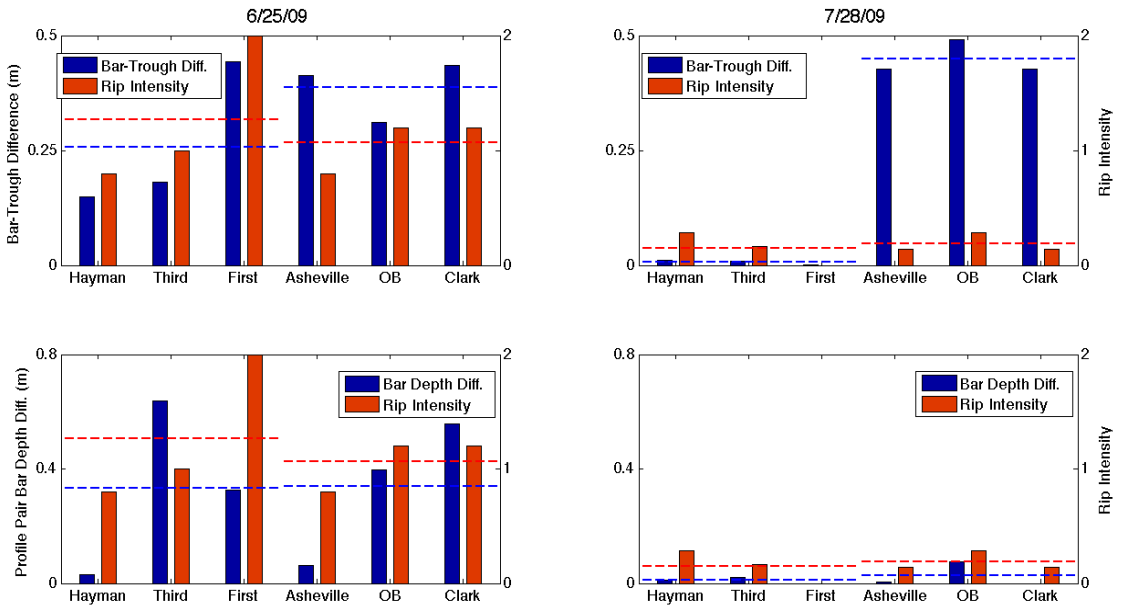

Figure 4.22 Shown are plots of the difference between the bar depth and trough depth along a particular profile (upper), and the cross-sectional (two-dimensional) trough volume along a particular profile (lower). Dashed lines indicate the average values over the northern or southern three locations. The data is from surveys completed at KDH on June 25 (left) and July 28 (right) of 2009.

different large-scale alongshore bar system, as the three southern locations have relatively large bars and the three northern locations have small bars (Figure 4.22). None of the bars demonstrate much small-scale alongshore variability in depth. The three southern locations have bar-trough differences similar to the locations with the largest bars on June 25th (~0.5 m), but have bar depth differences between profile pairs of only 0.01 m, 0.08 m and 0 m. For comparison, the four largest bar locations on June 25th had bar depth differences between profile pairs ranging from 0.33 m to 0.64 m. Rip intensity averaged over all six locations on July 28th is 0.2, much lower than the average of 1.2 during the first survey period. This suggests that relatively large bar systems with significant small-scale alongshore variability in depth produce greater rip intensity than instances when large bars have uniform small-scale alongshore depths. It is important to consider that the

wave direction for the July 28th time period is about 30 degrees further south from shore-normal than for the June 25th time period. When refracted the direction difference reduces to about 20 degrees. Since shore oblique wave incidence leads to lower rip intensity, the expectation is that both wave direction and differences in the bathymetry contribute to the variations in rip intensity.

4.5 Discussion

4.5.1 Rip intensity and the wave field

The cross-correlation analysis (Table 4.2) and calculation of rip intensity averages (Figures 4.7 and 4.8) demonstrate that significant wave height is the primary factor influencing rip intensity, while mean wave direction and directional spread provide some contribution. One way to interpret the results is that the wave height determines a baseline intensity level, which is then modulated depending on the direction and spread. Very low wave height days will never have intense rips regardless of the direction or spread. Conversely, very high wave height days will most likely have rips present, with the intensity of the rips influenced by direction and spread.

The relation of significant wave height to average rip intensity is of importance as a beach safety concern. There is a sharp increase in average rip intensity at the 0.8 m significant wave height bin and then a leveling off as wave height increases (Figure 4.7). This trend signifies a minimum wave height threshold at which hazardous conditions are likely (roughly 0.7 m). The implication of this finding is that moderate wave height conditions may be especially hazardous for swimmers. At wave heights just greater than 0.7 m, observed rip intensity on average can be nearly as high as when the wave height is

almost 2 m. However, when the wave heights are moderate the potential for a dangerous surf zone may not be as obvious, thus posing a greater safety risk.

The physical explanation for this apparent wave height threshold is less clear. It is possible that rip currents are generally weak for wave heights under ~0.7 m, as alongshore gradients in radiation stress may not be large enough to drive significant rip circulation. It may also be that waves under this threshold are too small to break over the surf zone bar in most cases and instead break directly on the shore. This could have the effect of greatly minimizing any alongshore variations in set-up and thus reducing or eliminating rip current flow. It is also possible that rip currents still occur under this threshold, but are so small that lifeguards do not observe them. Finally, there is the possibility that lifeguards underestimated rip intensity for wave heights larger than the threshold value (Hs of 1-2 m), thereby artificially creating an apparent threshold when in reality rip intensity increase with wave height is much more linear.

The shoaled and refracted wave height and direction alludes to the same relationship with rip intensity. Rip intensity is higher with larger waves and when wave incidence is close to shore-normal. However, the distributions of the shoaled and refracted wave heights exhibit a greater spread than the observed data. Wave fields consisting of longer and larger waves experience a greater increase in height than smaller and shorter waves (Figure 4.6). The distributions of refracted wave direction are more constrained than the observed data, as waves that approach from a large angle of incidence experience greater refraction when traveling from 12m to 3m depth. These differences signify the importance of considering the location in which the wave

measurements are collected (i.e. a wave incidence of 30 degrees at either 12m depth or 3m depth cannot be interpreted in the same manner).

The refraction and shoaling calculations applied here provide a simple mechanism to improve the portability of the results of this study. This is especially significant when considering rip current forecasting, as a predictive model will need to utilize standardized inputs. However, the simple methods used in this study may be compromised by complex bathymetry. In KDH in particular, the northern portion of the beach has highly variable bathymetry nearshore, which may alter the wave height and direction considerably (Figure 4.2). Further, the transformation of the directional spread from 12 m to 3 m depth is beyond a simple Snell's law calculation and thus is not included here. These limitations suggest the need for further analysis using nearshore modeled wave data.

Single swell wave conditions are slightly more favorable for rip current activity than wind sea. This is most evident for significant wave heights from 0.6 m to 1.2 m (Figure 4.11). The explanation for this result may lie in the different directional distributions of wind sea and single swell components. Wind sea originates from a wider range of directions, potentially limiting the increase in intensity caused by the increase in wave height (Figure 4.10). The relationship between average rip intensity and the directional spread is similar for both wind sea and swell, however the intensity observed at a spread of 25 degrees is greater for swell (Figure 4.11). Large wind sea conditions can often occur with greater spread than with similarly large swell conditions, this results in relatively fewer occurrences of large wind sea and very narrow spread (i.e. optimum rip intensity conditions). The average rip intensity dependence on mean direction is

comparable for both wind sea and swell, suggesting that despite which component is present the influence of direction is similar (Figure 4.11).

Contrary to bulk and swell data, the rip intensity shows some dependence on peak period for wind sea conditions (Figure 4.11). A fully developed wind sea will have larger wavelengths and longer periods, whereas there is no such dependence with swell or bulk measurements. For the instances of wind sea over the study period, significant wave height demonstrates a linear correlation with peak period, whereas no such correlation exists during instances of swell. Given that rip intensity shows no dependence with peak period for swell or bulk measurements, it is expected that wind sea period does not directly impact rip intensity, but rather is representative of a dependence on wave height. That rip current intensity is not influenced by wave period is counter to previous research that suggests that period influences rip current activity (Lascody, 1998; Engle et al., 2002). It is possible that in some wind sea dominated environments, the dependence of peak period on wave height leads to a correlation between peak period and rescues. A correlation between peak period and rescues may exist in this case because both peak period and rescues are dependent on wave height, and not because the peak period has a physical impact on rip intensity.

Previous research utilizing rip rescues found that single swell conditions were highly favorable for hazardous rip currents, while essentially no relationship was seen with wind sea (Chapter 3). Those findings are somewhat challenged here. Although swell conditions demonstrate higher rip intensity, wind sea dominated wave fields influence rip current intensity in a similar manner. The mildly contradictory results of Chapter 3 may be explained by the different observation methods. Chapter 3 suggests

that a lack of beach attendance and/or bather load during high wind sea days may be the primary reason for the poor correlation seen between rip rescues and wind sea components. A more accurate depiction of the influence of wind sea on rip currents may be presented here, since bather load does not impact the rip intensity estimates.

Wave fields that are dominated by two swells with oblique and opposing incidence may increase the likelihood of hazardous rip current activity (Chapter 3). Bi-directional wave fields have generated rip currents in numerical model and lab studies (Fowler and Dalrymple, 1990; Johnson and Pattiaratchi, 2006). This increase in rip activity may be caused by wave components with highly oblique incidence leading to constructive and destructive interference nearshore and corresponding alongshore-variable set-up gradients (Fowler and Dalrymple, 1990). Despite a small number of observations (22 days), the results suggest that instances with relatively large wave heights and large mean direction differences can lead to increased rip current activity (Figure 4.12).

4.5.2 Rip intensity and surf zone bathymetry

KDH appears to favor a summertime mode in which a substantial surf zone bar develops in the south compared to a small bar, or no bar at all, in the north. This mode favors a greater likelihood of hazardous rip currents in the southern portion of the beach. This dichotomy is found using rip rescues as a proxy for hazardous rip occurrence (Chapter 3). From 2001 to 2008 there were nearly twice as many rip current rescues made in the southern half of KDH compared to the north (339 to 177). In 2008 alone there were twice as many rescues in the south than in the north (48 to 24). This difference

is attributed at least in part to the presence of a surf zone bar in the south while the north generally had no bar present (Chapter 3).

The reason for this alongshore mode of surf zone bar development is less clear. The modification of the surf zone depends on wave energy and the likelihood of morphological re-organization (estimated by Ω). Low Ω values seem to favor larger surf zone bars in southern KDH and small or no bars in the north, while some instances of high morphological change (Ω>10) appear to generate more large-scale alongshore uniform bar systems. However, Ω values do not explain all of the variation between northern and southern KDH. It is likely that the previous surf zone morphology and sediment supply, as well as the wave conditions over the winter and early spring months influence bar formation in northern KDH.

The difference between northern and southern KDH may also relate to the nearshore bathymetry. The oblique bar features in the north of KDH fall within the margins of a paleo-river channel and overlie gravel outcrops that have shown a minimal response to large wave events (Browder and McNinch, 2006; Schupp et al., 2006). The oblique bars may transform the incoming wave energy such that it is less likely to generate or maintain a surf zone bar system, especially during low energy conditions. The southern region of KDH has demonstrated short-term and long-term accretion, while northern KDH has exhibited short term and long-term erosion (Schupp et al., 2006). The erosion rate in the northern region suggests either a low sediment supply or a divergence of sediment away from the area. This too would hinder bar creation in the area. Early in the summer of 2009, significant bar formation is evident along all of KDH following a relatively large re-organization event. This response suggests that although the shore

oblique bar morphology does not favor bar formation, a large wave event, or series of wave events, may lead to bar formation in northern KDH. Consistent low wave energy (weeks to months) may result in a shift to the favored alongshore mode where a more substantial bar exists in the south of KDH.

An additional consideration is sediment size, which can have a significant impact on Ω. The median sediment size of 0.18 mm was based on measurements at nearby Duck, NC (van Enckevort et al., 2004). However, sediment size varies both cross-shore and alongshore in and around the KDH region. Stauble et al. (2007) found more alongshore variability in sediment size in the northern, oblique bar region of KDH compared to southern KDH. Within the northern region between MHW and 2 m depth there are sediment sizes ranging from coarse (~ 0.5 mm) to fine (~ .12 mm). The calculation of Ω requires a median grain size, which is not available at each alongshore location. However, if northern KDH has a larger median grain size than southern KDH it could have a different modal morphology for the same ambient wave field. For example, if the median grain size is estimated at 0.28 mm instead of 0.18 mm, the modal range of Ω decreases from 3-4 to 2-3. When the grain size is large, Ω exceeds the threshold value of 6 only 11% of the time compared to 32% of the time for the smaller grain size. A larger grain size indicates a more reflective and morphologically stable modal state. If a large bar were not present, it would likely take a significantly larger wave event to create one. Thus, a larger grain size in northern KDH may contribute to the lack of large bar formation when compared to southern KDH, however a more detailed sediment analysis will have to be performed to form a definitive conclusion.

The alongshore variability of the surf zone bar has significant implications for beach safety and rip current forecasting. The differences between northern and southern KDH are site specific, however evidence for a consistent morphological response to varying wave energy could enhance the applicability of this study. The tendency for a region to develop a substantial bar system under low energy conditions may lead to an increase in rip current activity. Conversely, if bar formation is less likely in another region, rip current activity would be lower even if both regions experience the same wave conditions. A general understanding of the morphological response of a particular surf zone region may enable an estimation of the likelihood of the existence of a rip-favorable surf zone bar. For example, a binary proxy could be used to indicate a higher likelihood of rip favorable bar features within 3 days following a moderate to large (H_s ~1 m) wave event (or lower likelihood if not following the event). This proxy could be included in a rip current forecast system to improve overall prediction of rip current likelihood.

A more substantial surf zone bar that varies over small alongshore scales (~ 50 m) appears to increase rip current intensity. Alongshore variations in bar features can lead to variations in wave height necessary for an alongshore gradient in the radiation stress (Brander, 1999; Brander and Short, 2000; Haller et al., 2002; MacMahan et al., 2005). It has also been shown that steeper cross-shore and alongshore bathymetry gradients (i.e. a steep, tall bar with a narrow, deep rip channel) can result in stronger rip currents (Brander, 1999). The bar-trough depth difference and profile pair bar depth difference are relative indicators of the bathymetry gradients. Profile pairs with large values for both measurements should demonstrate increased rip intensity or occurrence.

Data limitations preclude a more definitive relationship between surf zone bathymetry and rip intensity. There were only three periods of simultaneous beach profile surveys and rip observations and the wave energy was generally low around survey dates. The lack of intense rip currents close to survey dates complicates the surf zone bathymetry – rip intensity comparison. The sampling of 12 to 14 profile lines presents a limited view of the surf zone bathymetry over 7.5 km and there may have been considerable variation in the bathymetry just beyond the survey locations. These limitations prompt the need for more robust surveying for future comparisons with large-scale spatial variations in rip intensity.

Lastly, the use of lifeguard observations to indicate rip current occurrence and intensity is an important consideration when interpreting the results of this study. There is some error to be expected in the lifeguard observations, as they are qualitative measurements. However, the lifeguards are trained observers, which provides reassurance in the validity of their estimates. The lifeguard observations also correspond well to instances of rip current rescues, providing additional validation. Averaging of all alongshore observations of rip intensity (up to 19 total), will also reduce the influence of possible over- or underestimation in a single guard's estimate. The importance of the guards observations cannot be understated. Use of rescue data alone has proven useful, however the limitation of bather load is a significant one. A dynamically consistent relationship between wave height and rip occurrence cannot be determined with rescue data alone as there are few bathers and correspondingly few rescues when wave heights are large. Using lifeguard observations overcomes this limitation. Further, similar lifeguard observations are relatively simple to perform in other locations with lifeguard

presence. The methods utilized in this study could provide a mechanism for obtaining a reliable measure of rip current occurrence and intensity at many other coastal locations.

4.6 Conclusions

Variations in rip intensity over large temporal and spatial scales are influenced by both the wave field and the surf zone bathymetry. Beach-wide variations in rip intensity on a daily basis are dependent on significant wave height, wave direction and directional spread. The highest levels of rip intensity occur for large waves arriving from near shore-normal with a narrow directional spread. The bar-trough depth difference and the profile pair bar depth difference influence rip intensity both temporally and spatially. The highest values of rip intensity occur when large surf zone bars exhibit significant differences in bar depth (~ 0.5 m) over 50 m alongshore.

Analysis of both the bulk and component spectral statistics suggest that significant wave height is the primary influence on rip intensity, while mean direction and directional spread provide secondary contributions. Peak period is insignificant to rip current intensity, except in the case of wind sea. The results here show peak period is only correlated to rip current intensity when it is tied to wave height (i.e. wind sea), and that wave period itself does not significantly impact rip intensity.

The significant wave height threshold value of 0.7 m is of particular importance. Average rip intensity increases dramatically at 0.7 m and observed intensity levels at just above the threshold are nearly as high as when significant wave height is close to 2 m. This threshold suggests a physical control on rip current occurrence or intensity at KDH. For example, wave heights under this threshold may not break over the surf zone bar,

reducing variations in set-up alongshore and reducing or eliminating rip current occurrence. The threshold is also of importance to beach safety, as it suggests that rip currents in moderate (apparently safe) surf conditions could be strong enough to influence swimmers. It is difficult to identify similar thresholds in either wave direction or directional spread. This may be in part due to difficulties in isolating the contributions of each variable due to interdependence.

The shoaled and refracted wave height and direction just outside the surf zone (3 m depth) demonstrate similar relationships to rip intensity as the measured values (12 m depth). However, the shape of the rip intensity distributions are different for the shoaled and refracted values. Most notably the range of wave directions is considerably more constrained at 3 m depth, suggesting the importance of measurement depth when considering the portability of this study. The simple Snell's law calculations used here may provide a mechanism to increase portability; an essential consideration if results of this study are utilized in a rip current forecast model.

The northern and southern portions of KDH develop different surf zone bar features over the course of the summer. Northern KDH tends toward small or no surf zone bars later in the summer, while southern KDH has larger bars. Low energy conditions (low Ω) may contribute to the development of this modal state, as wave energy is generally low over the summer and a complete morphological reset (Ω>10) rarely occurs. The explanation for this north-south modal state may lie in the variable nearshore bathymetry features at KDH as well as differences in sediment size and supply.

Rip currents are most intense when there are large bars with alongshore variable height. In a comparison of two survey dates with large bars in the southern portion of

KDH, the survey of bars with significantly variable alongshore depth over 50 m (~ .5 m) exhibited higher levels of rip intensity. This suggests that large surf zone bars may not generate intense rip currents if there is not sufficient alongshore variability, a result that is consistent with rip current dynamics. Differences in the mean wave direction during the survey periods confounds interpretation and additional observations are needed before a more definite relationship can be determined.

Despite some limitations, this study provides a starting point to the analysis of large-scale rip current variability, a subject matter that has lacked significant research attention. The importance of this type of large-scale analysis is two-fold: (1) It provides a basis for the understanding of rip current occurrence, intensity and variation over large areas, from days to years; and (2) it enables definition of quantifiable large-scale relationships between rip intensity and the wave field or surf zone bathymetry. Both present the opportunity for improved rip current prediction. In this sense, the analysis presented here may benefit both the scientific community and beach-going public.

CHAPTER 5

A PROBABILISTIC RIP CURRENT FORECAST MODEL

5.1 Introduction

Rip currents are the number one public safety risk at the beach. In 2010 there were 50 recorded rip current drownings and over 30,000 rescues on U.S. beaches (www.usla.org). The National Weather Service (NWS) Weather Forecast Offices (WFOs) issue categorical rip current forecasts (low, medium or high risk) for many populated coastal regions in the U.S. The present forecast model used by a number of NWS WFOs utilizes a rip risk index based on rip rescue and drowning research (Lushine, 1991; Lascody, 1998; Engle et al., 2002) with the specific structure of the model decided by each individual WFO. The forecast model used by the WFO in Morehead City, NC , for example, has been iteratively improved over the past decade and provides relatively good guidance to swimmers and life saving personnel. However, the accuracy of the model used at Morehead City and at other WFO's is hindered by a lack of observations assessing the impact of physical factors on hazardous rip current occurrence over large spatial (< 1km) and temporal (days to years) scales. Recent observational studies have enabled such an assessment (Dusek et al., 2011 and also Chapter 3; Chapter 4). The index method and categorical output of the NWS WFO models also has inherent functional limitations, for example, the need for the forecast to be manually calculated. A statistically based probabilistic forecast model

has been created to address the need for more robust and functional hazardous rip current prediction.

The probabilistic model is developed from rip intensity observations using a logistic regression formulation. Logistic regression is a common methodology for relating a binary response variable (in this case if hazardous rip currents are present or not) to one or more independent predictor variables (Hosmer and Lemeshow, 1989). Predictor inputs into the model include significant wave height, mean wave direction, tidal elevation and if the forecast is in a 72-hour post-event window. The output of a logistic regression model is the probability of a positive response (from 0 to 1) given the predictor inputs. This probabilistic output makes logistic regression a good model for weather related forecasts (Mason and Mimmack, 2002; Lo et al., 2007; Leroy and Wheeler; 2008), and lends itself to hazardous rip current prediction.

The probabilistic model presented is an initial step in creating a new rip current forecast framework. The use of bulk wave measurements and tidal elevation as predictors allows for portability and relative ease of implementation. Portability and functionality can be enhanced by using the output from wave and tide models, which could be easily input into the probabilistic model allowing for a multi-day forecast with relatively fine alongshore resolution (~ 1-5 km). The adaptable framework of the probabilistic model enables the modification or inclusion of predictors. This flexibility allows for the addition of more detailed wave field information (i.e. spectral components) and surf zone bathymetry measurements as additional data becomes available. Further, this type of probabilistic model bridges an eventual transition towards a nearshore circulation model approach, which is already being pursued (Voulgaris et al., 2011).

This paper first presents the observations used in the study, the present Morehead City NWS WFO index model (referred to as NWS model), the methodology used to create a logistic regression rip current forecast model, and statistics used for comparing the models to the observations and to each other (section 2). The physical and statistical basis for the inclusion of each predictor in the logistic regression rip current forecast model is addressed in section 3. The results and the assessment of model performance are provided through comparison to the performance of the NWS model in section 4. In section 5 we present a discussion of the model performance with a focus on the reasons for improvement over the present NWS model, along with limitations of the probabilistic model. Lastly, a summary and some conclusions are presented in section 6.

5.2 Methods

5.2.1 Study location

Observations were collected on the Outer Banks of North Carolina. Rip current intensity observations and lifeguard rescue data were collected at Kill Devil Hills (KDH), a relatively straight 7.5 km stretch of beach that faces the east northeast (63$\pm$2 degrees true). The region is wave dominated (mean annual significant wave height or H_s of 0.9 m; McNinch, 2004), with the summer months typically characterized by low energy swell (H_s = 0.4 – 0.6 m) and punctuated by storm events (H_s > 1m) on average every 8.5 days (Chapter 3). The surf zone and nearshore region of KDH is often either single or double-barred; one surf zone bar at 1-2 m depth, and one bar outside the surf zone at 4-5 m depth (www.frf.usace.army.mil/survey/frfsurvey.html). Tides are semi-diurnal (mean range of ~ 1m; Birkemeier et al, 1985).

5.2.2 Observational data

Observations utilized for this study are from three sources. The observations utilized for the creation of the probabilistic model were collected in a 2008-2009 field program at KDH (Chapter 4). The observations utilized for this field program include directional wave data from Acoustic Doppler Current Profilers (ADCPs), tidal elevation measurements, surf zone bathymetry profiles, and lifeguard rescues and observations of rip current intensity. The hindcast of the probabilistic model relies on records of lifeguard rescues made at KDH from 2001-2007 as well as wave data from a Waverider Buoy at nearby Duck, NC (Chapter 3). Lastly, the hindcast of the NWS rip current forecast model is generated from similar observations used by the NWS over the recent past (the NDBC buoy and tidal elevations described below).

Rip current observations

KDH Ocean Rescue lifeguards recorded daily observations of rip intensity at 19 different alongshore chair locations throughout the summers of 2008 and 2009. The observations were recorded in the late afternoon each day to estimate the average conditions occurring throughout the day. The rip intensity levels are described as follows (Chapter 4):

- 0 - No rip currents present
- 1 - Some low intensity rip currents present, may be hazardous to some swimmers
- 2 - Medium to strong rip currents present, will likely be hazardous to swimmers
- 3 - Very strong rip currents present, hazardous conditions

The record of lifeguard rescues at KDH from 2001 to 2009 provides an additional measure of rip current occurrence. A total of 741 rescues classified as rip related from these nine summers have been cataloged hourly (Chapter 3). Assuming that a rescue indicates the presence of a hazardous rip current, this record provides the time that hazardous rip currents occur at KDH. Hazardous is defined as a rip current of sufficient strength to cause a swimmer distress (or at least a level of 1 rip intensity). For hours when no rip current rescues are made, the rescue record provides no information regarding the occurrence of hazardous rip currents. As rip current rescues are tied to bather-load (i.e. people need to be in the water for a rescue to occur), a lack of rescues may either indicate a lack of rip current occurrence or simply that there were not bathers in the water (e.g. due to cold water, bad weather, large surf, etc.).

Directional wave data

Wave data were collected by two Teledyne RDI 600 kHz ADCPs in northern and southern KDH, deployed at 12 m depth. Both ADCPs sampled bi-hourly over the summers of 2008 and 2009. The binary ADCP data were processed into two-dimensional directional wave spectra and the corresponding bulk wave statistics (significant wave height, peak period, vector mean wave direction and directional spread; Kuik et al., 1988) were calculated using the open-source wave toolbox DPWP (Doppler Profiler Waves Processing Toolbox; Chapter 2). Spectra were further processed into wave components (i.e. wind sea and swell) using the MATLAB® toolbox XWaves (www.WaveForceTechnologies.com; Hanson and Phillps, 2001). For model creation,

bulk wave statistics were temporally averaged (bi-hourly samples from 10 am to 5 pm) to model daily rip current intensity (following Chapter 4), or were interpolated to hourly estimates to model hourly rip current rescues.

For the hindcast using the probabilistic model (2001-2007), wave observations are from a directional Waverider buoy maintained by the US Army Corps of Engineers Field Research Facility (FRF). The buoy is located 15 km NNW of the study site at 17 m depth and sampled hourly. Spectral coefficients are computed onboard the buoy using the Fourier coefficient method (Longuet-Higgins et al., 1963) and are then converted to calculate two-dimensional (2d) directional wave spectra and bulk spectral statistics. Waverider buoy wave statistics (e.g. significant wave height and mean direction) demonstrate a favorable comparison to ADCP wave statistics when both are shoaled and refracted to 3 m depth.

For the hindcasts using the NWS rip current forecast model (described in detail below), bulk wave statistics are from observations collected by National Data Buoy Center buoy 44014, located 64 nautical miles east of Virginia Beach, VA. The bulk wave statistics from this buoy are often used by the NWS when computing their rip current forecast for this region, and are used to replicate their forecasts as closely as possible. An additional hindcast of the probabilistic model was also performed with buoy data to assess the influence of the type of wave data on model performance.

Tidal and bathymetry data

Tidal data comes from two sources. For the probabilistic model creation and hindcasts, the observed water elevation from the FRF Pier is used, ~15 km NNW of

KDH. For the NWS model hindcast, the tidal elevation at Atlantic Beach Pier, NC is used, the same location historically used by the Morehead City NWS WFO for rip forecasts at KDH. From 2001-2003 the observed tidal elevations are used (observed data at this location was only available for this period), while for 2004-2009 the predicted tidal elevations are used.

The bathymetry data includes bar measurements sampled three times at KDH in 2009. Profiles were collected using an RTK GPS system and each profile transects seaward of the dune-line, in an approximately shore-normal direction, to the seaward edge of the surf zone (about 2 m depth). Each sample date includes two profiles (50 m apart) from six different alongshore locations. Various geometric profile features were identified in each profile. The most significant features relating to rip intensity are the bar-trough depth difference (the elevation difference from the bottom of the trough to the peak of the bar) and alongshore bar depth difference (difference in the depth of the bar peak between profile pairs; Chapter 4).

5.2.3 NWS model

The NWS rip current forecast model is a rip predictive index based on research completed on the east coast of Florida in 1991 (Lushine), 1998 (Lascody) and 2002 (Engle et al.). The exact model used at each local Weather Forecast Office (WFO) can be different although most follow the same framework. The model presented here (referred to as NWS model) follows the model used at the Weather Forecast Office in Morehead City, NC, which is used for rip forecasts at KDH and most of the Outer Banks. This model adds risk values calculated for four categories (wind, wave field, tide, and "other")

to assess the total risk of hazardous rip currents, which is rated as low, medium or high. The model uses a binary assessment of the wind and wave influence. The wind index value is 0 if winds are offshore (> 90 degrees from onshore shore-normal), and if winds are onshore (< 90 degrees from shore-normal) the index value is based on the wind speed (values of 0-5, Table 1). The wave field index value is 0 if the wave direction is offshore in deepwater, and is based on significant wave height and peak period if directed onshore (values of 0-8.5, Table 2). The tide index value ranges from 0 to 1 depending on the tidal height (high tide, HT, in height above Mean Lower Low Water) for a particular day (0 if HT < 4.5 ft; 0.5 if $4.5 \leq HT \leq 5$; 1 if 5 ft < HT), where high tide is used as a proxy for the daily tidal range. The "other" index category is used to manually adjust the forecast (from 0 to 1 points) if there is reason for the forecaster to believe rips might be more likely (e.g. if the day before was hazardous, if lifeguards report numerous rescues on the current day, etc.). These index point values are added together and hazardous rip risk is graded as low (total < 4), medium ($4 \leq$ total ≤ 5.5) or high (5.5 < total; Table 3).

The Newport, NC WFO (responsible for the Outer Banks) has reported a rip current forecast on a daily basis until 2009, when they began reporting a forecast up to three times daily (4am, 11am, 4pm). The hindcast in this study will be calculated either bi-hourly (2008 and 2009) or hourly (2001-2007) to simplify the comparison with the probabilistic forecast model. All inputs will be calculated based on the bi-hourly or hourly observations except for the tide value, which is kept constant on daily basis. There is no record of the "other" value, nor is it possible to calculate the "other" value for the hindcast and it is therefore set to 0 for all time periods. To allow for comparison of

Table 5.1 The wind speed calculation table for the NWS rip forecast model.

Speed (kt)	Value
≤ 9	0
10	1
11	1
12	1.5
13	1.5
14	1.5
15	2
16	2.5
17	2.5
18	3
19	3
20	4
21	4
22	4
23	4
24	5
25	5

Table 5.2 The wave field calculation matrix for the NWS rip forecast model. Value = 0 for all periods less than 8.

	Period (sec)												
Hs (ft)	**8**	**9**	**10**	**11**	**12**	**13**	**14**	**15**	**16**	**17**	**18**	**19**	**20**
1	0	1	1	1	1.5	1.5	1.5	1.5	2	2	2	2	2.5
2	0	2	2	2	2.5	2.5	2.5	2.5	3	3	3	3	3.5
3	0	3	3.5	3.5	4	4	4	4	4.5	4.5	4.5	4.5	5
4	4	4.5	4.5	4.5	5	5	5	5	5.5	5.5	5.5	6	6
5	5	5.5	5.5	5.5	6	6	6	6	6	6	7	7	7
6	6	6	6.5	6.5	6.5	7	7	7	7	7	8	8	8
≥7	7	7	7.5	7.5	7.5	8	8	8	8	8	8.5	8.5	8.5

Table 5.3 Example output of NWS rip forecast model on 8/26/2001

	Wind		**Wave Field**			**Tide**	**Total**
	Speed (kt)	Direction (from SN)	Hs (ft)	Period (s)	Direction (from SN)	HT above MLLW (ft)	**9 (High)**
Observation	15.4	43	5.7	10	18	4.6	
Risk Value	**2**		**6.5**			**0.5**	

the forecast to the probabilistic model, the categories (low, medium, high) are transformed to two different probabilistic scales: either (0, 0.5, 1) or (0.25,0.5,0.75). The index values are also normalized to a probabilistic scale (by the top 1% index value, or index = 10) to test model performance without the categorical transformation.

5.2.4 Logistic regression model

A logistic regression finds the best fit model relating a dependent binary response variable to one or more independent predictor variables. In this case, the predictors will be the physical observations (e.g. H_s) and the binary response variable will be the guards' rip current observations (0 if no rip, 1 if rip). The logistic regression model has been utilized often for forecasting since it has a probabilistic output between 0 and 1 (Mason and Mimmack, 2002; Lo et al., 2007; Leroy and Wheeler; 2008). The logistic regression model is as follows:

$$\pi(\mathbf{x}) = \frac{e^{g(\mathbf{x})}}{1 + e^{g(\mathbf{x})}}, \quad (5.1)$$

where $\pi(\mathbf{x})$ is the predicted likelihood of hazardous rip current occurrence given the predictor vector **x** and

$$g(x) = \beta_0 + \beta_1 x_1 + \beta_2 x_2 + \beta_m x_m, \quad (5.2)$$

also called the logit, for *m* predictors (Hosmer and Lemeshow, 1989). The importance of the logit representation is apparent, as it allows for a linear formulation of predictors in **x** and their coefficients. A maximum likelihood method is used to estimate the values for the coefficients $\boldsymbol{\beta}$, where the coefficient vector $\boldsymbol{\beta} = (\beta_0 \ldots \beta_m)$. Once the coefficients are estimated, p-values (denoted p_β-values going forward) are calculated using a chi-square

distribution to determine the significance of each predictor variable. Once the logistic regression model is determined, the likelihood of hazardous rip currents given a set of *m* predictors can be estimated. An example utilizing mean direction shows the fit of the logistic regression to the binary lifeguard observations (Figure 5.1). In this case, the binary lifeguard observations (0 or 1 – rip present or no rip present) are shown for a given wave direction along with the logistic regression modeled likelihood generated from the observations. The binned averaged observations fit the model closely, suggesting that the logistic regression is appropriate for these data.

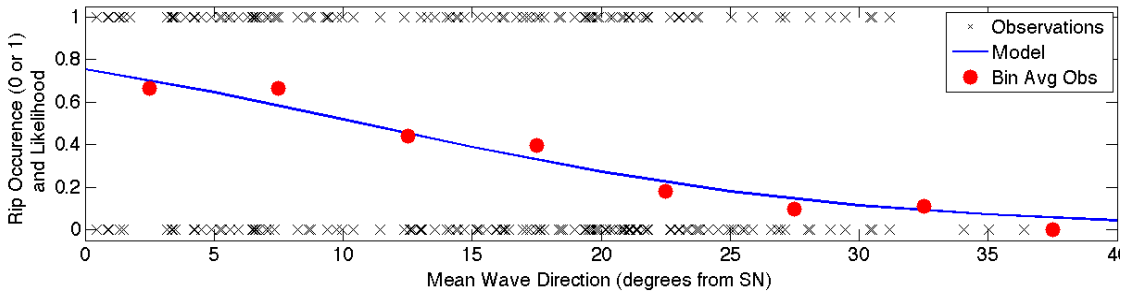

Figure 5.1 An example logistic regression plot of mean wave direction (from shore-normal). Shown are the lifeguard observations (black x; 0 = no rip, 1 = rip), the logistic regression model of those observations (blue line) and the 5 degree binned averaged observations (red circles).

5.2.5 Model validation

Two methods of model validation are employed: testing of model adequacy when building the model, and assessing model performance against independent data via a hindcast. When building the model, a goodness-of-fit test can provide an estimate of model fit against the observations used to create the model. One summary goodness-of-fit measure is the Pearson chi-square statistic,

$$\chi^2 = \sum_{i=1}^{n} \frac{\left[o_i - \hat{\pi}_i\right]^2}{\hat{\pi}_i\left[1-\hat{\pi}_i\right]}, \quad (5.3)$$

where the modeled values are $\hat{\pi} = \pi(\mathbf{x}, \boldsymbol{\beta})$, o are the observed values and i is the index of modeled-observed pairs (Hosmer et al., 1997). Evidence of lack-of-fit occurs when χ^2 is relatively large. Using the appropriate degrees of freedom will yield a p-value that denotes whether the model adequately fits the observations, where a p-value ≥ 0.05 indicates sufficient fit (denoted p_χ-value going forward). This goodness-of-fit measurement is used to determine the adequacy of the full multivariate model, $\bar{\pi}$ (not to be confused with p_β-values to assess coefficient significance).

One method used for assessing model performance against independent data is a comparison of hindcast estimates to rip current rescues from 2001-2007. Only times when rip current rescues are made can be used for comparison, since rescues only provide an indication of rip current occurrence. Model performance is determined by comparing the predicted hazardous rip current likelihood, $\dot{\pi}$, to the observed hazardous rip current occurrence (= 1 for every time period a rescue occurs).

The Brier Score is used to assess forecast performance against observations. The Brier Score is essentially a measure of the mean-squared error where

$$BS = \frac{1}{n}\sum_{i=1}^{n}(\hat{\pi}_i - o_i)^2, \quad (5.4)$$

and $\dot{\pi}$ are the model estimates, o are the observations (in this case all $o = 1$) with i being the index of the n observation-model pairs (Wilks, 2006). The BS will be between 0 and 1 with 0 being perfect agreement. The Brier Skill Score is a measure of forecast

improvement over a reference forecast, and can be used to relate the performance of the probabilistic rip forecast model to the NWS model. The Brier Skill Score is defined as

$$BSS = 1 - \frac{BS}{BS_{ref}}, \quad (5.5)$$

where BS is the Brier Score for the probabilistic model and BS_{ref} is the score for the reference or NWS model (Wilks, 2006).

5.3 Model Creation

5.3.1 Physical justification of predictors

The initial choice of predictors to include in the logistic regression model is based on evidence that they physically influence rip current activity. Previous research has suggested that the wave field, tide and surf zone bathymetry all influence rip current occurrence and intensity.

Wave Field

The aspects of the wave field that have been shown to influence rip current intensity are wave height, wave direction and directional spread. Rip intensity increases with wave height (Brander, 1999; Brander and Short, 2000; MacMahan et al., 2005; Chapter 3; Chapter 4), as larger waves increase set-up and the radiation stress gradients alongshore that drive rip current circulation. Rip intensity tends to be greatest when wave direction is close to shore-normal (Engle et al., 2002; MacMahan et al., 2005, Chapter 3; Chapter 4) as more oblique incidence results in increased inertia of the alongshore flow and drives stronger alongshore currents which can suppress cross-shore rip current flow (Svendsen et al., 2000; Kumar et al., 2011). Numerical models and

observations have also suggested that narrower directional spread may increase rip current activity (Johnson and Pattiaratchi, 2006; Chapter 3; Chapter 4). Some work has suggested that rip intensity increases with wave period (Engle et al., 2002; Lascody, 1998; Scott et al., 2009), however that relationship has not been seen at KDH (Chapter 3; Chapter 4). Analyses relating wave height and period to rip activity at KDH have also been performed (e.g. wave steepness), however a significant relationship was not observed.

Significant wave height and mean wave direction are refracted and shoaled from the observation depth to just outside the surf zone (3 m depth) for inclusion in the model. A simple wave energy conservation and Snell's law approach is used for the calculation (Chapter 4; Dean and Dalrymple, 2002). This wave transformation is applied to estimate the wave parameters that directly influence rip current circulation (i.e. the wave field at the point of wave breaking). Additionally, this transformation provides a standardized depth of wave field observation, which is especially important to the portability of the model.

Crossing wave trains are an additional hydrodynamic mechanism for rip current generation (Dalrymple, 1978; Kennedy, 2005). Constructive and destructive interference alongshore creates the alongshore radiation stress gradients necessary for rip current circulation. Crossing wave trains have been shown to generate rip currents in numerical model (Johnson and Pattiaratchi, 2006) and lab studies (Fowler and Dalrymple, 1990). A bi-directional wave field with two crossing swells has been shown to increase rip current occurrence as the angle between swells increases (Chapter 3). As such, an additional model input to consider when two swells are present is the direction difference between

two swells. As with the bulk wave parameters the swell direction is refracted to 3 m depth.

Tide

In numerous studies the tidal elevation has been shown to influence rip current intensity (Brander, 1999, MacMahan et al., 2005; Chapter 3). Rip currents tend to be more intense at low tide when there is increased breaking over the surf zone bar, while at higher tides there can be little or no breaking, significantly reducing rip current intensity. Voulgaris et al. (2011) utilized a numerical model to find that rip velocity could be up to 40% greater at low tide than at high tide. Additionally, at low tide the water level may be low enough over the surf zone bar that return flow within the surf zone is directed towards rip channels, strengthening rip intensity. The reference tidal datum used is Mean Sea Level (MSL), as a tidal level above or below MSL would be expected to decrease or increase rip intensity respectively.

Bathymetry

The presence of a surf zone bar and alongshore variations in bar height can create alongshore gradients in breaking wave height necessary for rip current circulation (Brander, 1999; Brander and Short, 2000; Haller et al., 2002; MacMahan et al., 2008). Thus, it is desirable to have information regarding the surf zone bathymetry to create the most accurate rip current predictive model. However, there does not exist, at present, a measurement technique to adequately monitor surf zone bathymetry over km scales on a daily basis. The three surf zone profile surveys performed in the summer of 2009 allow

for the inclusion of some bar information in the logistic regression model. The bar-trough depth difference and the alongshore bar depth difference represent the bar magnitude and alongshore bar variability respectively. These measurements correlate with rip current intensity in previous research and thus were chosen for inclusion in a logistic regression model (Chapter 4).

In many instances, (including for most rip current intensity observations in this study), information about the surf zone bathymetry is not available. An alternative is to incorporate a proxy for surf zone bathymetry measurements. In sandy, intermediate beaches (neither fully dissipative or reflective), large wave events can often lead to rip current favorable surf zone bathymetry shortly following the event (Calvete et al., 2005; Garnier et al., 2008; Lippmann and Holman, 1990). At KDH, rip current activity and intensity was seen to be relatively high in the 3 days following wave events for which H_s > 1 m (Chapter 3; Chapter 4). Thus, a binomial predictor variable was created as a proxy for bathymetric observations to indicate if the observation time period was within 72 hours of the peak of an event (1) or not (0).

5.3.2 Statistical justification of predictors

Given the predictors deemed physically influential to rip current occurrence, a statistical assessment of their influence must be made prior to inclusion in the forecast model. The first test to assess their statistical importance is to model the response to each predictor variable, x_d, individually. Using the observations of daily rip intensity (0 = no rip, 1 = rip) as the response variable, an assessment of the model, $\hat{\pi}_d$, is made where the logit is $g(x_d)$ and x_d is either significant wave height (H_s), vector mean wave direction (θ),

directional spread (σ_θ), peak period (T_p), 72-hour post event window (E_p), mean direction difference between two swells (Δ_θ), bar-trough depth difference (b_t) or alongshore bar depth difference (b_a). Wave steepness (S; ratio of H_s to wavelength) was also assessed for potential statistical significance.

The tide is a physically important predictor to include as well. However, the influence of tidal elevation on rip occurrence is not well resolved with the daily rip intensity observations due to the change in tidal elevation throughout the day (Chapter 4). To assess the statistical importance of the tide, hourly rip current rescues (0 = no rescue, 1=rescue) from the same time period (2008-2009) are used as the response variable of the model $\hat{\pi}_h$. For the logit $g(x_h)$, x_h is the hourly tidal elevation relative to MSL (η).

When modeled individually (i.e. x = one predictor) all predictors have significant p_β-values (< 0.05; Table 4), which suggests that each predictor should be tested for inclusion in a full, multivariate model (i.e. $\mathbf{x} = [H_s, \theta, \text{etc.}]$). For H_s and θ it was determined that a transformation ($\ln(H_s)$ and $|\theta|$) yielded an optimum logistic regression fit. This is signified by lower p_β-values as well as an improved assessment of (necessarily linear) fit (Figure 5.2). For the figure shown the observations (0 or 1) are bin averaged to obtain the observed likelihood and transformed to the logit scale. While the improvement to the fit of H_s is minor, the improved fit of θ is notable. As the logit is linear in x, a logistic regression is optimized when the logit function is monotonically increasing or decreasing. Since we expect rip intensity to decrease as the mean direction increases in either direction from shore-normal, $g(|\theta|)$ is monotonic, while $g(\theta)$ is not.

Three types of multivariate models will be considered: A model utilizing bulk wave parameters, a model for instances of two swells, and a model utilizing bulk wave parameters with surf zone bathymetry variables.

Table 5.4 List of all logistic regression coefficients for predictor variables modeled individually (*x*=one predictor).

Variable	β	p_β-value	Standard Error	Data Points	Response
H_s	4.65	$8.2x10^{-98}$	0.22	2313	Rip Intensity
$\ln(H_s)$	4.05	$3.2x10^{-118}$	0.18		
θ	-0.062	$1.6x10^{-46}$	0.004		
$\lvert\theta\rvert$	-0.11	$3.3X10^{-69}$	0.006		
σ_θ	-0.11	$1.1x10^{-72}$	0.006		
T_p	-0.043	0.021	0.019		
E_p	1.55	$7.2x10^{-42}$	0.11		
S	134.3	$5.7x10^{-78}$	7.18		
Δ_θ	0.016	0.033	0.007	327	
b_t	2.56	0.033	1.21	108	
b_a	4.36	$3.2x10^{-4}$	1.21		
η	-1.53	$9.0x10^{-9}$	0.27	1229	Rip Rescues

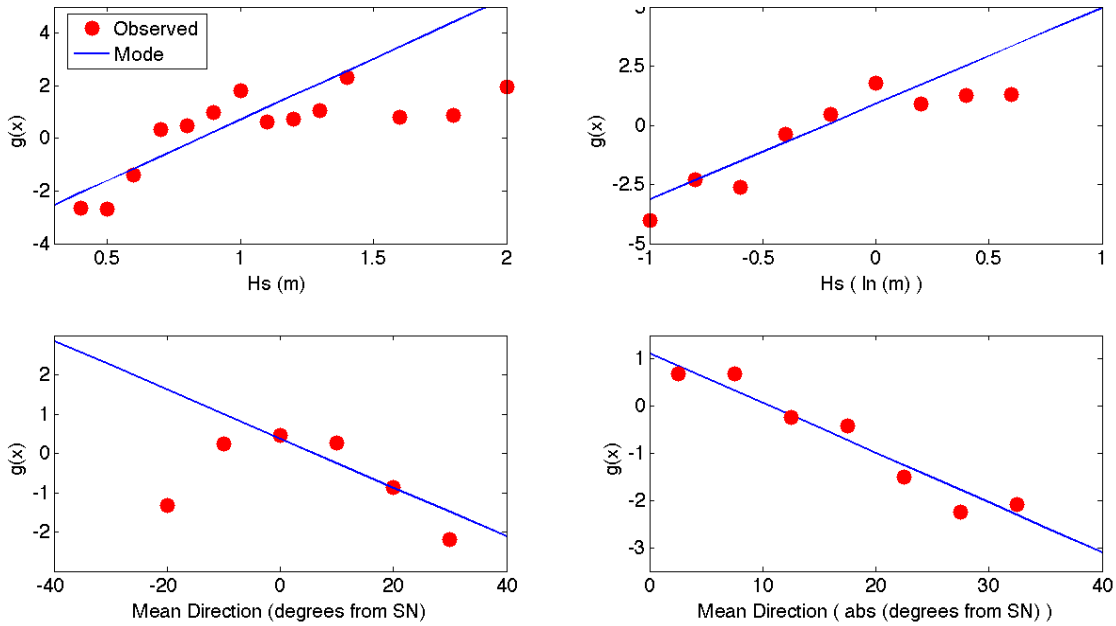

Figure 5.2 Plots of the modeled and observed data in logit (or *g(x)*) space. Shown are the significant wave height (upper left), natural logarithm of the significant wave height (upper right), mean direction (bottom left) and absolute value of the mean direction (bottom right). Rip occurrence observations (0 or 1) are bin averaged and transformed to the logit scale.

Hydrodynamic parameter model

When modeled individually, each bulk wave parameter, x_d, is statistically significant (p_β-value < 0.05; Table 4), suggesting its inclusion in the full model. However, when five bulk wave based variables are incorporated in the model together ($\mathbf{x_d} = [\ln(H_s), |\theta|, \sigma_\theta, T_p, E_p]$) the directional spread, σ_θ, becomes statistically insignificant (p_β-value = 0.23) and is removed from the model. The peak period approaches insignificance (p_β-value = 0.05). A borderline p_β-value may often support including a predictor in the model, however there is little physical evidence supporting the inclusion of peak period and thus it is removed from the model (Chapter 3; Chapter 4). Wave steepness was also considered for inclusion, however once spread and period were removed it was clearly statistically insignificant (p_β-value = 0.93). The remaining

predictors ($\mathbf{x_d}$ = [ln(H_s), |θ|, E_p]) are statistically significant, however it is important to validate that each predictor is well represented by a logistic regression.

Observations are plotted against the model output for each individual predictor (x=ln(H_s), x=|θ|), with the exception of the post-event variable, E_p, since it is binomial (Figure 5.3). Observations (0 or 1) are bin averaged to obtain the observed likelihood of rip occurrence for a given bin. The model fits the observations fairly closely, affirming that inclusion of these predictors in the logistic regression is appropriate.

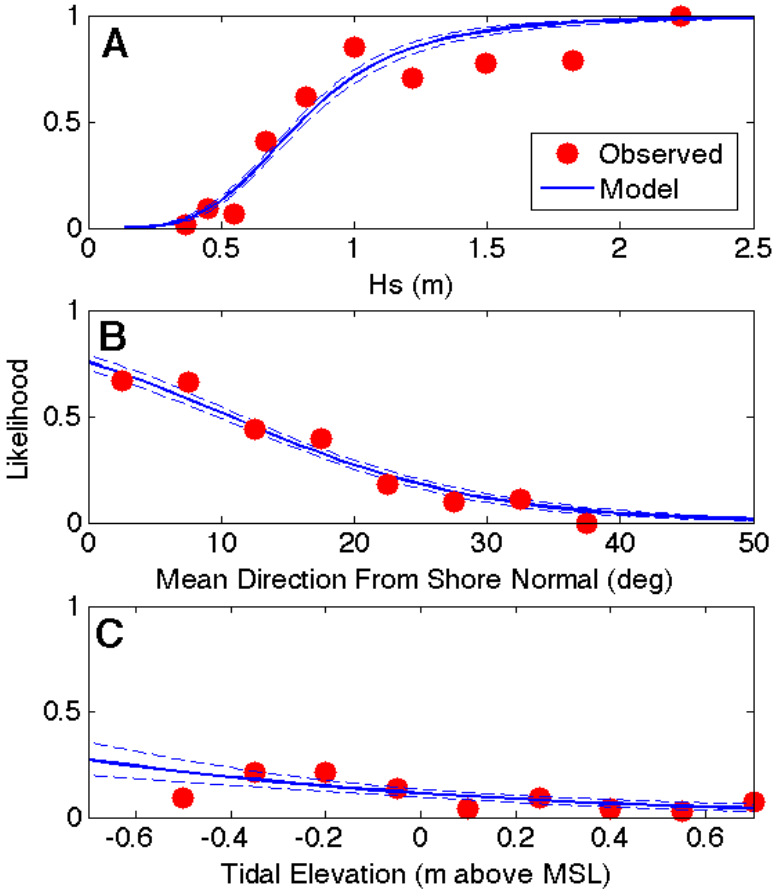

Figure 5.3 Plots comparing the average observed hazardous rip current likelihood to the probabilistic model for each individual predictor. Observed and modeled values are from lifeguard rip intensity observations and rescues at KDH in 2008 and 2009. Shown are significant wave height (top), mean directional from shore-normal (middle) and tide (bottom). Observations (0 or 1) are bin averaged to obtain the observed likelihood of rip occurrence. The 95% confidence limits (blue dashed) for the model are shown.

Further, the physical interpretation of the model plots, most notably with significant wave height, follow what has been seen previously. The model with significant wave height shows a dramatic increase in likelihood between 0.5 m and 1 m and then a leveling off with larger wave heights (Figure 5.3 A). This is precisely the relationship determined when analyzing the observations (Chapter 4), and thus provides confidence in the model. This aspect of the model also suggests the importance of moderate wave heights (~ 0.7 m) to hazardous rip occurrence. Lastly, the Pearson chi-square statistic for the model, $\mathbf{x_d} = [\ln(H_s), |\theta|, E_p]$), suggests a sufficient, but perhaps weak, fit (p_χ-value = 0.05, where $\geq$ 0.05 is sufficient fit).

The tide is a physically important predictor of rip current occurrence and $x_h=\eta$ is statistically significant when using hourly rip rescues as the response variable (Table 5.4). It is therefore desirable to include the tide in the model. An alternative model is considered where the predictors are hourly, $\mathbf{x_h} = [\ln(H_s), |\theta|, E_p, \eta]$, and the response is hourly rip rescue occurrence. When this model is calculated, the tidal coefficient is statistically significant. When the hourly rip rescue model is then calculated without the tidal coefficient (i.e. $\mathbf{x_h} = [\ln(H_s), |\theta|, E_p]$) the remaining three coefficients are statistically equivalent at one standard error to the hourly model with the tidal coefficient (Table 5.5). This comparison demonstrates that although the tidal coefficient is statistically significant, its inclusion in the model does not significantly alter the remaining three coefficients.

The deviance, or a measure of model error, can be utilized to determine if the hourly rip rescue model including the tide minimizes model error compare to the hourly model without the tide. The deviance is defined as (Hosmer and Lemeshow, 1989):

$$D = -2\sum_{i=1}^{n}\left[o_i \ln\left(\frac{\hat{\pi}_i}{o_i}\right) + (1-o_i)\ln\left(\frac{1-\hat{\pi}_i}{1-o_i}\right)\right]. \quad (5.6)$$

Table 5.5 The hydrodynamic parameter logistic regression model with the daily rip intensity response or hourly rip rescue response with and without tide

Daily Rip Intensity				
Variable	**β**	**p_β-value**	**Std E**	**Std Coeff.**
Intercept	1.05	$1.6\text{x}10^{-16}$	0.13	
$\ln(H_s)$	3.51	$4.8\text{x}10^{-69}$	0.2	2.43
$\lvert\theta\rvert$	-0.027	$2.6\text{x}10^{-5}$	0.007	-0.42
E_p	0.42	0.003	0.14	0.29
η	Not Included			
Hourly Rip Rescues				
Variable	**β**	**p_β-value**	**Std E**	**Std Coeff.**
Intercept	-1.19	$1.5\text{x}10^{-9}$	0.20	
$\ln(H_s)$	0.36	0.21	0.29	0.22
$\lvert\theta\rvert$	-0.074	$3.6\text{x}10^{-7}$	0.015	-1.59
E_p	0.63	0.003	0.21	0.45
η	Not Included			
Hourly Rip Rescues with Tide				
Variable	**β**	**p_β-value**	**Std E**	**Std Coeff.**
Intercept	-0.72	$9.8\text{x}10^{-4}$	0.22	
$\ln(H_s)$	0.42	0.16	0.30	0.25
$\lvert\theta\rvert$	-0.078	$8.0\text{x}10^{-7}$	0.016	-1.66
E_p	0.53	0.016	0.22	0.38
η	-1.70	$2.9\text{x}10^{-9}$	0.29	-1.17

In this case the hourly rip rescue model without the tide results in D = 762.7 and the hourly model with the tide improves to D = 709.7, a difference of 53. When a chi-square distribution is utilized with one degree of freedom (Hosmer and Lemeshow, 1989), this difference in deviance results in a p-value = $3x10^{-14}$. This suggests with a high degree of confidence that including the tide better captures the observations. Further, the coefficients for both $|\theta|$ and E_p of the daily rip intensity model are similar to the coefficients of the hourly rip rescue response with the tide (Table 5.5). The coefficient E_p is statistically equivalent for both responses. The wave height (H_s) coefficient is significantly different and was found to have a poor logistic regression fit with the rip rescues response (p_β-value = 0.16). The difference in the wave height coefficient is due to a lack of rescues at large significant wave heights. When wave heights are large, people tend not to be in the water due to poor weather or the large surf, reducing the bather load and the number of rescues. Rip current observations have no such dependence on bather load, and rip observations suggest high rip occurrence at large wave heights. These differences lead to significantly different coefficients when performing a logistic regression between wave height and either rip rescues or rip observations. There is not expected to be any systematic reduction in rescues from bather load due to tidal elevation, η, and inclusion of the tidal coefficient should not significantly influence the remaining three coefficients. Thus, it is reasonable to use the hourly tidal coefficient calculated with the rip rescue response in the daily rip intensity response model. This results in a mixed response model where $\mathbf{x} = [\ln(H_s), |\theta|, E_p, \eta]$).

Lastly, it is desirable to interpret the coefficients of the full model, ($\mathbf{x} = [\ln(H_s), |\theta|, E_p, \eta]$; Table 5.5), to determine their relative contribution to the output and to assure

that their influence follows what is dynamically expected. The fractional change in the likelihood of hazardous rip current occurrence can be determined by:

$$\psi = e^{c\beta_m}, \quad (5.7)$$

where β_m is the coefficient and c is the unit of change. Using this formulation, a 10 degree increase in mean direction from shore-normal would result in $\psi = 0.76$. In other words, hazardous rip current likelihood, π, reduces to 0.76 π with a 10 degree increase in mean direction. This follows the expectation that rip currents tend to be weaker with more oblique wave direction. If the forecast is within 3 days of the peak of an event, $\psi =$ 1.52 and thus a hazardous rip current is 1.52 times more likely, which follows the physical expectation. An increase in the tide by 0.1 m results in $\psi = 0.84$, or that the likelihood of a hazardous rip current is reduced from π to 0.84 π in this instance. This again follows the physical expectation that rip likelihood decreases with increasing tidal height. The wave height is slightly more difficult to interpret since the coefficient is for the natural logarithm of the wave height. In this case a significant wave height change from 0.5 m to 0.6 m would result in hazardous rip currents being 1.9 times more likely, which is inline with what is physically expected.

The interpretation of the coefficients suggest that significant wave height has the most influence over the model. Computing the standardized logistic regression coefficient supports this interpretation. The standardized coefficient is defined as:

$$\beta_{std} = \beta_m \sigma(x_m) \sqrt{\frac{\pi^2}{3}}, \quad (5.8)$$

where $\sigma(x_m)$ is the standard deviation of the predictor values (Hilbe, 2009). The magnitudes of the standardized coefficients show that with the daily rip intensity as the response, the significant wave height is clearly the most influential variable followed by wave direction and post-event (Table 5.5). With hourly rip rescues as the response, tidal height has a smaller standard coefficient than direction. This suggests that in the combined hydrodynamic parameter model ($\mathbf{x} = [\ln(H_s), |\theta|, E_p, \eta]$), the order of importance is significant wave height, mean direction, tidal elevation and post-event. The significantly larger standard coefficient of significant wave height indicates that wave height is the primary driver of hazardous rip occurrence and the remaining variables are of secondary influence.

Two-swell model

An additional model was considered for instances when two swells were present. There were 22 days when two swells were present, for a total of 327 predictor – response pairs. The coefficient for the mean direction difference, Δ_θ, is significant when modeled individually ($x_d = \Delta_\theta$; Table 5.4). That β is positive indicates that the likelihood of rip current occurrence, $\dot{\pi}$, increases as the direction between two swells increases, which follows previous research (Chapter 3). When Δ_θ is substituted for $|\theta|$ in the bulk wave parameter based model (i.e. $\mathbf{x_d} = [\ln(H_s), \Delta_\theta, E_p]$, the coefficient for Δ_θ remains significant, suggesting that this adjusted model may be a reasonable alternative for when two swells are present. However, the logistic regression does not fit the data very well (Figure 5.4 bottom), and relies on relatively few observations. Further, an assessment of goodness-of-fit shows that the model with Δ_θ substituted is only a slightly better fit (p_χ-

value = 0.36) than the model with $|\theta|$ (p_χ-value = 0.32). To incorporate the two-swell alternative model there would need to be branching logic to assess if each wave field consisted of one-swell or two-swells and then apply the appropriate model. Thus, the inclusion of the two-swell case would add significantly to the complexity of the model while only slightly improving fit, and is not considered further.

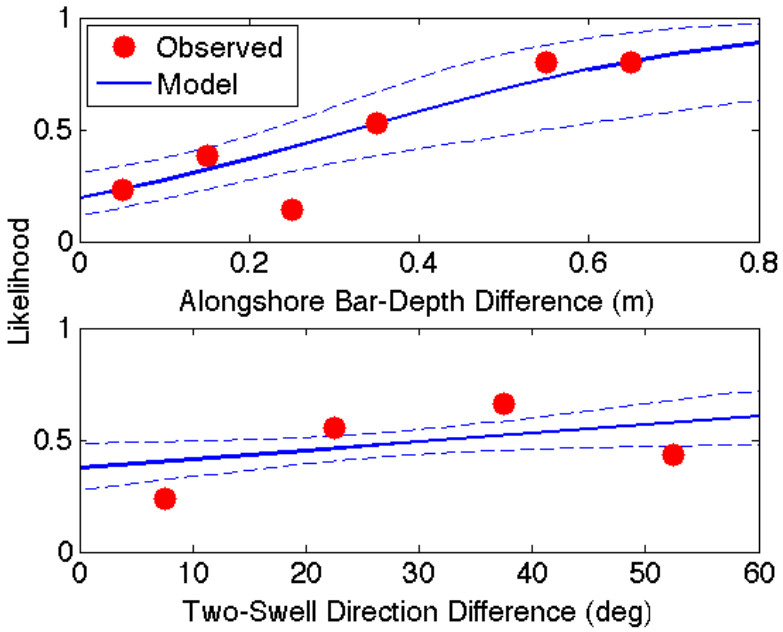

Figure 5.4 Plots comparing the average observed hazardous rip current likelihood to the probabilistic model for each individual predictor. Observed and modeled values are from lifeguard rip intensity observations at KDH in 2008 and 2009. Shown are the alongshore bar-depth difference (top) and the mean direction difference between two swells (bottom). Observations (0 or 1) are bin averaged to obtain the observed likelihood of rip occurrence. The 95% confidence limits (blue dashed) for the model are shown.

Bulk wave parameter model with bathymetry

Another alternative model includes the surf zone bathymetry information. The bathymetry predictors are bar-trough depth difference (b_t) and alongshore bar depth difference (b_a), which are assumed valid at a profile location for three days prior to and after the survey dates unless a large wave event occurs (Chapter 4). There are a total of

19 valid days over three survey dates, and on each date profiles were collected at six different alongshore locations. When paired with the corresponding lifeguard rip intensity observations as the binomial response variable, there are a total of 108 bathymetry – observation pairs of data. When each bathymetry input is used individually (x_d = b_t or b_a) in a logistic regression model, the coefficients for both variables are significant (p_β-value < 0.05; Table 4). The bathymetry inputs can then be substituted for the event variable (E_p), which serves as a bathymetry proxy in the bulk wave parameter model. When combined with the bulk wave parameters in the full model ($\mathbf{x_d}$ = [ln(H_s), |θ|, b_t, b_a]) only the alongshore bar-depth difference, b_a, has a significant coefficient. This result suggests that alongshore bar-depth variability impacts rip current occurrence. However, the logistic regression does not fit the observed data very well (Figure 5.4 top), reducing the overall confidence in the model. Additionally, the small sample size provides a very limited number of wave height and direction combinations (only 19 daily observations) with bathymetry data. The limited number of observations, particularly of wave direction, results in a model ($\mathbf{x_d}$ = [ln(H_s), |θ|, b_a]), where the |θ| coefficient is insignificant (p_β-value 0.61), adding to a lack of model confidence. Although bathymetry is physically important to rip current occurrence, and its inclusion in a model is somewhat supported statistically, the limited number of observations available prevent bathymetry from being considered further.

Chosen model

Given the above statistical analysis, the hydrodynamic parameter model with the rip intensity response, and the inclusion of the tide coefficient is chosen as the optimum

model ($\mathbf{x} = [\ln(H_s), |\theta|, E_p, \eta]$). Although KDH has demonstrated variable rip occurrence alongshore in the past (Chapter 3), as presently constructed, this model cannot account for these differences due to a lack of a bathymetry input. Thus, the model forecast is applied to all of KDH. The logit of the model with the appropriate coefficients can be written as (see Table 5.5 for p_β-values and standard errors):

$$g(\mathbf{x}) = 1.05 + 3.51H_s - 0.027|\theta| + 0.42E_p - 1.70\eta. \quad (5.9)$$

Model output can be shown in three dimensions (showing H_s, $|\theta|$ and η, with $E_p = 1$; Figure 5.5). In this case, the influence of each variable can be visualized. The primary importance of significant wave height is especially apparent, as when H_s < ~0.5 m rip currents are not likely, regardless of wave direction or tidal height.

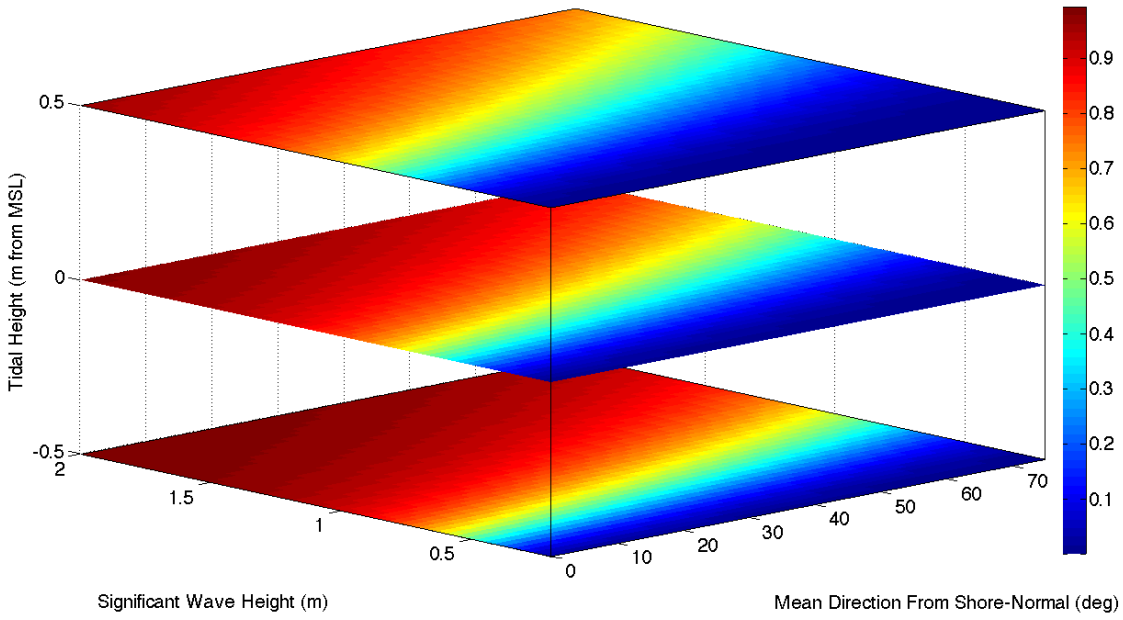

Figure 5.5 A three-dimensional plot showing the output of the probabilistic rip current forecast model. The influence of significant wave height, mean direction (absolute value from shore-normal) and tidal height on rip current likelihood (colorbar) is shown. In this case the post-event variable is held at 1. Coefficients used for this plot are shown in Eq. 5.9.

5.4 Results

5.4.1 Model hindcasts compared to rip intensities

A bi-hourly hindcast using both the probabilistic and NWS models was performed for the summers of 2008 and 2009. The hindcasts are compared to the daily beach-wide average rip intensity where the magnitude is retained (0,1,2, or 3). Two different hindcasts are completed to assess performance. The first hindcast is utilized to compare the probabilistic model and the NWS model with independent data. The 161 days of observations were split into two randomly sampled groups of data (of 83 and 78 days). The bulk wave based coefficients of the probabilistic model were then re-computed utilizing only one of the groups (83 days). The tide coefficient in eq. 5.9 was used since it was generated utilizing only rip rescue data. The logit of the probabilistic model using only this portion of the data is as follows:

$$g(\mathbf{x}) = 0.99 + 3.71\mathrm{H}_s - 0.025|\theta| + 0.46\mathrm{E}_p - 1.70\eta \text{. (5.10)}$$

The coefficients generated from the 83 day sample are all within one standard error of the coefficients generated from the entire 161 days. The remaining 78 days are then used for the first hindcast and comparison to the NWS model over this same period.

To assess performance, scatter plots are made between the daily average hindcast values (when guards are on the beach, 10am – 5pm) and the daily average rip intensity (Figure 5.6). In this instance, the index values of the NWS model hindcast are shown. The probabilistic model demonstrates a fairly strong linear relationship with rip intensity ($R^2 = 0.70$). There are no days of significant underforecasting (high rip intensity observations and low likelihood forecast), and relatively few days of significant overforecasting. The output index of the NWS model displays more scatter and a weaker

linear fit (R^2 = 0.54), especially at low model indices. In these cases, the NWS model underforecasts and outputs a "low" forecast when a portion of these days have moderate to high rip intensity. The NWS model output of "high" is quite reliable, as there are only 2 days of significant overforecasting. This comparison suggests that although both models perform reasonably well, the probabilistic model outperforms the NWS model, especially in some cases of moderate rip current intensity.

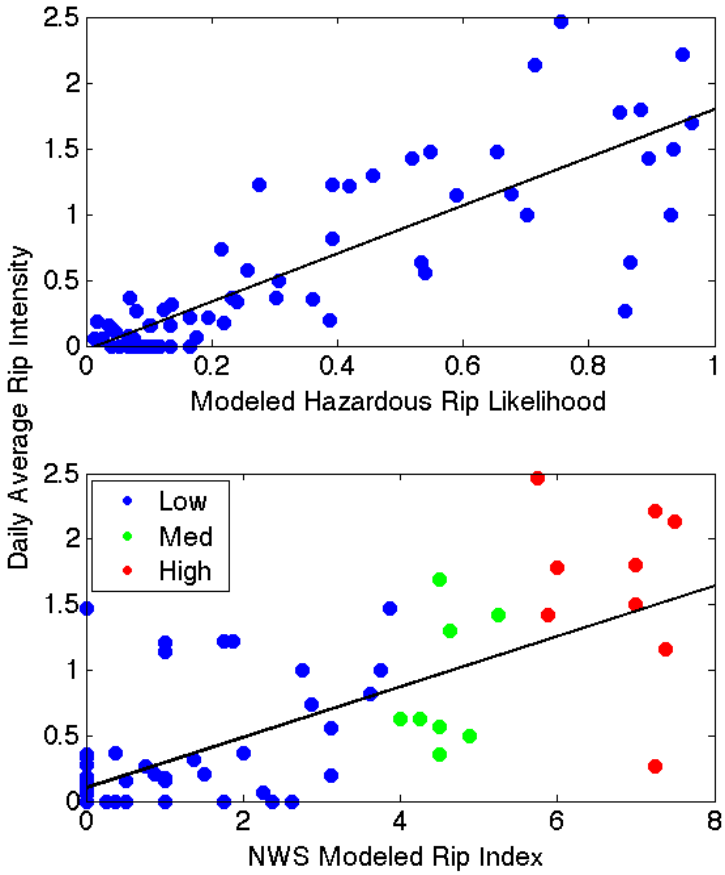

Figure 5.6 Scatter plots of the daily average observed rip intensity and the daily average hindcast of the probabilistic model (top) and NWS model (bottom) from a random sampling of 78 days in 2008 and 2009 at KDH. The NWS model hindcasted values are shown as index values with color coded forecast levels. The best fit linear regression line is shown (solid black).

A second bi-hourly hindcast is then created for all 161 days from 2008 and 2009, now utilizing the coefficients from the entire data set. The NWS model is represented with probabilities (0, 0.5, 1) replacing its categorical risk values. The time series of the bi-hourly hindcasts further suggests that both the probabilistic and NWS models compare favorably to the rip intensity observations (Figure 5.7). The probabilistic model appears to always accurately predict days of very high rip intensity, while displaying very few instances of significant overforecasting (high likelihood forecast and low observed rip intensity). The NWS model generally seems to identify instances of high rip intensity, however since the model is categorical the forecast often jumps back-and-forth between levels. The NWS model also displays few instances of overforecasting. Most importantly, as seen with the scatter plot, it is prone to underforecasts and misses some moderate rip intensity days entirely.

This comparison suggests that although both models perform reasonably well, the probabilistic model outperforms the NWS model, especially in cases of moderate rip current intensity. To more completely assess performance a comparison to rip rescue observations independent of the probabilistic model creation dataset will be used.

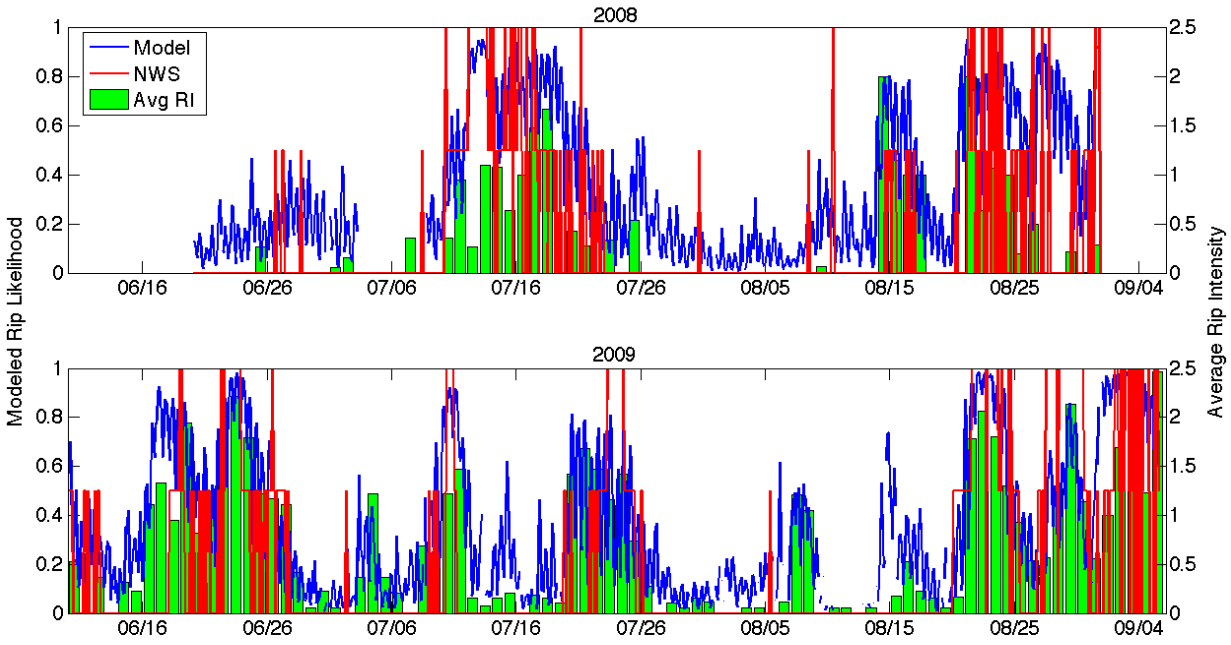

Figure 5.7 The daily average observed rip intensity and the probabilistic and NWS model hindcasts (bi-hourly) for the summers of 2008 (top) and 2009 (bottom) at KDH.

5.4.2 Hindcast with rip rescue comparison

Over the seven summers of rip rescue observations (2001-2007) there are 294 hours when at least one rip rescue was made. Each of these occurrences is a "positive" hazardous rip current occurrence (o = 1). The probabilistic model has a much higher mean value for these instances (0.66) compared to the NWS model utilizing the [0, 0.5, 1] scaling (0.19), the [0.25, 0.5, 0.75] scaling (0.35) or the normalized index scaling (0.24) suggesting superior performance. Part of this dramatic difference can be explained by the higher hindcast mean over all summers for the probabilistic model (0.40) compared to the NWS model (0.12, 0.31 or 0.16 respectively). However, the probabilistic model also displays a larger average increase during rip occurrences relative to the underlying mean (0.26) compared to the NWS model (0.07, 0.04 or 0.08 respectively).

Further evidence that the probabilistic model accurately predicts hazardous rip current events and outperforms the current NWS model is given by the Brier Score for instances when rescues were made. The probabilistic model has a BS = 0.15 (0 is perfect prediction), which suggests the model fairly accurately predicts hazardous rip occurrence. The NWS model has a BS = 0.75, 0.45 or 0.64 for the [0, 0.5, 1], [0.25,0.5, 0.75] and normalized index scaling respectively, which signifies comparatively poor performance. Using the Brier Skill Score to compare the models results in a BSS = 0.80, 0.67 or 0.77 depending on the scaling, or that the probabilistic model demonstrates a minimum of a 67% improvement in prediction of hazardous rip occurrence compared to the NWS model.

A subset of 75 hours when more than one rescue in an hour occurred can offer additional insight into performance. The times when multiple rescues occur in one hour provide greater confidence that there were clearly hazardous rip current conditions. For these cases the probabilistic model BS = 0.13 and the NWS model BS = 0.70, 0.43 or 0.63 depending on scaling. This results in a BSS = 0.82, 0.70 or 0.79, similar to the BSS for all instances of rescues, which further suggests that the probabilistic model is a significant improvement over the NWS model.

The improved performance of the probabilistic model may be due in part to functional improvements in the model, as well as because of superior input data. One of the chief differences in input data used for both models is the source of wave data. The NWS model utilizes deepwater wave field observations while the probabilistic model utilizes local wave field observations that more accurately depict the wave field as it exists at KDH. A hindcast of the probabilistic model using the same deepwater NDBC

buoy wave inputs as in the NWS model (shoaled and refracted to 3m depth) results in slightly decreased performance. The probabilistic model has a mean of 0.50 over the 294 hours of hazardous rip presence, an increase of 0.20 when compared to a mean of the entire data record (0.30). For the same 294 hours the probabilistic model has a BS = 0.31 and for the 75 hours when multiple rescues occur a BS = 0.30. Depending on the NWS index scaling used ([0,0.5,1], [0.25,0.5,0.75] or normalized index), the BSS for the 294 hours with at least one rescue is 0.59, 0.31 or 0.52. The BSS represents that the probabilistic model has a minimum of a 31% improvement over the NWS model using the same deepwater wave observations.

Instances of very high rip current activity, when many rescues are made over the course of a few days, are of particular importance to beach safety and thus are critical to accurately forecast. Two examples of such events occur over 4 days (100 hours) on August 1 to 5 of 2001 when there are 36 rescues and August 17 to 21 of 2005 when there are 22 rescues (Figure 5.8). In both cases the probabilistic model predicts the occurrence of hazardous rip current conditions with a fairly high degree of accuracy. The probabilistic forecast varies significantly over the course of the day depending on the tidal elevation, which had a relatively large range in these time periods, and predicts greater hazardous rip occurrence during low tide.

The NWS model demonstrates some degree of accuracy in the 2001 case, however it performs comparatively poorly in the 2005 case. The 2001 case begins with fairly large (H_s > 1 m) and long period (T_p ~ 11 s) waves close to shorenormal. Winds are onshore and moderate (~ 6 m/s). These conditions lead to high rip intensity forecasts for both the NWS model and the probabilistic model. Both models are reasonably

accurate in predicting the large number of rescues on August 2 and 3. However, in the later half of the 2001 case, wave height becomes more moderate (H_s ~ 0.7 m) and wind direction is offshore. The lower wave heights and offshore winds cause the NWS model to underforecast rip intensity on August 4, when 6 rescues occur. However, the probabilistic model indicates moderate intensity due to the moderate wave height and the low tidal elevation during the daytime.

The 2005 case is characterized by moderate wave heights with relatively short periods (6-10 seconds) as well as low winds. The NWS model tends to predict low rip intensity during low winds and also when the wave period is short (< 8 seconds), and thus underforecasts rip intensity in this instance. The probabilistic model does not include wave period or wind speed and accurately forecasts the likelihood of hazardous rip occurrence (Figure 5.8). It should be noted that the NWS WFOs manually account for rescues occurring on previous days (or even earlier in the day) when providing their rip forecast to the public. Thus, in both of these instances the NWS would probably issue a high rip risk in the hours or days following the initial large number of rip rescues even if the model prediction suggested otherwise. However, this manual adjustment factor was not recorded for these time periods and cannot be tested with this model hindcast.

Averaging predicted values over entire summers show that both models generally forecast consistent likelihood of rip occurrence, regardless of variations in the number of rescues from summer to summer (Table 5.6). This is not surprising since the total number of rescues can depend on a number of factors such as weather, water temperatures and beach attendance. The exception to this is 2003, when only 6 rip rescues were recorded over the entire summer. This was an unusually low number of

rescues for KDH, and both models capture this with their relatively low mean forecast levels for 2003.

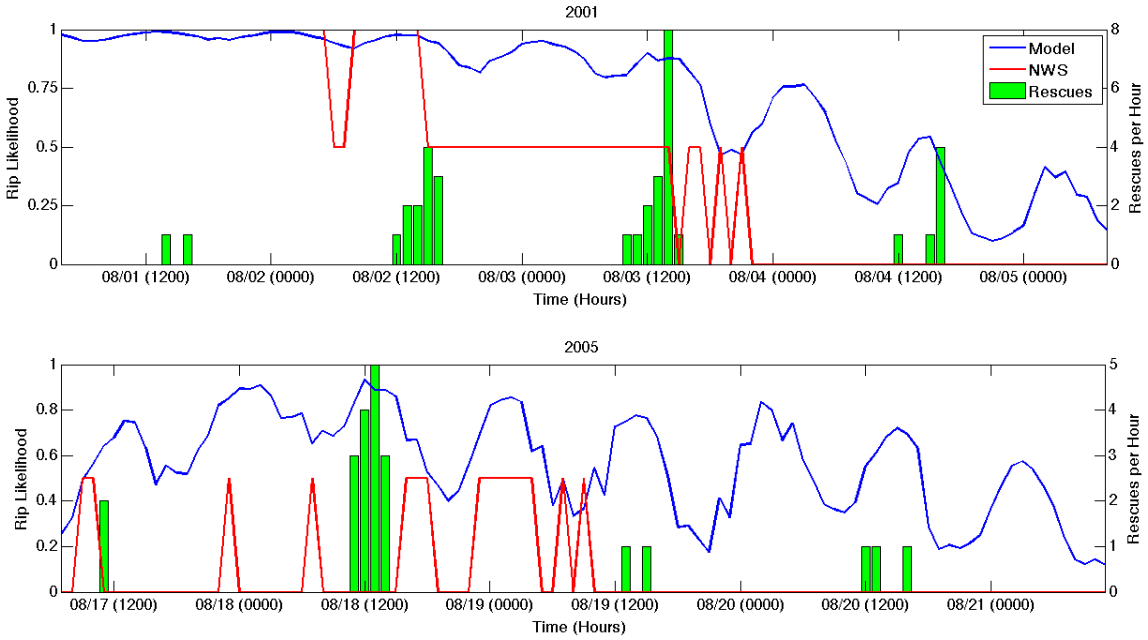

Figure 5.8 Two 100-hour case examples of the observed hourly rip current rescues and the probabilistic and NWS model hindcasts at KDH from August 2001 (top) and August 2005 (bottom).

Table 5.6 Total rescues and model averages for each summer at KDH

Year	**2001**	**2002**	**2003**	**2004**	**2005**	**2006**	**2007**	**Total**
Rescues	100	31	6	74	123	66	34	434
Prob. Model	0.41	0.44	0.31	0.45	0.41	0.37	0.42	0.40
NWS (0,0.5,1)	0.13	0.13	0.05	0.14	0.13	0.14	0.14	0.12
NWS (0.25,0.5,0.75)	0.31	0.31	0.28	0.32	0.32	0.32	0.32	0.31
NWS (Norm Index)	0.17	0.17	0.07	0.17	0.20	0.19	0.19	0.16

5.5 Discussion

5.5.1 Performance of probabilistic model and NWS model

The probabilistic model forecasts the likelihood of hazardous rip current occurrence with a Brier Score of 0.15 when compared to the occurrence of rip current rescues at KDH. Comparing the BS with that of the NWS model indicates the probabilistic model improves the forecast by at least 67%. Reasons for the forecast improvement are due to differences in both the type of model and the variables included.

One reason for model improvement is changing from a categorical index based model (NWS model) to a probabilistic logistic regression model. The categorical model can introduce inaccuracies when the forecast is close to the categorical cut-offs (low-medium or medium-high). In these instances even a slight change in wave field, wind or tidal measurements can cause a different level to be forecast, when in reality the slight difference would affect no real change in hazardous rip current likelihood (Figure 5.8). The probabilistic model has no such limitation because it is continuous. Additionally, the index approach is not statistically based and thus there is no method to assess if the indexed contributions of each variable are accurate. Each variable included in the probabilistic model has both a physical and statistical significance to rip current occurrence and thus its inclusion can be justified.

Both models include the wave field as a predictor. However they do so in different manners and this appears to influence model accuracy. Both models include wave height and direction, however the NWS model uses deepwater observations while the probabilistic model uses local wave observations shoaled and refracted to 3 m depth. When the deepwater observations are used in the probabilistic model, performance

decreases compared to using local wave inputs (BS = 0.31 compared to BS = 0.15). However, even with deep water wave inputs the probabilistic model outperforms the NWS model, indicating that the input source is not the only reason for improvement.

The NWS model uses only a binary representation for wave direction (with a cut-off at 90 degrees from shore-normal), whereas direction is a continuous predictor in the probabilistic model. This allows the probabilistic model to account for moderate direction differences which may significantly impact rip occurrence, especially in moderate wave height conditions. The NWS model includes wave period in its index as previous work utilizing rip rescues has suggested period significantly influences rip activity (Lascody, 1998; Engle et al., 2002). However, research completed at KDH has suggested that wave period does not influence rip intensity or occurrence (Chapter 3; Chapter 4). It is possible that in some wind sea dominated environments, the dependence of peak period on wave height leads to a correlation between peak period and rescues, however period is excluded from the probabilistic model since it has demonstrated little influence on rip occurrence at KDH. The inclusion of wave period negatively impacts the success of the NWS model when the period < 8 seconds, as the wave field index is then 0 regardless of wave height and direction. For instance, in the case of the extreme rescue event beginning on August 17, 2005 (Figure 5.8) peak period < 8 for a majority of the 100 hours shown. This results in the NWS model predicting low rip risk, when in reality hazardous rip occurrence is quite high.

The tidal influence on each model is especially apparent when comparing model forecasts. The probabilistic model includes the hourly tidal elevation as a continuous predictor, while the NWS model only includes a categorical tidal range for a given day.

The effect of this difference is most notable on days when there are large tidal ranges (Figure 5.8). In these instances there will often be relatively high levels of hazardous rip current occurrence when the tidal elevation is low and low levels of rip occurrence when the tidal elevation is high. The probabilistic model captures this variability well; on days of large tidal ranges the forecast can vary by more than 0.50 (Figure 5.8). The NWS model forecasts only a slight increase in rip likelihood for the whole day, thereby missing the major contribution of the tidal elevation on rip activity.

Wind speed and direction are included as predictors in the NWS model, but not in the probabilistic model. Outside of forcing the wave field, the wind has no direct physical influence on rip current occurrence. Therefore, the inclusion of wind may limit the accuracy of the NWS model. This is particularly evident when there are light winds, but favorable wave field and tidal conditions for rip occurrence. In some of these instances the NWS model forecasts low to medium rip likelihood, when in fact numerous rescues occur.

The rip current forecast model used by the Morehead City WFO is a specific version of the rip current index model developed by Lushine (1991), later enhanced by Lascody (1998) and Engle et al. (2002). Some of the improvements proposed by Engle et al. are not currently included in the Morehead City WFO model tested here, most notably the removal of wind speed and direction as factors. Further, the index method used for the variables included in this model enable a parameterization not possible with the Morehead City WFO model. When the index values are parameterized (using a log or linear fit) the total rip index for the Engle et al. model can be written as (Pers. Comm. – G. Voulgaris):

$$I = 2.98 + 0.16\log_{10}(T_p) + 0.54H_s - 0.22|\theta| - 1.9\eta \text{ . (5.11)}$$

Significant wave height, mean direction and tidal elevation are parameters common to both the Engle et al. and the probabilistic model (Eq. 5.9). While the variable signs are the same for both models, the relative magnitudes of each variable vary significantly. Most notably, the significant wave height appears to be much more important in the probabilistic model and the peak period is not included in the probabilistic model. These differences may indicate an improvement in the probabilistic model compared to the Engle et al. model, or may be primarily due to variations in wave and morphological conditions between locations. Testing of the probabilistic model at additional locations may provide further insight.

Development of the probabilistic model relies on the robust observational data set available at KDH. The probabilistic model is created and calibrated utilizing only local observations, while the NWS model is primarily based on previous work performed on the Florida coast, as until now there have not been sufficient observations on the North Carolina coast for adequate calibration. It is conceivable that a similar index based model calibrated more specifically to the North Carolina coast could result in improved performance. However, the statistical basis, functionality and flexibility of a logistic regression probabilistic model are preferred to an index based approach even if performance is similar otherwise.

5.5.2 Limitations of the probabilistic model

The probabilistic model is an initial attempt to create a simple hazardous rip current forecast that relies on observations (wave field and tide) available throughout most coastal regions. The model, as presently constructed, does not account for more complex aspects of rip current occurrence; namely surf zone bathymetry and components of the directional wave spectra. Previous research has shown that the surf zone bathymetry, and more specifically the surf zone bar, significantly influences rip current occurrence and intensity (Brander, 1999; Brander and Short, 2000; Haller et al., 2002; MacMahan et al., 2008). The inclusion of bathymetry is particularly important at KDH, as the northern and southern regions of KDH often have varying surf zone bar features which are believed to contribute to disparate rip activity between the regions (Chapter 4). The probabilistic model output for 2001-2007 was separated into north and south KDH to determine if performance was influenced by alongshore location. However, there were no significant differences between northern and southern KDH. Including information about the surf zone bar (bar-trough depth difference and alongshore bar depth difference) in the logistic regression model suggests that bar features may be important to predicting rip occurrence. Additionally, the relatively weak goodness-of-fit of the bulk wave forecast model (p_{χ}-value = 0.05) suggests that there is room for improvement. Inclusion of bar features could improve model fit, however, there are insufficient bar feature data in the present dataset to create a reliable model. Additional observations are needed to better assess how bar features may be included.

The bulk wave statistics used in the probabilistic model provide a general indication of the wave field. However, bulk statistics will not capture multiple wave field

components (e.g. two opposing swells) that may influence rip occurrence (Chapter 3). The mean direction difference between two swells is statistically significant when included in the logistic regression model, but the logistic regression fit is not optimal (Figure 5.4 bottom), and there are an insufficient number of data points (only 22 days) to use these results with much confidence. The binned observed values appear to peak between a 30 and 40 degree mean direction difference (Figure 5.4 bottom). A peak in the rip likelihood suggests that there may be an optimum or resonance direction difference between two swells when a maximum rip likelihood is reached. As the logit in a logistic regression assumes a linear fit, preconditioning to this data would be required to achieve the optimum fit (Hosmer and Lemeshow, 1989). Additional observations are required to assess this possibility.

The consideration of wave components could be utilized in a more sophisticated model that employs different predictors depending on what wave components are present. For example, wave fields consisting of one swell, swell and wind sea, or two swells might rely on different coefficients for predictors or different predictors entirely. In the case of two swells, as rip current creation is believed to be predominantly hydrodynamically driven, the influence of the surf zone bathymetry may be only marginal. A model relying on wave field components could be more robust and adaptable and provide increased accuracy. However, additional combined observations of rip intensity, wave components and surf zone bathymetry are needed to support model development.

The comparison presented here indicates the probabilistic model is an improvement over the current NWS index model; however, further validation is

desirable. The only independent data available to test the accuracy of the probabilistic model on an hourly basis is rip rescue occurrence. These observations provide only a limited number of data points to test model performance, and provide no indication of rip occurrence when rescues are not made. A more complete assessment could be accomplished by using similar rip intensity observations to those made at KDH in 2008 and 2009. Sadly, such a dataset was collected in 2010 but lost due to a lightning strike at the end of the summer.

It is expected that the model will perform reasonably well at locations with similar wave field, morphological and tidal characteristics. The mean wave height at KDH is 0.9 m (McNinch, 2004) and the summer morphology can be characterized as intermediate (not fully reflective nor dissipative) based on its Ω value (the non-dimensional fall velocity used to determine modal beach states) between 3 and 4 (Wright and Short, 1984; Chapter 4). The tide is considered microtidal with a mean range is about 1 m (Birkemeier et al., 1985). Thus, it is likely the model could be used at other morphologically intermediate beaches with similar tides and roughly 1m mean wave height. It is possible that the model could be adapted to locations outside these ranges, however the portability to such locations should be thoroughly assessed. Similarly, since the model has only been tested in the summer months, its performance in other seasons remains an outstanding issue. In warmer climates, swimming might be common in the late fall or winter months, which may have different wave field and morphological characteristics. In these instances further assessment of the model's portability would be beneficial.

5.6 Summary and Conclusions

This paper presents a probabilistic rip current forecast model that predicts hazardous rip current occurrence with a Brier Score of 0.15, which results in a 67% improvement over the current NWS model. The model utilizes a logistic regression formulation with predictor variables of significant wave height, mean direction, tidal elevation and 72-hour post event period. To calculate the coefficients for each predictor variable, the logistic regression is performed using hazardous rip current occurrence (i.e. intensity observations or rescues) observed at 19 lifeguard chairs at Kill Devil Hills, NC. The coefficients suggest that wave height is the primary driver of hazardous rip current occurrence, with the other three variables of secondary influence.

When assessed using an independent data set of rip current rescues from 2001-2007 the probabilistic model significantly outperforms the NWS model. When at least one rescue was made, the Brier Score for the probabilistic model is 0.15 (where 0 is perfect correlation) compared to a minimum score of 0.45 for the NWS model. The Brier Skill Score shows that the probabilistic model is a 67% improvement over the NWS model when predicting hazardous rip current occurrence. Additionally, the probabilistic model demonstrates a high level of accuracy when analyzing instances that are particularly hazardous to swimmers (i.e. when there are a large number of rescues). The probabilistic model has the added benefit of calculating a true probabilistic forecast compared to the categorical forecast currently implemented.

It is expected that the probabilistic model can be used to effectively forecast hazardous rip current occurrence at Kill Devil Hills and other locations with similar morphological, wave and tidal features. Further assessment would be beneficial,

particularly in locations different from KDH. One of the benefits of the logistic regression formulation is that if the model is found to be inaccurate at another location, the model coefficients could be adjusted to improve performance. It is envisioned that the model could be incorporated into the NWS forecast system with relative ease. Of particular importance is that wave model output currently used by some NWS WFOs could provide the necessary wave field inputs for the probabilistic model. This would enable a multi-day rip current forecast with relatively fine (1-5 km) resolution alongshore. Such a forecast could be integrated into the NWS graphical forecast system and displayed visually similar to other marine forecasts. An accurate, high resolution, and graphical rip current forecast could be utilized by ocean rescue personnel and the beach-going public to perhaps reduce the high number of rip current related rescues and drownings.

CHAPTER 6

CONCLUSIONS AND FUTURE RESEARCH

The influence of the wave field, tide and surf zone bathymetry on beach-wide rip current occurrence and intensity over daily to yearly temporal scales was determined through field work completed at Kill Devil Hills, NC. It was found that hazardous rip currents are more likely and more intense with large significant wave heights, shore-normal wave direction, low tide and an alongshore variable bar system. Specific relationships between these physical factors and rip current intensity were established. For example, observed rip intensity was found to increase dramatically at a significant wave height of about 0.7 m and then level-off at higher wave heights. The determination of relationships like this is pivotal to understanding large scale variability of rip currents, and has provided a basis for a probabilistic rip current forecast model. The probabilistic forecast model presented in Chapter 5 predicts hazardous rip current occurrence with reasonable accuracy (Brier Score = 0.15, where 0 is perfect prediction), which represents at least a 67% improvement over the present NWS forecast index used at the Morehead City, NC WFO.

The research presented in this dissertation has implications for both rip current science and public safety. One of the significant scientific results is the observed increase in hazardous rip current occurrence when the wave field consists of two swells

from opposing incidence. Although rip currents from crossing wave trains have been seen in lab and numerical model studies (Fowler and Dalrymple, 1990; Johnson and Pattiaratchi, 2006), this is believed to be the first instance in which it has been suggested from observations. This rip current forcing is of particular interest as it may be purely hydrodynamic and not depend on the surf zone bathymetry. The results presented here not only suggest that this type of rip formation occurs with some frequency, but that rips of this nature can be of significant velocity (enough to cause swimmers distress).

Another significant scientific result is the alongshore variability seen in rip current activity at KDH, and that this variability occurs due to both the wave field and the underlying morphology of the region. Generally, southern KDH displayed greater rip current activity than northern KDH. This appears to be in part due to southern KDH favoring more significant surf zone bar development. Further, the differences in bar development between northern and southern KDH appear to be most significant during extended periods of low energy conditions (low Ω), common in the summer. This result suggests that nearby (~ kilometer scale) coastal locations can have significantly different rip current characteristics, and that future rip research should take this into consideration. Large scale analysis is important to assess the rip current dynamics of a particular region. Future research should utilize observations (instrument based or visual) to consider potential large scale alongshore variability in rip occurrence.

In regards to public safety, the creation of the probabilistic rip current forecast model is clearly of primary importance. The probabilistic model presented predicts hazardous rip current occurrence with a reasonable level of accuracy (Brier Score = 0.15) and is an improvement over the present NWS forecast model in both accuracy (67%

improvement) and in functionality (a continuous probabilistic model compared to a categorical index model). Beyond an improvement in performance and functionality, a formalism is presented for probabilistic model development. The probabilistic model can be tested and adapted to other locations with relative ease if similar rip current observations are collected. The coefficients for the predictors can be modified or additional predictors can be added to improve performance. Additionally, the model can incorporate wave model output for wave field predictors, and thus bridge a potential transition to a fully numerical model approach.

The importance of the lifeguard observations to the creation of the rip current forecast model cannot be understated. The observations estimate the level of rip current intensity when rip current rescues do not occur. This is most notable during instances of moderate to large wave heights, when relatively few rescues may occur due to a lack of people in the water. Without the lifeguard observations an accurate relationship between significant wave height and rip current occurrence could not be determined. The use of the lifeguard observations introduces some uncertainties as it is a qualitative estimate of rip intensity. However, the lifeguards are trained observers and the use of 19 different observations over the entirety of KDH helps to mitigate this drawback. Further, this method of lifeguard observation of rip intensity could be easily reproduced in any locations lifeguards are present. These observations could be incorporated in the probabilistic rip current forecast model to calibrate the model for other coastal locations, greatly enhancing the portability and accuracy of the model.

Despite the results and applications presented here, there remain a number of research questions to address:

How do bi-modal wave fields influence rip intensity?

When two swells are present, rip activity has been shown to increase when the mean direction difference between the two swells is large (Chapter 2). Additionally, a logistic regression model incorporating the mean direction difference as a predictor variable suggests this same relationship (Chapter 4). However, there are an insufficient number of data points to provide enough confidence to include this predictor in the rip current forecast model. Additional rip intensity observations with corresponding nearshore wave field observations and surf zone bathymetry measurements are needed to determine a more specific relationship between bi-model spectra and rip current occurrence and intensity.

Why does Southern KDH favor increased bar formation compared to Northern KDH, and how does surf zone re-organization occur after large wave events at each location?

Southern KDH has shown a greater likelihood for more substantial surf zone bar presence than Northern KDH. Further, low energy conditions appear to favor this modal state. The most notable difference between Northern and Southern KDH is the presence of shore oblique bars (from 2 – 10 m depth) in the north and the bathymetry is characterized by shore-parallel isobaths in the south. Northern KDH also experiences short-term and long-term erosion while Southern KDH experiences short- and long-term accretion (Schupp et al., 2006). It is expected that both of these factors, nearshore bathymetry and accretion rate, influence differences in bar formation and re-organization between regions. It is possible that the shore oblique bars transform wave energy in a

manner less favorable for bar development or that a lack of sediment in Northern KDH reduces overall sand bar creation and size. A numerical model analysis of the wave transformation in each of these regions may help to answer these questions. Additionally, instrumentation in the surf zone and nearshore regions may help detect alongshore variations in the wave field transformation and sediment transport.

How does the probabilistic model perform at other locations?

The rip current probabilistic model was shown to forecast hazardous rip current occurrence fairly well at KDH (BS=0.15; Chapter 5). It is expected that the model will perform well at locations with similar morphological, wave field and tidal characteristics as KDH. However, it is unclear how the model will perform at locations with slightly different or significantly different coastal characteristics. Extension of the model to other beaches in North Carolina would be a simple means to assess model performance at locations characteristically similar to KDH. There are locations along the East Coast of the U.S. or the Gulf of Mexico that have slightly different morphological, tidal and wave field characteristics. The model could be assessed at three different locations, each of which may have only one characteristic that is significantly different than KDH. This may enable us to determine if the model fails for a particular instance (e.g. for a location with similar tidal and wave characteristics but a different morphology). Lastly, it is desirable to determine if the model could be utilized at locations that have much different characteristics than KDH. The Pacific Coast of the U.S. would be significantly different from KDH (larger wave heights, longer periods, more reflective beach states with more variable sediment characteristics, etc.) and testing could determine if the model is

portable to these types of locations with some modification to the predictor variable coefficients.

What improvements can be made to the probabilistic model and how can it be incorporated into the National Weather Service forecast system?

Although the performance of the probabilistic model in forecasting hazardous rip occurrence is encouraging, the Pearson chi-square test calculated during creation of the forecast model suggests additional variables may need to be included (p-value = 0.05; where p-value $\geq$ 0.05 is sufficient fit). Additionally, the alternative models utilizing the swell direction difference or surf zone bar characteristics suggest these predictor variables may be important to rip current prediction. As previously addressed, additional data collection is essential for determination of the influence of bi-modal wave fields on rip current occurrence and intensity. If more certainty can be established with the bi-modal logistic regression coefficients, a branching-logic forecast system could employ different forecast models depending on the number of swell components. Further, although surf zone bar features are important to rip activity, the difficulty in obtaining detailed measurements of these features complicates utilizing surf zone bar characteristics in a forecast model. An alternative to direct bathymetry measurements may be the incorporation of camera systems (e.g. Argus; Holman et al., 2006 and Turner et al., 2007). Photo analysis can identify the presence of a surf zone bar and some of the alongshore variability present in the bar system. These observations could potentially be utilized in a logistic regression model as an estimation of surf zone bar characteristics.

It is envisioned that a nearshore wave model, e.g. SWAN (Simulating WAves Nearshore), could provide the necessary wave field inputs to the probabilistic forecast model. Some NWS WFO's are currently using SWAN for wave field forecasts every 6 hours on a 5 km grid. The SWAN forecasts could be input into the probabilistic model with relative ease and would enable a graphical rip current forecast with similar spatial and temporal resolution. This graphical forecast could then be incorporated within the NWS Graphical Forecast Editor (GFE) and be presented on the NWS website along with other marine forecasts.

It is hoped that this dissertation can be a starting point to answering these questions, and that future research will continue to improve our scientific understanding of rip currents over large spatial and temporal scales. As evident with the creation of the probabilistic model, advancements in rip current research can be immediately utilized to improve rip current forecasting and potentially reduce the number of future rip current rescues and drownings.

APPENDIX A

DESCRIPTION OF DPWP PROCESSING SCHEME

Below is a description of the DPWP toolbox and additional modifications made to DIWASP. A code repository has been established at: trac.nccoos.org/dataproc/wiki/DPWP/docs.

The DPWP toolbox processes raw data from the ADCP or AWAC Doppler current profilers into directional wave spectra. The initial step of processing takes the raw binary data and converts it into ASCII files using Python. There are multiple ASCII files output for either the ADCP or AWAC. For the ADCP the output includes hourly ASCII files of the pressure record, the range to surface of each of four beams, the along beam radial velocity of each of four beams at 5 different vertical bin locations, as well as a file including date-time and system information. In addition, if the raw data includes interleaved currents data, a binary file of just currents data is created which can then be processed using TRDI's software or third party ADCP currents processing software.

For the AWAC the output includes hourly ASCII files of the pressure record, the range to surface of the vertical AST (Acoustic Surface Tracking) beam, the along beam radial velocity of each of three beams at one vertical bin location, and a file including date-time and system information. For the AWAC, if currents data is also recorded within the raw data, there are three ASCII files created that include a currents header file, currents tilt measurements, and a currents data file. Due to differences in the way the

ADCP and AWAC format their binary data, the AWAC currents data cannot be easily re-packaged into a binary data file readable by Nortek's software and thus are left as ASCII files. These can be analyzed within MATLAB® or other data analysis software.

After the ASCII files are generated the second step of the processing is completed within MATLAB®. A MATLAB® routine, Specmultiplot, (Figure 2.1) is called that takes either the ADCP or AWAC ASCII files and organizes the data into a data structure suitable for use with the wave spectral toolbox, DIWASP, an open-source waves spectral toolbox written in MATLAB® (Johnson, 2002). Prior to running DIWASP, Specmultiplot removes error values or bad data points from the ASCII records by identifying data points internally marked bad by the ADCP or AWAC and data values outside of 4 standard deviations of the mean calculated over one data record.

The DIWASP toolbox allows the user to input a variety of data types including pressure, surface elevation, vertical acceleration, sea surface slope, and horizontal and vertical velocities. In addition the user has numerous options in terms of how the directional wave spectra are generated. These include adjusting the directional and frequency resolution, choosing among a variety of spectral estimation methods and choosing the number of iterations to perform for iterative methods. Once the data structure is populated and the desired user options are selected, DIWASP outputs a directional wave spectral matrix, a graphical representation and information about the spectrum (significant wave height with confidence intervals, peak period, direction of peak period and dominant direction). For a complete description of the DIWASP toolbox see Johnson (2002).

Following the creation of the spectra by DIWASP, the MATLAB® routine creates time series plots of the significant wave height, peak period, direction of peak period and dominant direction. It then saves these plots, the individual directional spectra plots as well as a data structure including the spectra and all wave statistical data to the desired directory, thereby completing the processing scheme.

Changes to the original DIWASP code in addition to supporting radial velocity inputs include that the outdated MATLAB® spectral function 'csd' has been replaced in the code with the updated 'cpsd' and a slight change has been made to the inputs of the cpsd function. The size of the window used is now chosen based on the data length instead of the MATLAB® default of 8 windows. This prevents excessive zero padding that may negatively impact the results. The options selected in the cpsd function determine the degrees of freedom and allows the 95% confidence intervals to be calculated for the frequency spectra (Chapter 2). Additionally, the 1.1 version of DIWASP generated the frequency spectrum from the auto-spectrum of the first data input only. For the *p*-*u*-*v*-*w* and range data this same method is used in the updated version of the code. However, since the along beam radial velocity data is noisy compared to the typical pressure or range record, just using the one bin can result in a noisy frequency spectrum. Thus, the algorithm has been changed so that when using radial velocities to generate the spectra, the frequency spectra will be created using an average of the frequency spectra generated by all radial inputs instead of just the one listed first. In addition to improving the overall quality of the frequency spectra, an added benefit of using multiple radial velocities is the increase in the number of degrees of freedom and therefore, shrink confidence limits on the spectra and significant wave height estimates.

REFERENCES

Austin, M., Scott, T., Brown, Jef., Brown, Jen., MacMahan, J. 2010. Temporal observations of rip current circulation on a macro-tidal beach. *Continental Shelf Research. 30,* 1149-1165.

Birch, R., Fissel, D.B., Borg, K., Lee, V. and English, D. 2004. The capabilities of Doppler current profilers for directional wave measurements in coastal and nearshore waters. *Proceedings Oceans '04 MTS/IEEE/ Techno-Oceans '04. Kobe Japan*, IEEE Press, 1418-1427.

Birkemeier, W.A., Miller, H.C., Wilhelm, S.D., DeWall, A.E. and Gorbics, C.S. 1985. A User's Guide to the Coastal Engineering Research Centers (CERC's) Field Research Facility. Coastal Engineering Research Center, United States Army Corps of Engineers, Vicksburg, MS.

Boon, J.D., Green, M.O. and Suh, K.D. 1996. Bimodal wave spectra in lower Chesapeake Bay, sea bed energetics and sediment transport during winter storms. *Continental Shelf Research. 16 (15),* 1965-1988.

Bowen, A.J. 1969. Rip currents: 1. Theoretical investigations. *Journal of Geophysical Research 74,* 5467-5478.

Bowen. A.J. and Inman, D.L. 1969. Rip currents: 2. Laboratory and field observations. *Journal of Geophysical Research 74,* 5479-5490.

Brander, R.W. 1999. Field observations on the morphodynamic evolution of a low-energy rip current system. *Marine Geology. 157,* 199-217.

Brander, R.W. and Short, A.D. 2000. Morphodynamics of a large-scale rip current system at Muriwai Beach, New Zealand. *Marine Geology. 165,* 27-39.

Brodtkorb, P.A., Johannesson, P., Lindgren, G., Rychlik, I., Ryden, J. and Sjo, E. 2000. WAFO- a Matlab toolbox for analysis of random waves and loads. *Proceedings 10th International Offshore and Polar Engineering Conference. Seattle 3,* 343-350.

Browder, A.G. and McNinch, J.E. 2006. Linking framework geology and nearshore morphology: Correlation of paleo-channels with shore-oblique sandbars and gravel outcrops. *Marine Geology. 231,* 141-162.

Calvete, D., Dodd, N., Falques, A. and van Leeuwen, S.M 2005. Morphological development of rip channel systems: Normal and near-normal wave incidence. *Journal of Geophysical Research. 110,* C10006.

Capon, J. 1969. High-resolution frequency-wavenumber spectrum analysis. *Proceedings IEEE. 57*, 1408-1418.

Conover, W.J. 1999. Practical Nonparametric Statistics. John Wiley & Sons, Inc. New York, NY. 428-473

Cruz, J., MacKay, E. and Martins, T. 2007. Advances in wave resource estimation: measurements and data processing. *Proceedings 7th Euro Wave Tidal Energy Conference. Porto, Portugal*.

Dalrymple, R.A. 1978. Rip currents and their causes. *Proc. 16th Conference on Coastal Engineering. Vol. II,* 1414-1427.

Dean, R.G. and Dalrymple, R.A. 2002. Coastal Processes with Engineering Applications. Cambridge University Press. Cambridge, UK. 94-100

Dusek, G., Seim, H., Hanson, J. and Elder, D. 2011. Analysis of rip current rescues at Kill Devil Hills, North Carolina. In *Rip Currents: Beach Safety, Physical Oceanography and Wave Modeling.* CRC Press. S. Leatherman and J. Fletemeyer, editors.

Emery, W.J. and Thomson, R.E. 2004. Data Analysis Methods in Physical Oceanography: Second and revised edition. Elsevier B.V., Amsterdam, The Netherlands. 638pp.

Engle, J., MacMahan, J., Thieke, R.J., Hanes, D.M. and Dean, R.G. 2002. Formulation of a rip current predictive index using rescue data. *Florida Shore and Beach Preservation Association National Conference.*

Fowler, R.E. and Dalrymple, R.A. 1990. Wave group forced nearshore circulation. *Proceedings of 22nd International Conference on Coastal Engineering.* American Society of Civil Engineers, 729-742.

Garnier, R., Calvete, D., Falques., A. and Dodd, N. 2008. Modeling the formation and the long-term behavior of rip channel systems from the deformation of a longshore bar. *Journal of Geophysical Research. 113,* C07053.

Gorman, R.M., Bryan, K.R. and Laing, A.K. 2003. Wave hindcast for the New Zealand region: nearshore validation and coastal wave climate. *New Zealand Journal of Marine and Freshwater Research. 37,* 567-588.

Haller, M.C., Dalrymple, R. A. and Svendsen, I.A 2002. Experimental study of nearshore dynamics on a barred beach with rip channels. *Journal of Geophysical Research. 107 (14),* 1-21.

Hanson, J.L. and Phillips, O.M. 2001. Automated analysis of ocean surface

directional wave spectra. *Journal of Atmospheric and Oceanic Technology. 18*, 277-293.

Hanson, J.L., Tracy, B.A., Tolman, J.L. and Scott, R.D. 2009. Pacific Hindcast Performance of Three Numerical Wave Models. *Journal of Atmospheric and Oceanic Technology. 26,* 1614-1633.

Hashimoto, N., Nagai, T. and Asai, T. 1994. Extension of the maximum entropy principle method for directional wave spectrum estimation. *Proceedings 24th ICCE. Kobe, Japan 1*, 232-246.

Hashimoto, N. 1997. Analysis of the directional wave spectrum from field data. *Advances in Coastal and Ocean Engineering. World Scientific 3*, 103-143.

Herbers, T.H.C. and Lentz, S.J. 2010. Observing directional properties of ocean swell with an acoustic Doppler current profiler (ADCP). *Journal of Atmospheric and Oceanic Technology. 27,* 210-225.

Hilbe, J.M. 2009. Logistic Regression Models. CRC Press. Boca Raton, FL. 637 pp.

Hoitink, A.J.F. and Schroevers, M. 2004. Validation of ADCP surface wave measurements in a shelf sea. *Proceedings Oceans '04 MTS/IEEE/ Techno-Oceans '04. Kobe Japan,* 1444-1451.

Hoitink, A.J.F., Peters, H.C. and Schroevers, M. 2007. Field verification of ADCP surface gravity wave elevation spectra. *Journal of Atmospheric and Oceanic Technology. 24,* 912-922.

Holman, R.A., Symonds, G., Thornton, E.B., and Ranasinghe, R. 2006. Rip spacing and persistence on an embayed beach. *Journal of Geophysical Research 111,* C01006.

Holthuijsen, L.H. 2007. Waves in Oceanic and Coastal Waters. Cambridge University Press. Cambridge, UK. 387 pp.

Hosmer, D.W. and Lemeshow, S. 1989. Applied Logistic Regression. John Wiley and Sons, New York, NY. 307 pp.

Hosmer, D.W., Hosmer, T., Le Cessie, S., Lemeshow, S. 1997. A comparison of goodness-of-fit tests for the logistic regression model. *Statistics in Medicine. 16,* 965-980.

Jeans, J., Primrose, C., Descusse, N., Strong, B. and van Weert, P. 2003. A comparison between directional wave measurements from the RDI Workhorse with waves and the Datawell Directional Waverider. *Current Measurement Technology, 2003, Proceedings of the IEEE/OES 7th working conference on.* 148-151.

Johnson, D. 2002. DIWASP, a directional wave spectra toolbox for MATLAB® ®: User Manual. Research Report WP-1601-DJ (V1.1), Centre for Water Research, University of Western Australia.

Johnson, D. and Pattiaratchi, C. 2004. Transient rip currents and nearshore circulation on a swell-dominated beach. *Journal of Geophysical Research. 109, C02026.*

Johnson, D. and Pattiaratchi, C. 2006. Boussinesq modeling of transient rip currents. *Coastal Engineering. 53,* 419-439.

Kennedy, A.B. 2005. Fluctuating circulation forced by unsteady multidirectional breaking waves. *Journal of Fluid Mechanics. 538,* 189-198.

Kobune, K. and Hashimoto, N. 1985. Estimation of directional spectra from the Maximum Entropy Principle. *Proceedings 5th International OMAE Symposium. Tokyo,* 80-85.

Kuik, A.J., van Vledder, G. Ph. and Holthuijsen, L.H. 1988. A method for the routine analysis of pitch-and-roll buoy wave data. *Journal of Physical Oceanography. 18,* 1020-1034.

Kumar, N., Voulgaris, G. and Warner, J.C. 2011. Implementation and modification of a three-dimensional radiation stress formulation for surf zone and rip-current applications. *Coastal Engineering. 58(12),* 1,097-1,117.

Larson, M. and Krauss, N. C. 1994. Temporal and spatial scales of beach profile change, Duck, North Carolina. *Marine Geology.* 117, 75-94.

Lascody, R.L. 1998. East central Florida rip current program. *National Weather Digest. 22 (2),* 25-30.

Leroy, A., and Wheeler, M. C. 2008. Statistical prediction of weekly tropical cyclone activity in the southern hemisphere. *Monthly Weather Review. 136,* 3637-3654.

Lippmann, T.C. and Holman, R.A. 1990. The spatial and temporal variability of sand bar morphology. *Journal of Geophysical Research. 95,* 11,575-11,590.

Lo, F., Wheeler, M. C., Meinke. H., Donald, A. 2007. *Monthly Weather Review. 135,* 3506-3520.

Long, C.E. and Atmadja, J. 1994. Index and bulk parameters for frequency-directional spectra measured at CERC Field Research Facility, September 1990 to August 1991, Miscellaneous Paper CERC-94-5. US Army Engineer Waterways Experiment Station, Vicksburg, MS.

Long, C.E. and Oltman-Shay, J. 1991. Directional characteristics of waves in shallow water, technical report CERC-91-1. US Army Engineer Waterways Experiment Station, Vicksburg, MS.

Longuet-Higgins, M.S., Cartwright, D.E. and Smith, N.D. 1963. Observations of the directional spectrum of sea waves using the motions of a floating buoy. In: *Ocean Wave Spectra*. Prentice-Hall, Englewood Cliffs, NJ, pp. 111–136

Longuet-Higgins, M.S. and Stewart, R.W. 1964. Radiation stress in water waves, a physical discussion with applications. *Deep-Sea Research 11 (4),* 529-563

Lushine, J.B. 1991. A study of rip current drownings and related weather factors. *National Weather Digest. 16 (3),* 13-19.

MacMahan, J.H., Reniers, A.J.H.M., Thornton, E.B. and Stanton, T.P. 2004. Infragravity rip current pulsations. *Journal of Geophysical Research. 109,* C01033.

MacMahan, J.H., Thornton, E.B., Stanton, T.P. and Reniers, A.J.H.M. 2005. RIPEX: Observations of a rip current system. *Marine Geology. 218,* 113-134.

MacMahan, J.H., Thornton, E.B. and Reniers, A.J.H.M. 2006. Rip current review. *Coastal Engineering. 53,* 191-208.

MacMahan, J.H., Thornton, E.B., Reniers, A.J.H.M., Stanton, T.P. and Symonds, G. 2008. Low-energy rip currents associated with small bathymetric variations. *Marine Geology. 255,* 156-164.

McNinch, J.E. 2004. Geologic control in the nearshore: shore-oblique sandbars and shoreline erosional hotspots, Mid-Atlantic Bight, USA. *Marine Geology. 211,* 121-141.

Nortek AS. 2004. AWAC User Guide, for firmware version 1.10 onwards. Nortek AS.

Oltman-Shay, J. and Guza, R.T. 1984. A data-adaptive ocean wave directional-spectrum estimator for pitch and roll type measurements. *Journal of Physical Oceanography. 14,* 1800-1810.

O'Reilly, W.C., Herbers, T.H.C., Seymore, R.J. and Guza, R.T. 1996. A comparison of directional buoy and fixed platform measurements of Pacific swell. *Journal of Atmospheric and Oceanic Technology. 13,* 231-238.

Pawka, S.S. 1983. Island shadows in wave directional spectra. *Journal of Geophysical Research. 88,* 2579-2591.

Pedersen, T. and Lohrmann, A. 2004. Possibilities and limitations of acoustic surface tracking. *Proceedings Oceans '04 MTS/IEEE/ Techno-Oceans '04. Kobe Japan,* 1428-1434.

Rorbaek, K. and Andersen, H. 2000. Evaluation of wave measurements with and Acoustic Doppler Current Profiler. *Oceans 2000 MTS/IEEE Conference and Exhibition. 2,* 1181-1187.

Schupp, C.A., McNinch, J.E. and List, J.H. 2006. Nearshore shore-oblique bars, gravel outcrops, and their correlation to shoreline change. *Marine Geology. 233,* 63-79.

Scott, T., Russell, P., Masselink, G., Wooler, A. and Short, A. 2007. Beach rescue statistics and their relation to nearshore morphology and hazards: A case study for southwest England. *International Coastal Symposium. Journal of Coastal Research, Special Issue. 50,* 1-6.

Scott, T., Russell, P., Masselink, G. and Wooler, A. 2009. Rip current variability and hazard along a macro-tidal coast. *International Coastal Symposium. Journal of Coastal Research, Special Issue. 56,* 895-899.

Shepard, F. P., Emery, K.O. and LaFond, E.C. 1941. Rip currents: A process of geological importance. *Journal of Geophysical Research 49(4),* 337-369.

Shore Protection Manual. 1984. 4th ed., 2 vols, U.S. Army Engineer Waterways Experiment Station, Coastal Engineering Research Center, U.S. Government Printing Office, Washington, DC.

Siegel, E., Malzone, C. and Pedersen, T. 2004. Chesapeake Bay AWAC evaluation. Nortek Technical Note TN-021. October, 5 2004.

Stauble, D.K., Birkmemeier, W., Forte, M.F. and Dennis, W.A. 2007. Fill Suitability characterization of a complex coastal area: Dare Country, North Carolina. *Proc. 2007 National Conference on Beach Preservation Technology.*

Strong, B., Brumley, B.H., Terray, E.A. and Stone, G.W. 2000. The performance of ADCP-derived directional wave spectra and comparison with other directional wave measurements. *Oceans 2000 MTS/IEEE Conference and Exhibition. 2,* 1195-1203.

Svendsen, I.A., Haas, K.A. and Zhao, Q. 2000. Analysis of rip current systems. In: Edge, B.L. (Ed.), *Coastal Engineering, Proceedings of the 27th International Conference.* American Society of Civil Engineers, New York, 1127-1140.

Tracy, F.T., Tracy, B.A. and Hanson, J.L. 2006. Sorting out waves with a fast sort algorithm. *ERDC MSRC Resource (Fall 2006).* U.S. Army Engineer Research and Development Center, Vicksburg, MS, 6 pp.

Turner. I.L., Whyte, D., Ruessink, B.G., Ranasinghe, R. 2007. Observations of rip spacing, persistence and mobility at a long straight coastline. *Marine Geology, 236,* 209-221.

van Enckevort, I.M.J. and Ruessink, B.G. 2003. Video observations of nearshore bar behaviour. Part 1: alongshore uniform variability. *Continental Shelf Research. 23,* 501-512.

van Enckevort, I.M.J. and Ruessink, B.G. 2003. Video observations of nearshore bar behavior. Part 2: alongshore non-uniform variability. *Continental Shelf Research. 23,* 513-532.

van Enckevort, I.M.J., Ruessink, B.G., Coco, G., Suzuki, K., Turner, I.L., Plant, N.G. and Holman, R.A. 2004. Observational of nearshore crescentic sandbars. *Journal of Geophysical Research. 109,* C06028.

Voulgaris, G., Kumar, N. and Warner, J.C. 2011. Methodology for prediction of rip currents using a three-dimensional numerical, coupled, wave current model. In *Rip Currents: Beach Safety, Physical Oceanography and Wave Modeling.* CRC Press. S. Leatherman and J. Fletemeyer, editors.

Wilks, D.S. 2006. Statistical Methods in the Atmospheric Sciences: Second Edition. Academic Press. Burlington, MA. 627 pp.

Work, P.A. and Bystrom E. 2005. Triaxys wave buoy and RD Instruments 1200khz ADCP: Comparison of primary directional wave parameters. Tybee Roads, GA. 26pp.

Wright, L.D. and Short, A.D. 1984. Morphodynamic variability of surf zones and beaches: A synthesis. *Marine Geology. 56,* 93-118.